



UNIVERSITY  
OF TRENTO - Italy  
DEPARTMENT OF INDUSTRIAL ENGINEERING

---

---

XXVIII cycle

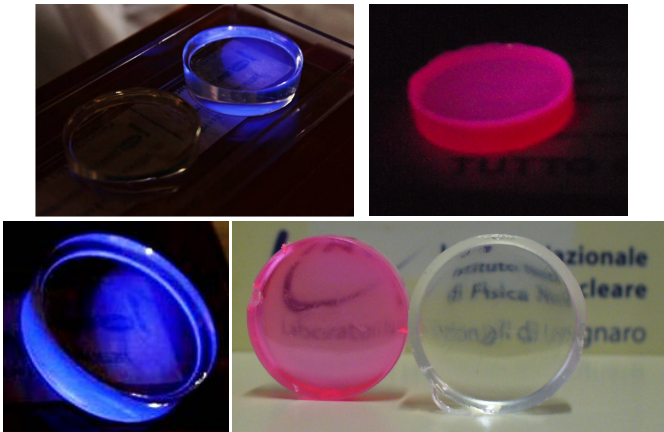
Doctoral School in Materials Science and Engineering

---

---

## Polysiloxane based neutron detectors

Matteo Dalla Palma



---

---

April 2016

---

---

# POLYSILOXANE BASED NEUTRON DETECTORS

Matteo Dalla Palma

E-mail: Matteo.DallaPalma@unitn.it

Approved by:

Prof. Alberto Quaranta, Advisor  
Department of Industrial Engineering  
*University of Trento, Italy.*

Ph.D. Commission:

Prof. Vigilio Fontanari,  
Department of Industrial Engineering  
*University of Trento, Italy.*

Prof. Eugene A. Olevsky,  
Department of Mechanical Engineering  
*San Diego State University, USA.*

Prof. Gino Mariotto,  
Department of Computer Science,  
*University of Verona, Italy.*

University of Trento,  
Department of Industrial Engineering

April 2016

**University of Trento - Department of  
Industrial Engineering**

**Doctoral Thesis**

**Matteo Dalla Palma - 2016  
Published in Trento (Italy) – by University of Trento**

**ISBN: - - - - -**

*To my family*



## Abstract

In the last decade, neutron detection has been attracting the attention of the scientific community for different reasons. On one side, the increase in the price of  $^3\text{He}$ , employed in the most efficient and the most widely used neutron detectors. On the other side, the harmfulness of traditional xylene based liquid scintillators, used in extremely large volumes for the detection of fast neutrons. Finally, the demand for most compact and rugged systems pushed by the increased popularity of neutron imaging, neutron scattering and neutron diffraction techniques.

Polysiloxanes could help addressing some of the existing issues regarding neutron detection thanks to their unique properties. For this reason, in this work, polysiloxane scintillators have been developed and characterized, with a special attention to their optical properties and their time response. In particular, this thesis describes the investigation of the scintillation performances of several different polysiloxane liquids. The results have been connected with the optical properties of the material, in turns linked to its molecular structure, allowing to select the most suitable polysiloxane solvent for liquid scintillators. The timing properties of scintillating mixtures employing the best performing polysiloxane solvent were consequently analyzed as a function of the primary dye concentration, with a special focus to the pulse shape discrimination (PSD) capability of the material. PSD is indeed one of the most important characteristic of liquid scintillators, and one of the factors determining their large use.

Beside polysiloxane liquids, time response of polysiloxane plastic scintillators was also investigated with the aim of studying their PSD capability. At the moment, indeed, only few examples of plastic scintillators capable of PSD exist, and also in those cases some criticalities emerged connected with stability issues and efficiency. Production of red emitting polysiloxane plastic scintillators is also described in this work, analyzing the energy transfer process between dyes in order to optimize the readout with an avalanche photodiode. This would allow overcoming some issues connected with the use of photomultiplier tubes, in more compact and rugged systems.

Finally some preliminary results about the HYDE experiment are presented. This project aims at the development of a hybrid detector for neutrons, combining a 3D silicon diode with a suitable neutron converter, in order to produce a compact efficient neutron detector with good spatial resolution. With this goal different types of converters for fast and thermal neutrons were tested and the performances of 3D and planar devices were compared.



# Table of contents

Introduction .....	1
Chapter I.....	5
Radiation detection and scintillation detector .....	5
<b>1.1 Radiation-Matter Interaction.....</b>	<b>5</b>
1.1.1 Heavy charged particles .....	5
1.1.2 Electrons.....	7
1.1.3 Photons.....	8
1.1.3.1 Photoelectric effect .....	8
1.1.3.2 Compton Effect .....	9
1.1.3.3 Pair production.....	10
1.1.4 Neutrons .....	10
1.1.4.1 Slow neutrons .....	11
1.1.4.2 Fast neutrons.....	12
<b>1.2 Scintillation detectors .....</b>	<b>14</b>
1.2.1 Inorganic scintillators .....	15
1.2.2 Organic scintillators .....	16
1.2.2.1 Organic crystals.....	16
1.2.2.2 Liquid scintillators .....	16
1.2.2.3 Plastic scintillators .....	17
1.2.3 Scintillation process in organic scintillators.....	18
1.2.3.1 Ionization and excitation of the matter .....	18
1.2.3.2 Energy transfer .....	20
1.2.4 Luminescence of organic molecules.....	23
1.2.4.1 Excited state .....	23
1.2.4.2 Radiative decay .....	24
<b>1.3 Neutron detection.....</b>	<b>25</b>
1.3.1 Scintillators for neutron detection .....	27
Chapter II.....	31
Materials and methods .....	31
<b>2.1 Polysiloxanes.....</b>	<b>31</b>
2.1.1 Properties of polysiloxanes.....	31

2.1.2	Polysiloxane plastic scintillating materials .....	33
2.1.2.1	<i>Cross-linking reactions</i> .....	35
2.1.3	Polysiloxane liquid scintillating materials .....	37
<b>2.2</b>	<b>Dyes</b> .....	<b>39</b>
2.2.1	2,5-Diphenyloxazole (PPO) .....	39
2.2.2	Lumogen Violet.....	40
2.2.3	Lumogen Red .....	41
<b>2.3</b>	<b>Samples preparation</b> .....	<b>43</b>
2.3.1	Polysiloxane plastic scintillators.....	43
2.3.2	Polysiloxane liquid scintillators .....	44
<b>2.4</b>	<b>Characterization techniques</b> .....	<b>45</b>
2.4.1	Optical measurements.....	45
2.4.1.1	<i>UV-Vis spectroscopy</i> .....	45
2.4.1.2	<i>Steady state fluorescence spectroscopy</i> .....	45
2.4.1.3	<i>Fluorescence lifetime measurements</i> .....	46
2.4.2	Scintillation light yield measurements.....	47
2.4.2.1	<i>Plastic scintillators</i> .....	47
2.4.2.2	<i>Liquid scintillators</i> .....	49
2.4.3	Pulse shape analysis .....	51
2.4.3.1	<i>Pulse shape discrimination</i> .....	51
2.4.4	Time resolved ion beam induced luminescence (TRIBIL) ...	52
<b>Chapter III.....</b>		<b>53</b>
<b>Polysiloxane liquid scintillators.....</b>		<b>53</b>
<b>3.1</b>	<b>Introduction.....</b>	<b>53</b>
<b>3.2</b>	<b>Experimental part.....</b>	<b>54</b>
<b>3.3</b>	<b>Optical properties of polysiloxane liquids.....</b>	<b>56</b>
3.3.1	Absorption spectra.....	56
3.3.1.1	<i>Absorption spectra of polysiloxane liquids</i> .....	56
3.3.1.2	<i>Absorption spectra of scintillating solutions</i> .....	57
3.3.2	Fluorescence spectra .....	59
3.3.2.1	<i>Fluorescence of polysiloxane liquids</i> .....	59
3.3.2.2	<i>Fluorescence of scintillating mixtures</i> .....	61
<b>3.4</b>	<b>Scintillation response of polysiloxane liquids .....</b>	<b>66</b>
<b>3.5</b>	<b>Conclusions.....</b>	<b>70</b>
<b>Chapter IV .....</b>		<b>73</b>
<b>Pulse shape discrimination in polysiloxane liquid scintillators .....</b>		<b>73</b>

4.1	<b>Introduction</b> .....	73
4.2	<b>Experimental part</b> .....	74
4.3	<b>Fluorescence analysis</b> .....	74
4.4	<b>Fluorescence lifetime analysis</b> .....	76
4.5	<b>Scintillation lifetime analysis</b> .....	79
4.6	<b>Scintillation light yield</b> .....	86
4.7	<b>Pulse shape discrimination capability</b> .....	87
4.8	<b>Conclusions</b> .....	92
<b>Chapter V</b> .....		93
<b>Time response of polysiloxane plastic scintillators</b> .....		93
5.1	<b>Introduction</b> .....	93
5.2	<b>Experimental part</b> .....	94
5.3	<b>Fluorescence emission analysis</b> .....	94
5.4	<b>Fluorescence lifetime analysis</b> .....	99
5.5	<b>Time resolved ion beam luminescence (TRIBIL)</b> .....	102
5.6	<b>Scintillation light yield</b> .....	107
5.7	<b>Scintillation pulses</b> .....	108
5.8	<b>Conclusions</b> .....	110
<b>Chapter VI</b> .....		113
<b>Red emitting polysiloxane scintillators</b> .....		113
6.1	<b>Introduction</b> .....	113
6.2	<b>Experimental part</b> .....	114
6.3	<b>Fluorescence and energy transfer</b> .....	114
6.3.1	Fluorescence emission .....	114
6.3.2	Energy transfer analysis .....	118
6.4	<b>Scintillation light yield analysis</b> .....	126
6.4.1	PMT measurements .....	126
6.4.2	APD measurements.....	128
6.5	<b>Neutron response</b> .....	132
6.6	<b>Conclusions</b> .....	132
<b>Chapter VII</b> .....		135
<b>HYDE experiment</b> .....		135
7.1	<b>Introduction</b> .....	135
7.2	<b>Experimental part</b> .....	136

7.2.1	Device structure.....	136
7.2.2	Polysiloxane deposition .....	137
7.2.3	Thermal neutron converters deposition .....	138
7.2.4	Neutron Tests .....	142
7.2.4.1	<i>Fast neutrons</i> .....	142
7.2.4.2	<i>Thermal neutrons</i> .....	142
<b>7.3</b>	<b><i>Performances of 3D hybrid detectors</i></b> .....	<b>143</b>
7.3.1	Fast neutrons.....	143
7.3.2	Slow neutrons .....	144
<b>7.4</b>	<b><i>Conclusions</i></b> .....	<b>148</b>
	<b>Conclusions and Future Perspectives</b> .....	<b>149</b>
	<b>List of Abbreviations and Acronyms</b> .....	<b>153</b>
	<b>References</b> .....	<b>155</b>
	<b>Scientific production</b> .....	<b>169</b>
	HYDE and scintillators.....	169
	Other activities.....	169
	Proceedings.....	170
	LNL annual reports.....	170
	<b>Acknowledgment</b> .....	<b>173</b>

# Introduction

The attention of the scientific community to neutron detection has been continuously increasing for more than 60 years (Figure 1), mainly due to the broad range of applications in many fields, ranging from nuclear physics [Leo1987], to homeland security [Joyce2012], materials analysis [Vartsky2003], medicine [Kirov2005], fusion science [Kaschuck2000] and more. In the last decade in particular, the research on this topic experienced a fast growth, boosted by the increased popularity of neutron characterization techniques (neutron imaging, neutron scattering and neutron diffraction), by homeland security issues connected with terrorism threats and by the  $^3\text{He}$  shortage [CRSreport2010].

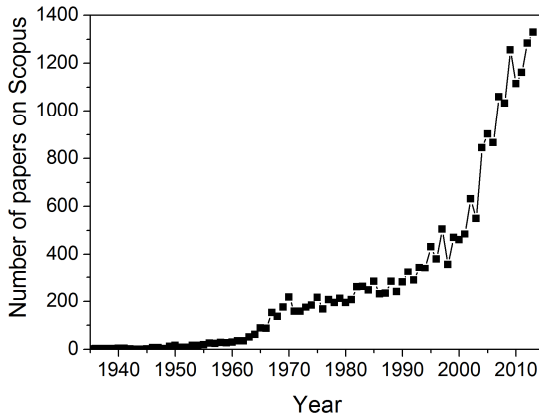


Figure 1. Annual distribution of the number of papers on "Neutron Detector" in Scopus database.

$^3\text{He}$  has been traditionally the most used material for neutron detection, especially in the detection of thermal neutrons or in systems detecting fast neutrons after a moderation stage, mainly due its high efficiency and low sensitivity to  $\gamma$  rays [Kouzes2011]. After September 2001, however, the increase in the demand for this gas due to homeland security reasons and the contemporary decrease in its production, following non-proliferation treaties, reduced the availability of this material, consequently increasing its price [CRSreport2010, Hurd2014]. This fact triggered the research for valid  $^3\text{He}$  alternatives [Kouzes2010] and a number of new systems with interesting characteristics were recently developed in its replacement. As regarding direct fast neutrons detection, liquid scintillators are one of the most used alternatives since their pulse shape discrimination (PSD) capability allows

achieving very good gamma rejection rates. Best performing liquid scintillators, based on xylene, have however some drawbacks connected with their high toxicity, high volatility and high flammability. The obvious solution to overcome these problems is the replacement of toxic solvents with less harmful ones, and strong efforts have been put in the development of new solutions [Chang2015, Joyce2012, OKeefe2011, Bentoumi2013] but, despite the good results achieved, at the moment they do not seem to equal the performances of xylene based scintillators [Pawelczak2013].

Polysiloxane liquids could also play a role in this research for new, less hazardous solvent, given their very good chemical stability, excellent thermal stability, very low toxicity, low flammability, low volatility (lower than  $10^{-4}$  torr at room temperature) and high flash point (more than  $200^{\circ}\text{C}$ ) [GelestMSDS]. For this reason, in this work, several possible polysiloxane solvents were tested as liquid scintillators, analyzing their optical properties and their gamma rays response (Chapter III). This investigation allowed selecting 1,1,5,5-tetraphenyl-1,3,3,5-tetramethyltrisiloxane (TPTMTS) as the best performing solvent. Since one of the key characteristic of liquid scintillators is their pulse shape discrimination capability, TPTMTS based mixtures were also investigated in this sense, analyzing their time response at various concentrations of primary dye and under different type of excitation (Chapter IV).

Another possible way to overcome these problems regarding the toxicity and volatility of liquid scintillators would be the use of plastic scintillators. At present however, their use for neutron detection is mainly hindered by their very poor pulse shape discrimination performances. Many attempts have been done in the last decade to overcome this problem, as reviewed in [Bertrand2015], and recently, the first commercial plastic scintillator with PSD capability entered the market [EJ-299-33]. Many of these attempts however were not so effective or efficient, and also the commercial EJ-299-33 is still under evaluation, both as regarding its performances [Cester2014, Pozzi2013] and its long term stability.

The interesting properties of polysiloxane materials could help overcoming also this issue, allowing to achieve an efficient PSD at lower PPO concentrations with the consequent reduction of long term stability problems. In order to investigate the possibility to achieve pulse shape discrimination with polysiloxane plastic scintillators, their time response has been investigated at different PPO concentrations with different excitations and the results are reported in Chapter V.

Beside these aspects, in many applications of neutron detection, from medical diagnostic [Levin2003, Pilcher1998, Chen1999], to nuclear [Katagiri2004] and high energy physics [Deiters2000], radiation monitoring [Li2012, Foster2008] and homeland security [Athanasiaades2005, Byrd1992], the need is growing for new more compact detectors in order to improve the spatial resolution in imaging systems and to achieve the integration of the detector in multifunctional devices. One of the key

steps to reach this goal is the replacement of cumbersome PMTs with more compact photodetectors. This could also allow overcoming some of the main problems of this type of device like high sensitivity to magnetic fields, large power consumption, fragility and damageability when exposed to intense light. At the moment, however, their performances in terms of gain, noise and quantum efficiency are hardly reached by other systems. This leadership is however being challenged by recent improvements in silicon based photodetectors, and Avalanche Photodiodes are very promising candidates to assume this role thanks to their very high quantum efficiency, compactness, insensitivity to magnetic fields, low power consumption, durability and good energy resolution [Holl1995, Moszynski2002, Karar1999, Schmelz1985]. One of the main factors limiting the widespread of APD detectors in coupling with scintillators is that the spectral efficiency of these devices is higher in the red part of the visible spectrum, with the maximum responsivity often above 700 nm, therefore having a non optimized spectral matching with most scintillators. Following this consideration, the shifting of the scintillator emission to longer wavelength could allow improving the spectral matching between APD responsivity and scintillator emission [Kalivas2012].

Chapter VI describes the development of red emitting polysiloxanes plastic scintillators, through the introduction of a third dye in the elastomeric matrix with the aim of improving the optical coupling with APD.

Always with the aim of the development of a compact and efficient neutron detector, in the last period there has been an increasing attention towards solid state neutron detectors [McGregor2013]. In this framework the INFN HYDE experiment aims at the development of a pixel hybrid detector for neutrons, by combining a 3D silicon diode with a suitable neutron converter. This could allow producing a new compact detector with good spatial and temporal resolution, capable of interesting neutron imaging performances that could find applications in many fields. With this aim, in Chapter VII, the preliminary results on the investigation of the performances of a first design of 3D silicon sensors filled with different type of converters for fast and thermal neutrons are reported and compared with the results of planar silicon diodes.



# Chapter I

## Radiation detection and scintillation detector

### 1.1 *Radiation-Matter Interaction*

In order to understand the behaviour of any radiation detector, including scintillators, it is crucial to understand the way the radiation to be detected interacts with matter. Different kinds of radiation interact in different ways depending on their mass, charge and energy. For this reason, for an optimal detection of a specific radiation field a dedicated detector has to be used, which might not be effective in detecting a different kind of radiation. For instance, silicon based semiconductor detectors are very efficient and widely used in heavy charged particle detection, but the same detectors are generally inefficient in the detection of high energy photons or neutrons. For the purposes of this work, radiations can be divided into four main classes:

- Heavy charged particles, comprising heavy ions (e.g. alpha particles), protons, mesons.
- Electrons (e- and e+).
- Electromagnetic radiations (X-rays and  $\gamma$ -rays).
- Neutrons.

#### 1.1.1 **Heavy charged particles**

The interaction of heavy charged particles with matter occurs mainly through a succession of coulombic interaction between the charged particle and the electronic orbitals of the material. In these inelastic interactions, the energy of the particle is transferred to the atoms in the medium, leading to the excitation and ionization of the electrons along the path. The secondary electrons coming from these ionizations sometimes have enough energy to cause further excitations and ionizations and in this case they are called  $\delta$ -rays. Excitations and ionizations are exploited to detect the passage of the particle in the medium, which might be a solid, a liquid or a gas. Since these inelastic interactions are very frequent, this process occurs very quickly and the particle travels a very short distance in the medium before completely losing its energy. Furthermore, due to the great difference between the mass of the electrons and that of the incident particle, it undergoes almost no deflection during these interactions. So, since scattering with materials nuclei is much less frequent, the particle track can be very well approximated with a straight line.

Heavy charged particles of particular importance for this work are alpha particles and protons. The former are doubly positively charged  ${}^4\text{He}$  ions ( ${}^4\text{He}^{2+}$ ), widely used for detectors energy calibration, and also exploited for thermal neutron detection, since alpha particles are emitted by  ${}^{10}\text{B}$  and  ${}^7\text{Li}$  after neutron capture. The latter are exploited for fast neutron detection in organic scintillators, as explained more in detail later.

The energy loss of this kind of radiation depends not only on the particle, but also on the medium where this radiation travels. More in detail the specific energy loss,  $-\frac{dE}{dx}$ , for a particle with energy  $E$ , rest mass  $M$  ( $\gg m_0$  which is the electron rest mass), velocity  $V$  ( $= \beta c$ ) and charge  $ze$ , crossing a medium having  $N \frac{\text{atoms}}{\text{cm}^3}$ , with atomic number  $Z$ , can be expressed using the *Bethe formula*:

$$-\frac{dE}{dx} = \frac{4\pi e^4 z^2}{m_0 v^2} N Z \left[ \ln \left( \frac{2m_0 v^2}{I} \right) - \ln(1 - \beta^2) - \beta^2 \right] \quad (1)$$

where  $I$  is an empirical constant depending on the ionization and excitation potential of the material. This formula shows that the heavier and denser is the medium, the larger is the specific energy loss.

An important parameter connected to the specific energy loss is the range of the particle, defined as the thickness of material at which the number of particles is reduced to 50%, and represents the mean distance travelled by the particle in that medium.

A very common  $\alpha$  source used also in this work is the one based on  ${}^{241}\text{Am}$ , that decays emitting  $\alpha$  particles with energy of 5.486 MeV (85%), 5.443 MeV (13%) and 5.388 MeV (1%). At this energy, the range is about 3 cm in air and is as short as 44  $\mu\text{m}$  in a typical polysiloxane based material. Protons of the same energy, due to their smaller mass, have a range respectively of 30 cm and 430  $\mu\text{m}$  (data from SRIM simulation [SRIM]).

A consequence of the *Bethe formula* is that the loss of energy along the track is not constant for heavy charged particles, but it is higher at the end of their path, so that the plot of  $-\frac{dE}{dx}$  vs.  $x$  shows a peak in the specific energy loss at the end of the particle path, known as *Bragg peak* (Figure I. 1).

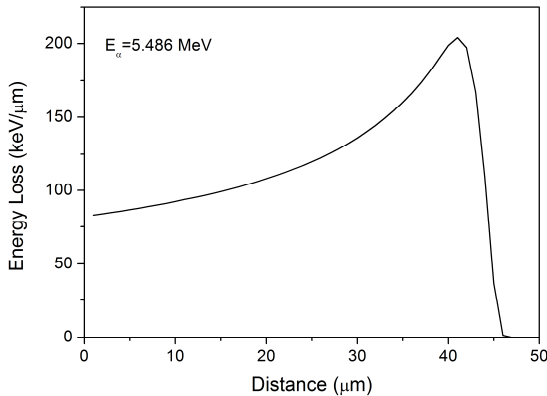


Figure 1. 1. Specific energy loss profile along the path for a  $^{241}\text{Am}$   $\alpha$  particle in polysiloxane (spectrum achieved by SRIM simulation [SRIM]).

### 1.1.2 Electrons

Also high energy electrons ( $\beta^-$ ) and positrons ( $\beta^+$ ) lose their energy through excitation and ionization of the matter, but interactions occur at lower rate than with heavy charged particles. Furthermore, due to their lower mass, they lose larger energy fractions in scattering with electrons (more common) and nuclei (rarer). For this reason they don't follow a straight track, but a tortuous path, so that observed range and real path can have different lengths (real path can be up to 4 times longer), and their track can undergo large deviations from the straight line especially after collisions with nuclei. As an example, the observed range for 1 MeV  $\beta$  rays in polysiloxane is about 4 mm, almost 100 times longer than alpha particles [Birks1964].

The specific energy loss due to collisions inside the material can be described by an equation very similar to the *Bethe formula*, but beside this, at high energies (around 10 MeV), another effect becomes important. This effect is called *bremsstrahlung* and consists in the emission of electromagnetic radiation due to the acceleration of the particle in the electric field of the nuclei. For the purpose of this work, the detection of electrons is mainly connected with the detection of  $\gamma$ -rays, as explained in the next paragraph. For this reason, since the energies involved in the process are usually below 5 MeV, the *bremsstrahlung* effect will be considered as negligible.

### 1.1.3 Photons

High energy electromagnetic radiations are classified as X-rays and  $\gamma$ -rays depending on their origin: X-rays are photons emitted by excited electronic orbitals of atoms, while  $\gamma$ -rays are emitted from atomic nuclei, as an effect of radioactive decays or nuclear reactions. The detection of high energy photons usually exploits three different mechanisms, depending on the material and on the energy of the radiation: *photoelectric absorption*, *Compton scattering* and *pair production*. All of them lead to complete or partial energy transfer from the photon to an electron, whose energy can be detected. Depending on the material and on the radiation energy, these processes can also occur simultaneously. The importance of the different processes as a function of energy in polysiloxanes are shown in Figure I. 2

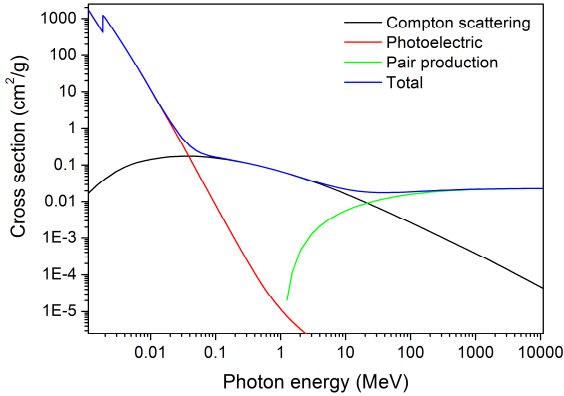


Figure I. 2.  $\gamma$ -rays cross section for the different types of photon interactions as a function of energy in a polysiloxane material (data achieved from [NIST2010]).

#### 1.1.3.1 Photoelectric effect

In the photoelectric process, the photon is absorbed by an electron in the atomic orbital of the medium. The energy of the photon is high enough to cause the ionization of the material and the ejection of the electron with energy equal to:

$$E_{e^-} = h\nu - E_B \quad (2)$$

being  $h\nu$  the photon energy and  $E_B$  the electron binding energy.

This electron can later cause excitation and ionization in the material, allowing the detection of the radiation. As a first approximation, the probability to have photoelectric effect is proportional to  $\frac{Z^n}{E_\gamma^{3.5}}$ , being  $n$  a number between 4 and 5. For

this reason, photoelectric effect is the main process for relatively low energy photons and is much more important in elements with high atomic number. Following these considerations it is clear that in light materials, typical for organic scintillators, photoelectric effect is almost negligible if no high Z element is added [Cho1975, Bertrand2014, Hamel2011a].

### 1.1.3.2 Compton Effect

The Compton Effect is usually the most effective process for organic materials in the energy range between 0.1-0.5 MeV and 10 MeV that is the energy of the most used  $\gamma$  sources. For this reason this is the process exploited also by plastic scintillators (and polysiloxane ones among them) for the detection of  $\gamma$  rays, and is particularly important for this work.

During this kind of elastic process,  $\gamma$ -ray interacts with an electron, considered at rest, and transfers part of its energy to it. This electron recoils with a certain angle  $\phi$  with respect to the direction of the incoming photon, and with a certain energy  $E_e$ , while the photon scatters with a different angle  $\theta$  and an energy  $E'$ . The energies of the scattered photon and of the recoil electron depend on the scattering angle of the photon, so that:

$$E' = \frac{E}{1 + \frac{E}{m_0 c^2}(1 - \cos\theta)} \quad (3)$$

$$E_e = E - E' \quad (4)$$

Following these equations, depending on the photon scattering angle, the energy of the recoil electron can vary between 0 and a maximum value ( $E_{e_{max}}$ ), known as *Compton Edge*, that takes the value:

$$E_{e_{max}} = \frac{E}{1 + \frac{m_0 c^2}{2E}} \quad (5)$$

The angular distribution of the scattered photons, calculated by Klein and Nishina [Klein1929], varies with the  $\gamma$  energy. At low energy this distribution is quite homogenous while it becomes peaked to the forward direction at higher energies (above 0.5 MeV). From this calculation, the energy distribution of recoils electron can be easily derived, and the corresponding energy spectrum is shown in Figure 1. 3. This is a very important result when dealing with detectors that operate in the energy range of Compton scattering, as in the case of plastic scintillators, since this is the expected energy spectrum for fixed  $\gamma$ -rays energy. As clear from the figure, unlike electrons and heavy charge particles, the energy spectrum of mono-energetic  $\gamma$ -rays in the Compton range is not a single peak, but a continuum going from 0 to  $E_{e_{max}}$ .

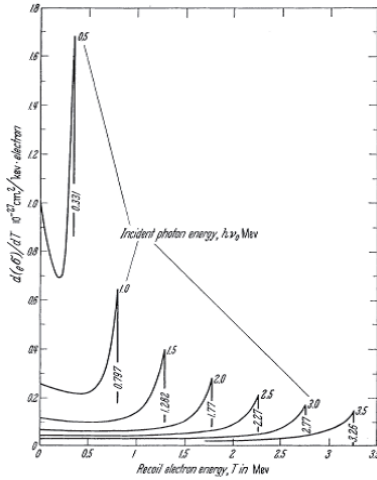


Figure 1. 3. Energy distribution of Compton recoil electrons for different  $\gamma$  energies [Evans1958].

### 1.1.3.3 Pair production

At energies higher than 10 MeV, the Compton scattering cross-section decreases and a third type of process becomes important. This process usually occurs in the electric field of the atomic nucleus, where the high energy photon is totally absorbed to create an electron-positron pair. In order to create this pair, a minimum energy of  $2m_e c^2 = 1.02 \text{ MeV}$  is needed, so that this process cannot occur for  $\gamma$  energies below 1.02 MeV. Over this threshold, the energy in excess is transformed into kinetic energy, so that:

$$E_{e^-} + E_{e^+} = E_\gamma - 2m_e c^2 \quad (6)$$

Also in this case then, as in the case of the photoelectric effect, the measured energy spectrum is a single peak, with an energy corresponding to  $E_\gamma - 2m_e c^2$ .

### 1.1.4 Neutrons

Neutrons, similarly to photons, have no electric charge and for this reason they cannot experience coulombic interactions with electrons or nuclei in the material. Unlike the other types of radiation, neutrons interact only through the strong force within the nuclei, but since this force requires a very short distance ( $\sim 10^{-13} \text{ cm}$ ), the interactions are much rarer than the Coulombic ones, so that they can travel several centimetres in a medium without being scattered or absorbed. As a consequence, in order to have an efficient neutron shield or an efficient neutron detector usually large volumes are required. Neutron interactions with matter occur

mainly in two ways: in the first case neutrons are completely absorbed by a nucleus, causing its excitation and the consequent decay through a neutron-induced nuclear reaction, with the emission of heavy charged particles, other neutrons and, in some cases, gamma rays; the second type of interaction instead is elastic scattering between the neutron and a nucleus of the material.

The cross section of these processes has strong energy dependence, and for this reason, historically, neutrons have been classified depending on their energy into fast, epithermal, thermal and cold neutrons (Table I. 1). A wider classification divides neutrons into fast and slow neutrons with the division set around 0.5 eV, corresponding to the cadmium cut-off energy (i.e. the energy where the neutron absorption cross-section of cadmium falls abruptly). It has to be remarked that this limit and the previous classification are not univocally defined and different authors have proposed different boundaries for the two groups [Herwig2009, Knoll2000, Leo1987].

Table I. 1. Neutron classification [Herwig2009]

Neutron classification	Energy (meV)	Velocity (m/s)	$\lambda$ (nm)
Cold	<1	<437	>0,9
Thermal	25	2187	0,18
Epithermal	1000	13832	0,029
Fast	>1000	>14832	<0,029

#### 1.1.4.1 **Slow neutrons**

The interaction of slow neutrons with matter occurs mainly by neutron capture reactions. The cross section of these processes, excluding the effect of resonance peaks, shows a  $\frac{1}{v}$  dependence (being  $v$  the neutron speed), so that at low neutron energies the reactions are the most probable. The most employed elements for the detection of slow neutrons are those allowing, through the (n, $\alpha$ ), (n,p) or (n,t) reactions, to convert neutrons into heavy charged particles that can be promptly detected with almost 100% efficiency. It is also crucial to have a high cross-section, in order to reduce the volume of the detector and increase the efficiency. This explains why  $^3\text{He}$ ,  $^{10}\text{B}$  and  $^6\text{Li}$  are the most used elements for slow neutrons detection. These isotopes have a very high cross section (Figure I. 4) and allow a prompt neutron conversion respectively through the reactions  $^3\text{He}(n,p)^3\text{H}$ ,  $^{10}\text{B}(n,\alpha)^7\text{Li}$  and  $^6\text{Li}(n,\alpha)^3\text{H}$ . Another isotope which is sometimes used for neutron detection is  $^{157}\text{Gd}$ . In this case the reaction doesn't produce heavy charged particles, but gamma rays, through the reaction  $^{157}\text{Gd}(n,\gamma)^{158}\text{Gd}$ . These  $\gamma$ -rays are more difficult to be

detected, but the incredibly high cross section of this reaction, which is almost 100 times higher than the other mentioned reactions (Figure I. 4) can make it convenient in some cases.

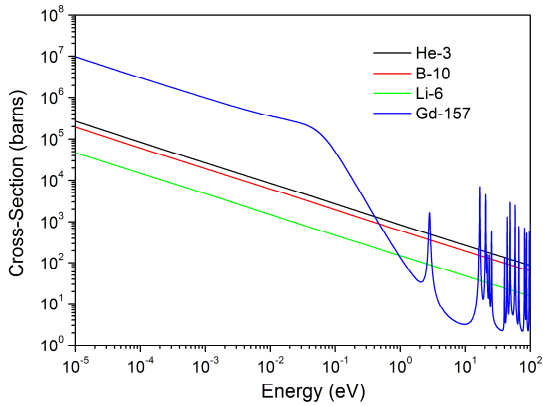


Figure I. 4. Neutron absorption cross-sections for the most used reactions in slow neutron detection [ENDF].

#### 1.1.4.2 Fast neutrons

At high energies, especially over the keV range, the neutron absorption cross section falls and a different process becomes important (Figure I. 5): the elastic neutron scattering. In this type of interaction neutrons transfer part of their energy to the nucleus they collide with. As a consequence this nucleus recoils with energy  $E_R$  while neutrons are slowed down or even stopped.

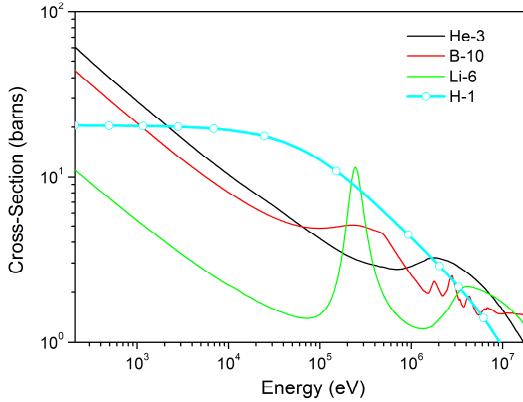


Figure I. 5. Comparison between neutron elastic scattering cross section in hydrogen and the neutron absorption cross section of the most used slow neutron converter in the keV-MeV range.

More in details, the energy of the recoil nucleus can be expressed as:

$$E_R = \frac{2A E_n}{(A+1)^2} (1 - \cos\theta) \quad (7)$$

where  $A$  is the mass number of the recoil nucleus,  $E_n$  is the incoming neutron energy and  $\theta$  is the scattering angle of the neutron in the centre of mass coordinate system. For  $\theta = \pi$ , i.e. for head-on collisions, the recoil nucleus has the maximum energy, equal to:

$$E_{R_{max}} = \frac{4A E_n}{(A+1)^2} \quad (8)$$

It follows straightforwardly that with hydrogen atoms ( $A=1$ )  $E_{R_{max}} = E_n$ , meaning that the neutron transferred all its energy to the nucleus. From these considerations it is clear that the best materials to slow down neutrons and to exploit the energy of the recoil neutrons are light hydrogen rich materials.

For neutrons having  $E_n < 10 \text{ MeV}$  scattering on hydrogen atoms, the angular distribution of the recoil nuclei can be considered as isotropic, and since the energy distribution is strictly correlated to the angular distribution, the energy spectrum can be regarded as a horizontal line with a constant number of counts for energies going from 0 to  $E_n$  (Figure I. 6). This is a special case of particular importance since hydrogen atoms can acquire the highest recoil energy in elastic scattering with neutrons (Eq.8). For this reason, hydrogen rich materials are the most used target for the detection of fast neutrons. This mechanism is also particularly important for this work since it is exploited in liquid and plastic scintillators, including polysiloxane

scintillators, for the detection of fast neutrons, as seen more in details in the next paragraphs.

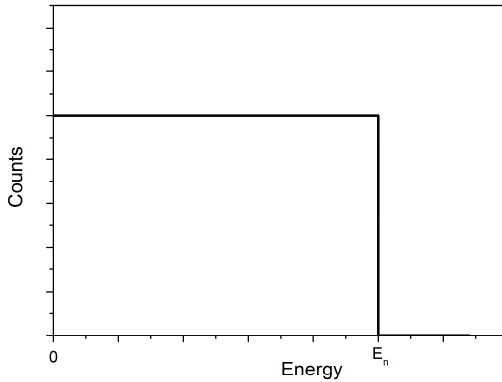


Figure 1.6. Expected energy spectrum of recoil protons produced by scattering on neutrons with energy below 10 MeV on hydrogen atoms.

## 1.2 Scintillation detectors

Scintillation detectors played a major role in many nuclear physics experiments, starting from the famous Rutherford experiment in 1909, when the light pulses were counted by sight [Geiger1909] up to now, in ATLAS and CMS detectors [Seiden2012] when much more advanced photodetectors are employed.

The working principle of scintillating materials is based on the emission of light pulses produced by the excitation and ionization of the material induced by ionizing radiations. These light pulses can be detected and used to achieve information about the particles originating them. At the basis of the scintillation process is the property called luminescence, which is the ability of a certain material to decay from an excited state through the emission of light.

Depending on the type of material used for this application, scintillators are classified as:

- Inorganic scintillators
- Organic scintillators
  - Organic scintillating crystals
  - Liquid scintillators
  - Plastic scintillators

The popularity of scintillating materials is due to their versatility that allows them to be employed both for counting and for spectroscopy, to their fast response,

especially in organic scintillators, to their relatively low cost (plastic and liquids) and, with the partial exception of plastic scintillators, to their capability to distinguish the type of radiation exploiting the Pulse Shape Discrimination (PSD) technique.

Ideally, the characteristics that a scintillator should have are [Knoll2000]:

- High scintillation efficiency
- Linearity between particle energy and light output
- High transparency, especially at the emission wavelength
- Emission wavelength matching the maximum sensitivity of the photodetector
- Fast decay time
- High manufacturability also in large volumes
- High refractive index (close to that of photodetector window)
- Low cost
- Pulse shape discrimination

At present, no material possesses these properties all together and for this reason, several scintillators exist, that are optimized for different specific applications and for the detection of different types of radiation.

### **1.2.1 Inorganic scintillators**

Usually inorganic scintillators are inorganic crystals emitting light due to the presence of impurities or crystallographic defects. Their luminescence therefore is not an intrinsic property of the material itself, but comes from its crystallographic structure. The most used inorganic scintillators are alkali halide crystals, usually doped with heavy metal elements like thallium. Classical examples of this group are NaI(Tl) and CsI(Tl) scintillators, that are two of the most used ones. Many other examples of inorganic scintillators exist, among them it is worth mentioning the very fast BaF<sub>2</sub> and tungstates such as CaWO<sub>4</sub>, the first scintillating material used at the end of nineteenth century [Weber2002], and PbWO<sub>4</sub>, more recently discovered (80s) and massively used in the CMS calorimeter at CERN LHC [Zhu2004] due to its high density and fast decay [Zhang2001]. For neutron detection, crystals based on Li compounds (LiI:Eu, LiBaF<sub>3</sub> and Li<sub>6</sub>Gd(BO<sub>3</sub>)<sub>3</sub>:Ce) have been developed and, more recently, Cs<sub>2</sub>LiYCl<sub>6</sub>:Ce (CLYC) has been employed in both gamma and neutron detection [Smith2013]. The main advantage of inorganic scintillators is given by their high light output, their good linearity, the good energy resolution, the high stopping power, due to their high density, and the high radiation hardness. They have however in many cases the drawback of having a slow decay time and of being highly hygroscopic. Furthermore, the crystal growth technique used to produce them is not trivial and doesn't allow the fabrication of large size crystals. This makes these materials much more expensive than their plastic or liquid counterparts and also more difficult to be produced.

## **1.2.2 Organic scintillators**

Differently from inorganic scintillators, the luminescence of organic scintillators is an intrinsic property of the molecules that constitutes the material, so that it is retained even in vapour state. Scintillation of organic materials is usually given by the emission of light following an electronic transition from the excited state to the ground state of aromatic groups that are the fundamental component of any organic scintillator. The main advantages of organic scintillators are the very fast response, with decay times usually shorter than 10 ns, the possibility to be produced easily and at reasonable prices, even in large size (for plastics and liquids), and the high hydrogen content, that allow them to be used for fast neutron detection. The control of impurities is less stringent than in inorganic crystals, but it is still very important since it is reported that the contamination of some elements, especially oxygen in liquid scintillators [Birks1964, O'Keeffe2011], can lead to quenching effects that reduce the light yield and the time performances of the scintillators. The main drawback of organic scintillators is that the scintillation light yield is usually lower than in their inorganic counterpart, and this is reflected also in a poorer energy resolution. Furthermore they proved to be less radiation hard than their inorganic counterpart, thus limiting their use where low radiation doses are present.

Depending on their physical form, organic scintillators can be mainly divided into three classes: pure crystals, plastic and liquid scintillators.

### **1.2.2.1 Organic crystals**

Organic crystals were the first type of organic scintillators to be used, in 1947, with the discovery of naphthalene crystals [Brooks1979]. Within organic scintillators they are the materials with the highest scintillation efficiency, even if their fragility, the anisotropy that reduces the energy resolution and the difficulty to produce them in large volumes and cut them in the desired shape and size made their use uncommon. The most used organic crystals are anthracene (best light yield), stilbene (pulse shape discrimination) and naphthalene. Anthracene crystals, in particular, remain the reference standard for organic scintillators as regarding the light output.

### **1.2.2.2 Liquid scintillators**

Liquid scintillators are based on a solution of one or more organic dyes inside an organic solvent. If only solvent and one solute are present, the system is called binary scintillator; if two dyes are present, it is a ternary scintillator, and so on. The aim of the dyes is to improve the efficiency of the system and to shift the emission to longer wavelengths in order to reduce self-absorption, improve the spectral matching with the detector and also to increase the radiation hardness [Zorn1990]. The emission of the solvent, in fact, occurs around 290-320 nm, and its quantum

efficiency is too low to be exploited for scintillation. For this reason a highly efficient solute, called primary dye, is dissolved in the base, thus collecting the excitation from the solvent and emitting it with higher efficiency at longer wavelengths. Both solutes and solvents need to have aromatic groups in order to be able to emit light after radiation excitation.

The main advantages of liquid scintillators are their fast response and the very large detection volumes that can be achieved easily and with reasonable costs so that they become the only affordable option in large scale facilities [Araki2005, Zhan2013, Kraus2006]. Furthermore, in order to detect slow neutrons, they can be easily doped with neutron absorbing materials like Gd [Beriguet2014],  $^6\text{Li}$  [Bass2013] and especially  $^{10}\text{B}$  [Birks1964, Swiderski2008], which is at present the most common solution. Liquid scintillators also proved to be fairly radiation hard, harder than plastic scintillators [Zorn1990], since they lack a rigid structure that could be damaged by radiations, leading to yellowing and absorption of dye emission. As mentioned above, a drawback of these scintillators is their strong sensitivity to dissolved oxygen that seems to act as a quencher both for the solvent and for the solute [Seiger1956], [Berlman1961a]. For this reason sealing and deaeration are required in order to achieve the best performances from these materials. Furthermore most efficient and therefore most used liquid scintillators (e.g. xylene and trimethylbenzene) have also some drawbacks due to toxicity, volatility and flammability of the aromatic solvents employed and these concerns become more than an issue when very large volumes of these materials are needed. Therefore, in the last decade, new solvents have been developed with low toxicity and low volatility, e.g. linear alkylbenzene (LAB) [Marrodan2009, Lombardi2013], diisopropyl-naphthalene (DIN) [Lombardi2013] or phenyl-o-xylene (PXE) [Marrodan2009, Back2008].

### **1.2.2.3 Plastic scintillators**

Plastic scintillators are solid solutions where one, two or, in few cases, three different dyes have been dissolved in an organic matrix. Similarly to organic liquid scintillators, the presence of aromatic groups within the matrix is crucial to have an efficient scintillator, and for this reason, the most used materials are polystyrene and most of all polyvinyltoluene. This type of materials can be easily produced, with low cost, and in many shapes and dimensions, so that they represent the only feasible solution whenever a solid, large volume detector is needed. In this case, an important parameter to be considered is the attenuation length, representing the length at which the intensity is decreased by the 63%, mainly due to self-absorption of dye emission. An issue to be considered, especially when operating in harsh environments, is the radiation hardness of plastic scintillators, which is not always very high, since many plastic matrices show a reduction in the transparency due to the creation of radical species during irradiation [Barashkov1996, Busjan1999]. Another aspect that has to be taken in mind when using plastic scintillators based on

polyvinyltoluene or polystyrene is that they are attacked by many common organic solvents such as acetone, toluene, benzene, and they can also undergo crazing, with the formation of a cracks network on the surface that affect the optical quality of the scintillator [Leo1987]. Also plastic scintillators, similarly to liquids, can be easily doped in order to improve the sensitivity to some specific kinds of radiation, the most significant cases are plastic scintillators loaded with heavy elements, mostly lead, for x-rays and  $\gamma$ -rays detection (especially imaging) [Hamel2011b, Koshimizu2015] and boron, lithium or gadolinium loaded scintillators for slow neutron detection [Britvich2005, Normand2002, Breukers2013, Ovechkina2009].

### **1.2.3 Scintillation process in organic scintillators**

When a particle releases its energy in a scintillator, a fraction of this energy is used to excite the molecules of the solvent or the matrix. This excitation is then partially transferred to one or more dyes that are responsible for the emission of light. The overall process is very fast, since it occurs in few nanoseconds, but it is composed of different steps, where several competing processes can occur leading to different non-radiative de-excitation paths. For this reason, only a fraction of the initial particle energy is finally converted to light. This fraction depends on the scintillation efficiency of the material,  $S$  and is usually around 3-4% of the particle energy. Beside  $S$ , other important properties of an organic scintillator are the scintillation emission spectrum, that, in case of plastic and liquid scintillators, depends on the last emitting dye, and is important because it has to match the region of maximum efficiency of the photodetector, but has also influences on other parameters like the attenuation wavelength and the radiation resistance; another crucial property is the scintillation decay time, that depends once again on the characteristic of the dyes and affects the acquisition rate.

In order to understand more in details the working principle of a scintillator, the scintillation process can be conveniently divided into two main parts: a first part, when the particle releases its energy in excitations and ionizations, leading to the excitation of the main constituent of the scintillator (organic crystal, solvent or polymeric matrix); and a second part, when this excitation is transferred, through different steps, at the emitting dye, responsible for the final emission, through the process called fluorescence. Since organic crystals will not be part of this work, only the case of plastic and liquid scintillators will be treated from now on.

#### **1.2.3.1 Ionization and excitation of the matter**

During its passage through the matter, a charged particle loses its energy through electromagnetic interactions with electrons and in few cases with nuclei. This interaction causes the excitation and ionization of the material within a distance of

several molecular diameters from the track, and in case the transferred energy is high enough, secondary electrons (known as  $\delta$  rays) can also be ejected from the atomic orbitals inducing more ionization and excitation further from the path. In such a way, a particle leaves behind a track of excited molecules, radicals, ions, secondary electrons and fragments, whose density depends on the specific energy loss of the particle,  $\frac{dE}{dx}$ .

Since, in plastic and liquid scintillators, exclusively the aromatic molecules in the first excited singlet state,  $S_1$ , can transfer their energy to the fluorophores [King1966], only a small fraction (roughly 3-4%) of the energy released along the path will finally be converted into scintillation light, while the larger part will be used in ionization of the material, excitation of non-fluorescent species or it will be dissipated through non radiative processes like thermal de-excitation and recombination. The latter occurs especially within the track, where a high density of ions and radicals is created, and ionization quenching occurs, reducing the intensity of the emitted light by molecular collisions. This process explains the reason for the lower scintillation light yield of alpha particles in comparison to electrons of the same energy, and accounts for the non-linear behaviour of the scintillation with the radiation energy.

After being excited to higher singlet excited states,  $S_2$  or  $S_3$ , the molecules of the matrix undergo a very fast vibrational relaxation process ( $10^{-11}$  s), called *internal conversion*, to the lowest singlet excited state,  $S_1$ . This process has almost unitary efficiency when occurring in regions of low ionization density, while, in case of high  $\frac{dE}{dx}$ , it is strongly affected by ionization quenching which is acting in the same time scale [Brooks1979, Voltz1966, Fuchs1970].

As mentioned above, in order to produce scintillation light, the molecules need to be in the  $S_1$  state. This state can be populated not only by direct excitation, but also by ions recombination or by a process called triplet annihilation [Laustriat1968], in which two excited triplet states interact to give rise to an excited and a ground singlet state, following the scheme:



These triplet states are mainly formed in ion-electron recombination processes, when triplet and singlet excited states are formed in a 3:1 ratio. Since the excited singlet states coming from triplet annihilation form later, their emission occurs at longer time, giving rise to a slower component in the emission, called delayed fluorescence [King1966]. Furthermore, since triplet annihilation occurs mainly due to ion recombination, which is acting in competition to the ionization quenching process, this delayed component is less sensitive to ionization quenching, and its relative intensity, in comparison to the prompt component, will be more intense the higher is the density of ionized states, thus depending on  $\frac{dE}{dx}$ . This consideration is at the origin of the pulse shape discrimination (PSD) technique, allowing to distinguish different particles on the base of the shape in time of the scintillation pulse [Brooks1979, Laustriat1968].

The relationship between the intensity of the scintillation light emitted per length unit,  $\frac{dL}{dx}$ , and the specific energy loss has been studied in details by many authors. A very popular mathematical formulation of this dependence is the one proposed by Birks [Birks1964]:

$$\frac{dL}{dx} = \frac{S \frac{dE}{dx}}{1 + kB \frac{dE}{dx}} \quad (9)$$

where  $S$  is the scintillation efficiency,  $B \frac{dE}{dx}$  is the density of ionized species, depending on the specific energy loss, and  $k$  is the ionization quenching parameter. An alternative formulation was proposed by Wright [Wright1953]:

$$\frac{dL}{dx} = \frac{A}{2B} \ln \left( 1 + 2B \frac{dE}{dx} \right) \quad (10)$$

Finally a most complicated but most accurate relation was introduced by Voltz et al. [Voltz1966], dividing the contribution to the scintillation intensity in two components, respectively due to the prompt and the delayed emission. This relation seems to fit in a better way the experimental data also for heavy charged particles [Brooks1979]. In the limit of small  $\frac{dE}{dx}$  instead, they all reduce to the linear relation:

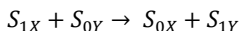
$$\frac{dL}{dx} = S \frac{dE}{dx} \quad (11)$$

that has been experimentally verified for fast electrons.

### 1.2.3.2 Energy transfer

After reaching the first excited singlet state,  $S_1$ , the molecule of the solvent (solid or liquid) can undergo some different processes in order to return to the ground state  $S_0$ . This de-excitation can occur either radiatively, with the emission of a photon, or non-radiatively. In the first case, the photon can be absorbed by another solvent or matrix molecule, in the so called *radiative energy migration* process; in particular, if it is absorbed by a primary dye molecule, the process is called *radiative energy transfer*. Non-radiative decay, instead, can occur by *non-radiative energy migration* to another base molecule, by *non-radiative energy transfer* to a primary dye molecule or by quenching and thermal de-excitation.

The *energy transfer* process in particular is very important, since it is the one allowing the excitation of the dye through the matrix aromatic groups. Indicating X as the matrix or the solvent fluorophore, Y as the primary dye and Z as the secondary dye, the energy transfer process from X to Y can be schematized in the following way:



where  $S_{0X}$  and  $S_{1X}$  represent respectively the ground and excited singlet state of the solvent, and  $S_{0Y}$  and  $S_{1Y}$  are those of the primary dye. In an efficient plastic or liquid scintillator, this process is strongly competing with other de-excitation processes. Especially non-radiative energy transfer is particularly important in the scintillation process, since it is faster and more efficient than the radiative energy transfer, involving the emission and re-absorption of photons and since it allows in some cases also the transfer of triplet excitation energy [Kaschke1988]. The rate of non-radiative transfer increases with the amount of dye and for this reason, in liquid or plastic scintillators, where high primary dye concentrations are typically employed, this mechanism becomes the leading one for the transfer of the solvent or matrix excitation energy. At lower dyes concentrations, instead, the dominant process is the radiative one, since the average molecule distance becomes larger than 3-10 nm usually required for an efficient non-radiative interaction [Lakowicz2006].

From several studies performed on liquid and plastic scintillators, it appears that the energy transfer from solvent or matrix to primary dyes occurs mainly by non-radiative processes, through long range dipole-dipole interactions [Birks1964] between molecules with similar energy levels, and thereafter also called *resonance energy transfer*.

This mechanism has been studied by Förster [Forster1959], so that it is also known as Förster energy transfer. Following his formulation, the energy transfer rate of this process follows the equation:

$$k_T = \frac{1}{\tau_D^0} \left( \frac{R_0}{r} \right)^6 \quad (12)$$

where  $\tau_D^0$  is the donor lifetime in absence of acceptor,  $r$  is the donor-acceptor distance and  $R_0$  is the so called *Förster radius*, representing the donor-acceptor separation at which transfer rate and decay rate ( $= \frac{1}{\tau_D^0}$ ) are equal.

The *Förster radius* can be calculated as:

$$R_0^6 = \frac{9000(\ln 10)\kappa^2\Phi_D^0}{128\pi^5 N_A n^4} \int_0^\infty I_D(\lambda)\epsilon_A(\lambda)\lambda^4 d\lambda \quad (13)$$

where  $\kappa^2$  is an orientation factor and assumes the value of  $\frac{2}{3}$  in case of randomly distributed freely rotating molecules and the value of 0.476 in case of rigid media where the molecules rotation is slower than the de-excitation rate [Valeur2001].  $N_A$  is the Avogadro's number,  $n$  is the refractive index of the medium in the wavelengths region of interest,  $\Phi_D^0$  is the donor quantum yield in the absence of transfer, and the last term represent the overlap integral between donor emission (normalized to  $\int_0^\infty I_D(\lambda) d\lambda = 1$ ) and acceptor molar absorption coefficient ( $\epsilon_A$ ). From this equation it follows that a large overlap between donor emission and acceptor absorption, and high donor efficiency lead to larger values of the *Förster radius* and in turn to higher non-radiative energy transfer rate. For this reason, it is important that the primary dye dissolved in the solvent or scintillator matrix has an absorption

spectrum very well overlapping with the matrix or solvent emission spectrum, together with high quantum efficiency. From Eq.12, it also follows that the transfer rate is inversely proportional to the sixth power of the intermolecular distance between donor and acceptor. This means that this kind of process is much more efficient at high concentrations, when this distance is small, so explaining why the primary dye is usually dissolved in the matrix with concentrations in the order of 1% wt. If the process involves excited triplet states, the transfer mechanism is slightly different: in this case, the only dipole-dipole interaction is not sufficient and the transfer occurs by electron exchange mechanism, occurring at shorter distances since it needs a certain degree of orbital overlap [Forster1959, Valeur2001].

In case of binary systems, the energy transfer from the base to the primary dye is mainly non-radiative, due to the high concentration of the latter. This is especially true in liquid scintillators, where the molecular diffusion contributes to bring the excitation close to the acceptor molecule [Birks1970a], while a certain amount of non-radiative one cannot be excluded in plastic scintillators [Hallam1978]. In any case, after the excitation is transferred to the primary dye, light is emitted through radiative decay by the latter. In case of ternary systems, a further step is required in order to transfer the excitation to the secondary dye. Since this secondary solute is dissolved in the system at much lower concentration, the intermolecular distance between the two dyes is not small enough to allow complete non radiative transfer, and the process partially occurs also via radiative transfer, through the emission of a photon from the primary dye, and its re-absorption by the secondary one [Birks1964, Birks1970a]. At the end of this process the light emission occurs almost entirely from the secondary dye, by radiative de-excitation.

The energy transfer efficiency from primary to secondary dye and especially from matrix or solvent to primary dye is favored by another process, called *energy migration*. It can occur both radiatively and non-radiatively, but in plastic or liquid scintillators, the latter, appears to be the dominant one. This process seems to be driven by short range exchange interactions between adjacent aromatic groups both in liquids and in plastics [Zhang1995, Horrocks1974, Hirayama1968, Mathad1986, Birks1966].

In liquid scintillators, the energy migration is further facilitated also by thermal diffusion of excited molecules that contributes, together with non-radiative processes, to bring the solvent excitation close to the acceptor molecule.

In plastic scintillators, instead, the higher rigidity of the system hinders molecular diffusion and only energy migration based on dipole-dipole or exchange interactions are possible.

## 1.2.4 Luminescence of organic molecules

### 1.2.4.1 *Excited state*

As already mentioned, the property at the basis of the scintillation capability of a certain material is the luminescence, which is the ability to decay from electronic excited states through emission of photons.

Excitation can be induced by several different processes (chemically, mechanically, thermally, electrically,...), but in case of scintillation, the most important processes are photoluminescence, induced by the absorption of photons, and radioluminescence, that is at the base of scintillation and in which the excitation is induced by ionizing radiations.

In case of atomic transitions, since the mass of the nucleus is several orders of magnitude larger than that of the electron, electronic transitions are much faster than the consequent rearrangement of the nuclei, which can thus be considered in a fixed position during the excitation (Franck-Condon principle). After the transition has occurred, the new electronic configuration changes the electric field felt by the nucleus, that begins to oscillate around a new equilibrium position. For this reason, electronic excited states can be divided into different vibrational sublevels having slightly different energies one from each other. Since at the end of the excitation process, the nucleus is not yet in the new equilibrium position, the electronic transition occurs at higher vibrational sublevels. After the transition, the system dissipates the excess energy, bringing the excited electron to lower vibrational sublevels. This non-radiative relaxation is called *internal conversion*. In case of luminescent species, the system cannot completely dissipate the excess energy in a vibrational way, but once the lowest sublevel of the excited state has been reached, the return to the ground state occurs radiatively with the emission of a photon, in a much longer time than the excitation or than the internal conversion. Similarly to the excitation, also the decay follows the Franck-Condon principle, so that, after coming back to the ground state, further vibrational relaxation is needed to reach the lowest vibrational sublevel of the fundamental state (Figure I. 7).

Following this mechanism, the energy needed to excite the molecule, and that emitted in the de-excitation are different, and the absorption of the photon and its emission occur at different wavelength. This difference is called *Stokes Shift*.

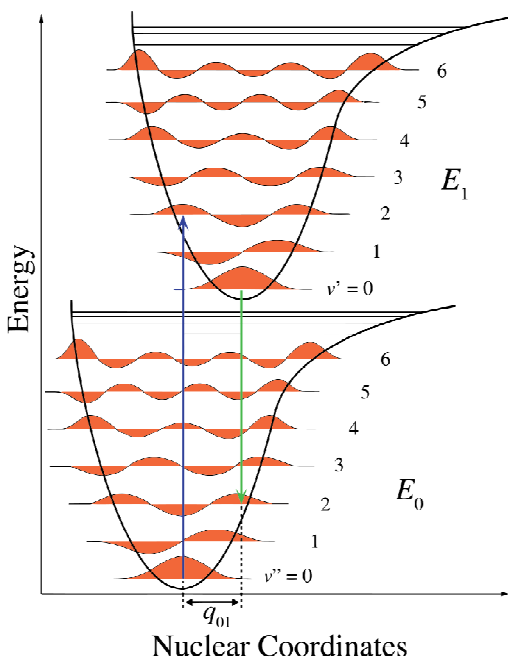


Figure I. 7. Franck-Condon diagram for an electronic transition showing the difference in energy between excitation and de-excitation.

In organic compounds, luminescence is associated to the presence of conjugated molecules, especially aromatics. The presence of unsaturated bonds (with  $sp$  or  $sp^2$  hybridization), allows the electrons to occupy  $\pi$  orbitals. If more  $\pi$  orbitals are present next one each other, they form a delocalized system whose excited state is responsible for luminescence ( $\pi \rightarrow \pi^*$  transition).

#### 1.2.4.2 Radiative decay

Luminescence can be divided into two main radiative processes: fluorescence and phosphorescence. The former is the decay from an excited singlet state ( $S_1$ ) to a ground singlet state ( $S_0$ ),  $S_1 \rightarrow S_0$ , where the electron in the excited state and its counterpart in the ground state have antiparallel spin. This is an allowed transition and therefore it occurs efficiently and quickly ( $10^{-8}$  to  $10^{-9}$  s) with the emission of a photon.

Phosphorescence instead is the decay from an excited triplet state ( $T_1$ ) to a ground singlet state ( $S_0$ ). The triplet state  $T_1$  has slightly smaller energy than the corresponding singlet state  $S_1$ , and is characterized by excited and ground state electrons having parallel spin. Triplet states can be populated by ion recombination,

as explained in the previous section (1.2.4.1) or from the excited singlet state, by a non radiative process called *inter-system crossing*. The transition  $T_1 \rightarrow S_0$  is forbidden by selection rules and the emission of photons occurs then slowly ( $10^{-3}$ -1 s) and less efficiently.

There is also a third kind of radiative emission, called delayed fluorescence and already mentioned earlier. In this process, lasting for a period of  $10^{-7}$ - $10^{-3}$  s, the decay from the excited triplet state to the ground singlet state doesn't occur directly, but through the interaction with another molecule in the same excited triplet state. The result of this interaction is the formation of an excited and a ground singlet state,  $T_1 + T_1 \rightarrow S_1 + S_0$ .  $S_1$  decays by fluorescence but, due to time needed for the triplet state interaction to occur, the photon is emitted at delayed times.

The most important parameters needed to characterize a fluorescent molecule are the lifetime ( $\tau$ ) and the quantum efficiency ( $q$ ). The former describes the time evolution of the intensity of the light emitted by the fluorophore, and usually follows an exponential decay.

$$I(t) = I_0 e^{-\frac{t}{\tau}} \quad (14)$$

If the emission is the sum of different component, or in case also delayed fluorescence occurs, the decay can be multi-exponential, presenting two or more different decay time constants.

$$I(t) = A e^{-\frac{t}{\tau_1}} + B e^{-\frac{t}{\tau_2}} \quad (15)$$

The quantum efficiency instead is the ratio between the emitted photons and the absorbed ones, and can be expressed as:

$$q = \frac{k_f}{k_f + k_{nr}} \quad (16)$$

where  $k_f$  is the radiative emission rate and  $k_{nr}$  is the non radiative one that can be due to phenomena like quenching, inter-system crossing or energy transfer.

### 1.3 Neutron detection

The most important characteristics for a neutron detector are: high efficiency, good time resolution, efficient neutron/gamma discrimination, good neutron energy resolution and good pulse height resolution [Harvey1979]. No neutron detector can however fulfil all these requirements at once, and for this reason, different applications requires different detectors, depending on the specific need (e.g. neutron counting, neutron spectroscopy, neutron imaging), on the neutron energy range (fast or slow) and on the specific conditions (high gamma background, required volume, ...).

As already explained in the section 1.1.4, different detection mechanism has to be exploited depending if the aim is the detection of fast or slow neutrons.

Fast neutron detection generally occurs in three different possible ways. A first technique is to exploit neutron moderation, using water, heavy water, paraffin or polyethylene, in order to slow neutrons down to thermal energies and detect them using neutron induced nuclear reactions, as seen in the previous paragraph. This is the case of one of the most used neutron detector, called *Bonner Sphere*. A second possible strategy is to exploit neutron induced reactions that have a relatively high cross section to the desired energies, similarly to what has been seen for slow neutrons. At these higher energies however the cross section is usually much lower than for slow neutrons. Typical exploited reactions are  ${}^3\text{He}(n,p){}^3\text{H}$  and  ${}^6\text{Li}(n,\alpha){}^3\text{H}$  that show a resonance peak in the MeV range. A third type of detector, which is probably the most common one in this field, directly detects the recoil nuclei produced in the elastic interactions. This technique has the advantage that the energy of the recoil nuclei is somehow dependent from the neutron energy, and thus it allows to perform neutron energy spectroscopy, not possible in the other types of detector.

Table I. 2. Main characteristics of most used slow neutron absorbers.

Converter	$\sigma$ (25 meV) [barns]	Reaction products	Q-value
${}^3\text{He}$	5353	H (0.573 MeV), $\alpha$ (0.191 MeV)	0.764 MeV
${}^{10}\text{B}$	3870	$\alpha$ (1.47 MeV), ${}^7\text{Li}$ (0.84 MeV) $\alpha$ (1.78 MeV), ${}^7\text{Li}$ (1.01 MeV)	2.31 MeV (94%) 2.79 MeV (6%)
${}^6\text{Li}$	945	$\alpha$ (2.05 MeV), ${}^3\text{H}$ (2.73 MeV)	4.78 MeV
${}^{157}\text{Gd}$	256000	Several products with energies below 100 keV	-

As regarding thermal neutron detection, it usually relies on the neutron capture reaction described above. The neutron converter and the reaction products however can be detected in several different ways depending on the application. The main types of slow neutron detectors are gas detectors, scintillator detectors and solid state detectors. Gas detectors can be filled by a neutron converting gas ( ${}^3\text{He}$  or enriched  $\text{BF}_3$ ). The products of the neutron capture reaction ionize the gas itself, and the so formed ions are accelerated causing further ionization before being collected at the electrodes. A slightly different version of gas detectors is represented by boron lined counters, where the neutron conversion is not performed by the gas, but by a thin layer of enriched boron deposited on the wall of the gas container. The reaction products of the boron capture reaction are responsible for the gas ionization that is collected by the electrodes in the same way as before [Knoll2000].

A different type of thermal neutron detectors is represented by solid state detectors where a thin layer of converter (usually enriched B or enriched  $\text{B}_4\text{C}$ , but also  $\text{LiF}$ ) is

deposited over a microstructured solid state detector, that allows to detect the reaction products coming from the converter [Herwig2009, McGregor2009, Mendicino2014]. Finally, thermal neutron detection can also be efficiently fulfilled by scintillators, as treated below.

### 1.3.1 Scintillators for neutron detection

Table I. 3. Main properties of EJ-301 and EJ-309 liquid scintillators and EJ-299-33 plastic scintillators, all of them with PSD capability.

Properties	EJ-301	EJ-309	EJ-299-33
Type of scintillator	PSD liquid	PSD Liquid Low Toxicity	PSD plastic
Light Output [% anthracene]	78	75	56
Photon yield [ph/MeVee]	12000	11500	8600
$\lambda_{em}$ [nm]	425	424	420
H atoms [ $10^{22}$ cm $^{-3}$ ]	4.8	4.37	5.13
C atoms [ $10^{22}$ cm $^{-3}$ ]	4.0	5.46	4.86
Electrons [ $10^{23}$ cm $^{-3}$ ]	2.3	3.17	3.55
Density [g/cm $^3$ ]	0.874	0.964	1.08
Fast Decay Time [ns]	3.2	3.5	5
Long Decay Times [ns]	32.3; 270	n. a.	140; 150
FoM (th. 100 keVee)	2.2 (3"x3")	1.9 (2"x2")	1.5 (2"x2")

Organic scintillators are widely used as neutron detectors because of their versatility and their suitability to produce large detectors volumes, relatively easily and at reasonable prices. Organic liquid and plastic scintillators are mostly composed by hydrogen and carbon atoms and for this reason they are able to detect fast neutrons, exploiting the neutron recoil reaction. So far, the most employed materials in this field have been organic liquid scintillators, because the possibility to easily produce very large scintillator volumes allows for good detection efficiency that would not be achievable with organic crystals like stilbene or anthracene. But most of all, the success of liquid scintillators is due to their capability to perform pulse shape discrimination (PSD), which is a key aspect for neutron detection since it allows to

distinguish neutrons from the gamma background [Brooks1979]. In this respect, the best liquid scintillators, and still the most used is the xylene based EJ-301 (or its equivalent BC-501A or NE-213). These liquids have the drawback of toxicity, flammability and volatility, requiring sealing and consequently reducing the handiness of the system. To overcome this issue, non toxic solvents were tested [Chang2015, Joyce2012, OKeefe2011, Bentoumi2013], and a new low toxicity, low volatility liquid scintillator with PSD capability entered recently the market [EJ-309ds] (Table I. 3).

The ultimate solution to these problems however would be the replacement of liquid scintillators with plastic scintillators having the same performances. This would allow detecting fast neutrons in an easier way, also combining in the same device charged particles detection.

For this reason, recently, strong efforts have been put in the development of plastic scintillators capable of PSD [Bertrand2015, Zaitseva2012], but the suitability and stability of these new products is still under investigation [Cester2014] and for this reason, at the moment, plastic scintillators are employed as fast neutron detection only in the few cases when gamma discrimination is not a concern because of relatively low background or because other discrimination techniques, e.g. time of flight (ToF), can be applied [Agosteo2016]. In order to produce PSD plastics, different strategies have been employed so far: composite scintillators, addition of triplet harvesting materials and increase of the triplet-triplet interaction.

The first method consists of inserting organic crystal, capable of PSD in transparent inert matrix [Tarasenko2013], with the drawback of low scintillation light output due to light scattering by crystals. The second smart method consists of the addition to the organic matrix of triplet harvesting dyes, emitting at different wavelength and with a longer lifetime, allowing a combination of spectral discrimination and pulse shape discrimination [Feng2012], but with the drawback of a much longer time response, in the order of  $\mu\text{s}$ , typical of triplet harvesting organometallic compounds.

Finally, the most used technique so far employed to enhance PSD capability of plastic scintillation has been the strong increase of the primary dye concentration, in order to favor the dye molecules interaction and in turn increase the triplet-triplet interaction probability. The first attempt was reported by Brooks in 1960 [Brooks1960], and other followed until very recently [Zaitseva2012, VanLoef2014]. Even if his technique seems to be the most promising and it also brought to the commercialization of EJ-299-33 plastic scintillator, the performances reached so far are still lower than liquids [Cester2014, Pozzi2013], and the scintillators seems to have problems related to the long term stability of the high dye concentrations (up to 30 wt%) dissolved in the matrix [Bertrand2015].

Organic scintillators find applications also in the field of slow neutron detection thanks to the ease of doping them with Li, B or Gd containing compounds, as already mentioned in previous sections. On the market, several different formulation exist of plastic scintillators doped with boron concentration up to 10%, e.g. BC-454

[BC-454ds] or EJ-254 [EJ-254ds] or liquid scintillators doped with Gd [EJ-331ds, BC-521ds] or  $^{10}\text{B}$  (EJ-339A, BC-523A). The main issue in this case is to find the most suitable compound in order to achieve the highest solubility without affecting the performances. In case of boron containing mixtures, the most used molecules are carboranes [Pawelczak 2014], boric acid [Britvich2001] and other metallorganic compounds [Bollinger1957]. In case of lithium, Li-methacrylate [Breukers2013], lithium salts [Bass2013] and more complex metallorganic compounds [Zaitseva2013] have been successfully employed. Finally, gadolinium has been incorporated in organic systems, by using different aromatic and non-aromatic metallorganic complexes [Ovechina2009, Bariguete2014]. All these systems have some advantages and disadvantages. Boron is at the moment the most used solution because it has a quite high abundance of  $^{10}\text{B}$  in the natural mixture and thus, in most cases, enrichment is not needed, with great cost saving. It is also a well known and documented element, and the high cross-section allows achieving very good efficiencies. On the other side, the energy released by the reaction products is not so high in comparison to other possible elements. Furthermore, enrichment is not so easy, and in case enriched boron is needed the price of the system is strongly increasing. Finally, some problems have been encountered with the toxicity of boron compounds and also with their volatility that is reducing the long term stability of the scintillator. Lithium instead has the advantage of a higher energy produced during the neutron capture reaction, increasing the scintillation light yield and also allowing for a better pulse height discrimination. From the chemical point of view, Li compounds are easier to produce, but despite these advantages, the hygroscopicity of most Li compounds and most of all, the lower cross-section are intrinsic limits of this element, hindering its diffusion. Finally, gadolinium is one of the elements with the highest thermal neutron cross-section. Unfortunately, the doping of organic materials with Gd complexes is not straightforward. Furthermore, its reaction products are mainly low energy x-rays and  $\gamma$ -rays that due to their long range can also escape from the material without being detected, cannot be easily distinguished from the background, and doesn't allow good neutron-gamma discrimination.

The main advantage of organic scintillator in the field of thermal neutron detectors is represented by their fast response, which is in some cases orders of magnitude faster than other scintillators. In terms of efficiency and scintillation light output, instead, their performances are lower than inorganic scintillators, which are, at the moment, the most common scintillating system. In this field, in the last years, there have been a large number of newly developed crystals, based on Li, B, Gd or a combination of them. Not all of them entered the market, but some of them proved to be very interesting materials.

Differently from organic materials, where the most used converter is  $^{10}\text{B}$ , in case of inorganic scintillators, the most used element is by far  $^6\text{Li}$ . The first materials to be developed in this group were  $^6\text{Li}$ -glass(Ce),  $^6\text{Li}$ (Eu) and  $\text{ZnS}^6\text{LiF}$ , with the latter

having the highest light output, but being limited to thin slabs due to low transparency.

In the last decade, a new class of compounds have been developed, with very interesting properties. This class of materials, called elpasolites, has composition  $A_2LiMX_6:Ce$ , ( $A=Cs, Rb, M=Y, La, Sc, X=Br, Cl, I$ ) (see [Van\_Eijk2012] and references therein), and has been developed after the discovery of the interesting properties of  $Cs_2^6LiYCl_6:Ce$  (CLYC) scintillators. Are part of this class  $Cs_2^6LiYBr_6:Ce$  (CLYB),  $Cs_2^6LiLaCl_6:Ce$  (CLLC),  $Cs_2^6LiLaBr_6:Ce$  (CLLB), all of them showing very high light output, but also having the drawback of strong hygroscopicity.

Table I. 4. Comparison between the most used inorganic scintillators for thermal neutron detection. Properties of boron doped plastics and liquids are also reported.

Scintillator	Density [g/cm <sup>3</sup> ]	Neutron Light yield [ph]	Gamma Light yield [ph/MeV]	$\tau_f$ [ns]	PSD
$^6LiF/ZnS$	2.6	160 000	75 000	>1000	Yes
$^6LiI:Eu$	4.1	50 000	12 000	1400	No
$^6Li$ -glass:Ce	2.5	6000	4000	75	Yes
$Cs_2^6LiYCl_6:Ce$ (CLYC)	3.3	70 000	22 000	1000	Yes
$Cs_2^6LiYBr_6:Ce$ (CLYB)	4.1	90 000	24 000	1000	Yes
$Cs_2^6LiLaCl_6:Ce$ (CLLC)		110 000	35 000	1000	Yes
$Cs_2^6LiLaBr_6:Ce$ (CLLB)		180 000	60 000	>270	Yes
$^6LiBaF_3:Ce$	5.3	3500	5000	1; 34; 2100	Yes
$^6Li_6Gd(BO_3)_3:Ce$	3.5	40000	14000	200; 800	No
Organic Plastic	$\approx 1$	$\approx 650$	8600	$\approx 2$	No
Organic Liquid	$\approx 0.9$	$\approx 900$	10000	$\approx 3$	Yes

# Chapter II

## Materials and methods

### 2.1 Polysiloxanes

The scintillators produced and studied in this work, liquid or plastic, are made by materials belonging to the category of polysiloxanes, commonly known also as silicones. These polymers are composed by a main backbone, formed by silicon and oxygen atoms, regularly alternated, and by organic substituents, attached to the silicon atoms of the main chain. Many of the optical and chemical properties of the material depend on the type and distribution of these substituents. Furthermore, in case of rigid polysiloxane, is the reaction between side groups that allows the formation of intermolecular bonds (cross-linking) conferring to the polysiloxane, mechanical properties typical of elastomeric materials.

#### 2.1.1 Properties of polysiloxanes

The main difference between polysiloxanes and other common organic polymers, including polyvinyltoluene (PVT) and polystyrene (PS) usually used for plastic scintillators, is the composition of the main chain, where the usual C-C bonds are replaced by the stronger Si-O bonds, having a bond energy of 445 kJ/mol against 346 kJ/mol for C-C bonds [Tiwari2014]. This difference is the reason for the very high chemical and thermal stability (the operating temperature can range in some cases from -100 °C up to over 300°C [Polymer\_Ency]). Furthermore silicones have high flexibility and T<sub>g</sub> as low as -125 °C for poly(dimethylsiloxane) (PDMS) that rises to -30 °C for poly(methyl-phenylsiloxane) (PMPS), as a consequence of the increased rigidity due to the presence of phenyl substituents [Mark2005]. These properties are related to the length of the Si-O bond (1.64 Å), longer than the C-C bond (1.53 Å), to the regular succession of substituted silicon and non substituted oxygen, to large Si-O-Si bond angle (143°, against 110° for the standard tetrahedral structure) and to the low torsional barrier, that confers high chain mobility to the material. The higher free volume connected with these properties allows much higher dye mobility in comparison to polystyrene or epoxy resins [Chu1990]. The low T<sub>g</sub> value, is important in our case because it hinders the occurring of *crazing*, that strongly reduces the transparency of the material. This phenomenon is instead a problem for standard plastic scintillators, based on the more rigid PVT or PS, having a T<sub>g</sub> as high as 90°C. Beside all these interesting properties another very important reason for choosing polysiloxane matrixes, or solvents, is the radiation hardness of this material. In standard plastic scintillators, radiation breaks C-H or C-C bonds, producing free radicals that cause the yellowing of the material, and the consequent light yield reduction. This process occurs at higher radiation doses in polysiloxanes, due to

their stronger bonds. This resistance is further increased by the presence of phenyl side groups that absorb part of the radiation energy thanks to the  $\pi$  electrons in the aromatic ring, thus reducing the damages along the polymeric chain. Another advantage of polysiloxanes over standard organic materials is given by higher electron density along the main chain, due to the presence of the unpaired couples on the oxygen atom. This confers an higher electron mobility along the chain, thus allowing to increase the energy migration distance and to extend the protective effect of the phenyl groups over several monomeric units, differently from what occurring in PVT and PS [Koike1960]. In this respect, several data can be found in literature, reporting the superior performances of polysiloxane in terms of radiation hardness. [Quaranta2013, Bowen1989a, Quaranta2010a].

The addition of phenyl moieties to the polysiloxane chain gives to the material some more interesting properties, from a scintillator point of view. First of all it confers to the material an intrinsic fluorescence, crucial for scintillation, whose emission depends on the distribution and concentration of phenyl groups. If they are further one from each other than two monomeric units, the interaction with neighbours is hindered, and the emission, coming from the single monomeric unit, is centred at about 290 nm. If instead they are closer, the emission occurs at 320 nm, and is the typical emission coming from excimers [Itoh2001]: excited state dimers temporary formed from the interaction of an excited state phenyl group with a ground state one [Birks1967]. In any case, these compounds are characterized by the strong absorption of the aromatic moieties, occurring at 260 nm (Figure II. 1). The presence of aromatic groups allows also increasing the refractive index of the material to values close to glass and quartz. This is an important aspect, because it improves the optical matching with cuvettes and photodetector windows, thus reducing reflection light losses.

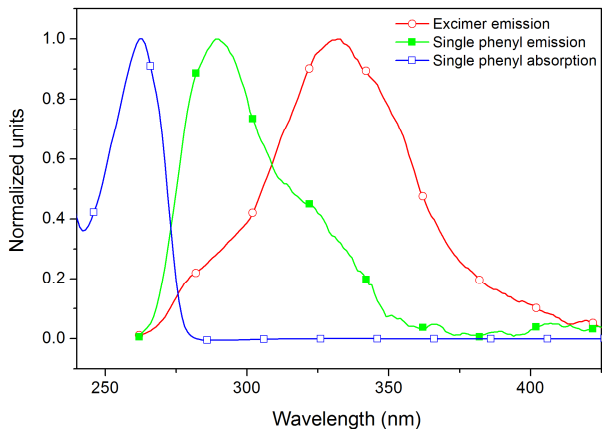


Figure II. 1. Comparison between absorption spectrum, single phenyl emission and excimer emission for phenyl substituted polysiloxane materials.

As regarding the mechanical properties of the materials, in case of plastic scintillators, the presence of the phenyl groups increases the rigidity of the material and therefore also its fragility. From the chemical point of view, instead, the presence of the aromatic moieties increases the dye solubility in the material. This is a very important issue because, low dye solubility can lead to aggregations that strongly reduce the efficiency of the fluorophore and in turn the light output of the scintillator. For this reason, in the cases when high dye concentrations need to be added, also a high phenyl concentration is needed, at the price of a higher fragility of the material.

### 2.1.2 Polysiloxane plastic scintillating materials

Within the large variety of polysiloxane resin, a good candidate to be chosen as scintillator matrix needs to be highly transparent in order to minimize light losses, it needs to have aromatic side groups along the main chain, in order to allow for scintillation, it needs to be homogeneous and with reasonable mechanical properties, in order to allow an easy handling of the samples. Furthermore, the starting components need to have a low enough viscosity in order to allow the complete mixing of the dyes, but also a long enough pot life to allow the complete removal of gases and bubbles that could originate inhomogeneities and light scattering. On the market a wide range of different possible alternatives is available, having different phenyl group concentration and distribution, different viscosity of the starting material and different cross-linking reactions.

The development of polysiloxane scintillators began almost 20 years ago, by Bowen and co-workers [Bowen1989a, Bowen1989b]. These works reported for this material

superior radiation hardness, showing no yellowing with doses up to 10 Mrad, far beyond the limit observed for typical PS or PVT based scintillators with scintillation light outputs ranging from less than 5% to 90% of a commercial reference sample (BC-408). The same group performed an extensive series of studies on the radiation hardness of polysiloxane scintillators doped with different types of primary dye, [Feygelman1990a], [Walker1989], secondary dyes [Feygelman1990b] and different phenyl concentrations [Harmon1991]. More than ten years later, Bell and co-workers exploited these interesting properties for the production of polysiloxane scintillators for thermal neutron detection, through the loading with boron or gadolinium [Bell2002], [Bell2004].

More recently, due to interesting properties of these materials, together with their low toxicity and low flammability of precursors, interest for polysiloxane scintillators was renewed. A deep analysis was performed focusing on the optimization of the scintillation performances of the materials, by varying the matrix composition, the mixture concentration and composition [Quaranta2010a], [Quaranta2010b], [Quaranta2013] by studying thermal neutron detection with the addition of o-carboranes at different concentrations [Quaranta2011] and fast neutron detection by TOF discrimination technique [Carturan2011].

On these basis, for the present work, two different materials have been chosen depending on the application: when dye concentrations up to 4% had to be dissolved, the chosen solution was poly(dimethylsiloxane-co-diphenylsiloxane) with 22-25mol% of diphenylsiloxane monomers (22PDPS) (Figure II. 2). This material was chosen for its higher scintillation light yield [Quaranta2010b]. When higher primary dye concentration needed to be added to the material, higher amount of phenyl groups was necessary and the chosen matrix was poly(methylphenylsiloxane) (100PMPS) (Figure II. 3), having poorer performances, but allowing a better solubility.

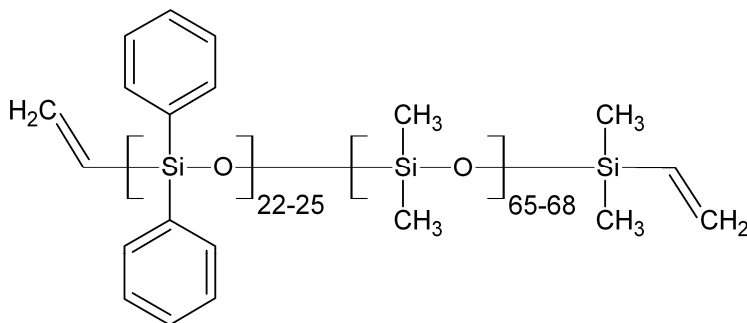


Figure II. 2. Molecular structure of poly(dimethylsiloxane-co-diphenylsiloxane) vinyl terminated.

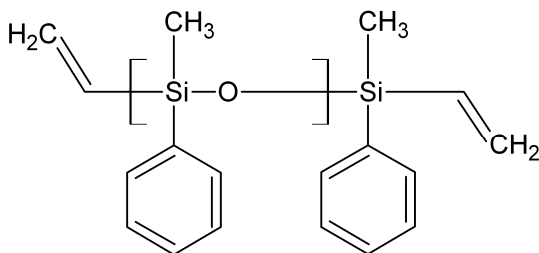


Figure II. 3. Molecular structure of poly(methylphenylsiloxane) vinyl terminated.

In order to be more formally correct, it is finally necessary to give a clarification about the classification of these materials as “polysiloxane plastic scintillators”. Even if the term “plastic” has become a synonym of polymers in common language, from the scientific point of view, polysiloxanes are not plastic materials, but elastomeric materials. Nevertheless, within this work, these materials are classified as “polysiloxane plastic scintillators” due to the strong similarities with other “plastic scintillators”. The scintillation process, the production technique (dissolution of dyes in a rigid matrix), the field of application of polysiloxane plastic scintillators is indeed very similar to traditional plastic scintillators, that are the real competitors of these materials, and that for this reason are also used as standard reference for the evaluation of their performances.

### 2.1.2.1 *Cross-linking reactions*

There are several possible cross-linking reactions that occur with the formation of an intermolecular network, and the consequent passage from a viscous material to an elastomeric matrix. These reactions can occur spontaneously after the exposure to atmospheric conditions as in the case of mono-component resins, or they can begin only after the addition of a second component, as in the case of bi-component resins. The reactions of interest for the present application are of two main types: condensation cure and addition cure.

Condensation cure is the most widely used type of reaction for commercial silicone. It is employed both with mono- and bi-component resins having hydroxide side groups (silanol) and other hydrolysable terminations. In presence of the atmospheric moisture, these groups react with the silanol group of other polymeric chains leading to the formation of cross-links (Figure II. 4). In all cases, by-products are formed in this process, that depends on the type of hydrolysable group and need to be removed from the material. Depending on the reaction occurring, it can be classified as alcoxy condensation, acetoxy condensation, amine condensation, and many others. The formation of by-products is one of the main problems for a possible use as scintillators, since, especially for bulk samples, they are difficult to be removed

and lead to the formation of pores and bubbles that reduce the transparency of the material.

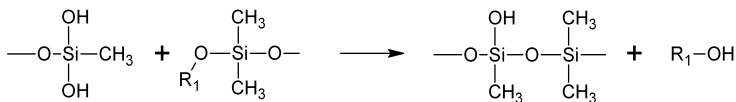


Figure II. 4. Schematic representation of the condensation cross-linking reaction, with formation of volatile by-products.

Another type of cross-linking reaction is represented by the addition cure. It relies on platinum catalyzed vinyl addition, also called hydrosilylation reaction, occurring from a terminal vinyl group and a hydrogen moiety of two different polymeric chains. The process is exploited in bi-component resins, with addition of platinum, in form of metallorganic complex, as catalyst. During this reaction no by-product is formed allowing for a good dimensional stability and a high transparency, since the formation of pores and bubbles is avoided. For this reason, this is the most used solution whenever very good optical properties are needed, and it is also the type of cross-linking exploited in this work. Some problems however may arise from the presence of the metallorganic compound that could absorb light and so reduce the transparency of the material. Therefore it is very important that no exceeding amount of platinum is added to the resin. The vinyl addition reaction is a type of room temperature vulcanization (RTV), but it can be much faster if it is carried at about 50°C-60°C. In order to further improve the optical properties, a cure moderator can be added to the starting mixture, allowing extend the pot life of the mixture to perform the complete deaeration of the material before the occurrence of cross-linking.

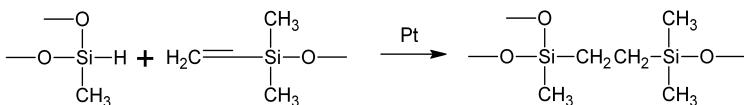


Figure II. 5. Schematic representation of platinum catalyzed vinyl addition.

A standard recipe for the preparation of a polysiloxane sample using this method consists of a certain amount of vinyl terminated polysiloxane (A part) with the addition of hydride terminated polyhydrosiloxane (B part), a cure moderator and a platinum complex, whose relative concentrations depend on the type of polysiloxane. There are several possible platinum compounds and cure moderators, with different performances and optimized for different materials and various production methods. For the purposes of this work, the moderator employed is 1,3,5,7-Tetravinyl-1,3,5,7-Tetramethyl-cyclotetrasiloxane, while Platinum-Divinyl-tetramethyl-disiloxane

complex in xylene has been used as catalyst. All the reagents used for this activity were purchased from ABCR GmbH.

### 2.1.3 Polysiloxane liquid scintillating materials

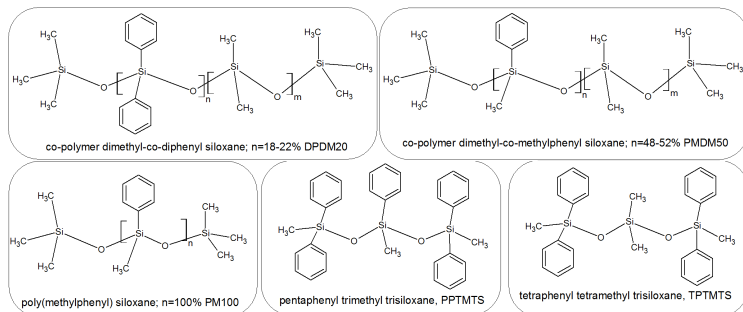


Figure II. 6. Molecular structure of the different polysiloxane liquids used in this work.

Polysiloxane liquids used in this work belong to a wide group of materials, having a polysiloxane main chain, with phenyl and/or methyl substituents attached to the silicon atoms and no reactive functional group, since no cross-linking reaction is desired. They have very different chain length, ranging from a minimum of 3 siloxane units up to more than 20, and consequently different molecular weights and viscosities. Also the concentration and the distribution of phenyl groups is not the same between molecules, and as it will be shown later, this is influencing the optical properties and so the scintillation response. Despite this differences, all this materials have some very interesting characteristic, as low toxicity, excellent chemical and thermal stability, good transparency, very low volatility (vapour pressure smaller than  $10^{-6}$  bar), high flash point (higher than  $220\text{ }^{\circ}\text{C}$ ).

A list of the liquid polysiloxanes used for this thesis, and their main physical properties is listed in Table II. 1, while Table II. 2 shows the HMIS codes (Hazardous Material Identification System) reported in the Materials Safety Data Sheet (MSDS) of each fluid, indicating the health hazard, the flammability and the physical hazard in a degree from 0 (lower) to 4 (higher) for every compound. It can be observed that no specific risk for health or environment is derived by the use of these materials. For comparison, HMIS indexes of EJ-301 and EJ-309 are also reported. All the liquids polysiloxanes used in this work were purchased from ABCR GmbH.

Table II. 1. Main properties of the polysiloxane liquids used in this work.

<b>Chemical name</b>	<b>Label</b>	<b><math>\eta</math> [cSt]</b>	<b><math>\delta</math> [g/ml]</b>	<b>MW</b>	<b>Phenyl [mol/l]</b>	<b>n</b>
18-22%-diphenyl-co-dimethylsiloxane	DPDM20	160	1.05	2000	3.9	1.49
48-52%-phenylmethylsiloxane-co-dimethylsiloxane	PMDM50	125	1.07	2100	4.7	1.5
Phenylmethylsiloxane	PM100	500	1.11	2600	7.6	1.53
1,1,5,5-tetraphenyl-1,3,3,5-tetramethyltrisiloxane	TPTMTS	38	1.07	485	8.8	1.55
1,1,3,5,5-pentaphenyl-1,3,5-trimethyltrisiloxane	PPTMTS	175	1.09	547	10	1.58

Table II. 2. HMIS index and cas number for the materials used in this work, as reported in the Materials Safety Data Sheet (MSDS). EJ-301 is also shown for comparison.

<b>Material</b>	<b>MSDS HMIS code</b>	<b>cas number</b>
DPDM20	1,1,0	68083-14-7
PMDM50	1,1,0	63148-52-7
PM100	1,1,0	9005-12-3
TPTMTS	1,1,0	3982-82-9
PPTMTS	1,1,0	3390-61-2
EJ-301	2,3,0	n. a.
EJ-309	1,1,0	n. a.

## 2.2 Dyes

In order to be used for scintillation, a dye needs to have some fundamental characteristics:

- Efficiency needs to be the closest possible to unity.
- High radiation resistance.
- High chemical stability, no reaction with matrix or solvent materials, with other dyes or with other elements in the operation environment, since these reactions could reduce the efficiency of the dye, or increase the absorption of the material.
- High solubility in the matrix or solvent.

Furthermore, in order to choose the proper dye for a certain system, it is extremely important to have a good overlap between base emission and primary dye absorption, between primary dye emission and secondary dye absorption and, in case of quaternary scintillators, between secondary dye emission and ternary dye absorption. This allows for an optimal energy transfer, crucial for good scintillation efficiency, as explained in the previous chapter.

Not all the organic dyes commercially available can satisfy the above requirements. In particular, radiation resistance is an issue for many organic substances, and also the solubility is not always possible in the required quantities. Among the dyes with the desired performances, 2,5-diphenyloxazole (PPO) and BASF Lumogen F series dyes [Lumogen] resulted to be very good candidates to be used in polysiloxane scintillators. The former is already largely employed in many liquid and plastic scintillators [Birks1964, Brooks1979, Lombardi2013] the latter have been specifically developed to be used as dyes for photovoltaic applications.

### 2.2.1 2,5-Diphenyloxazole (PPO)

2,5-Diphenyloxazole (PPO) (Figure II. 7) has been used as dye for liquid and plastic scintillator for a long time. Its use arises from the need to overcome the solubility of other common dyes, as p-terphenyl. Generally, the substitution of a phenyl group with an oxazole or oxadiazole group greatly increases the solubility of a linear aromatic chain, without affecting its quantum efficiency [Birks1964]. Furthermore, beside the high efficiency (close to 1) and the very good solubility also in polysiloxane, this dye shows also good radiation hardness [Quaranta2010c]. The excitation spectrum, centred at about 300 nm (Figure II. 8), is well matching the emission of the polysiloxane base, thus allowing a good energy transfer from the matrix or solvent to the primary dye. The PPO used in this work was scintillation grade 2,5-diphenyloxazole purchased from Fluka.

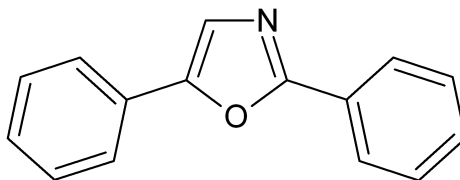


Figure II. 7. Molecular structure of the molecule 2,5-diphenyloxazole (PPO).

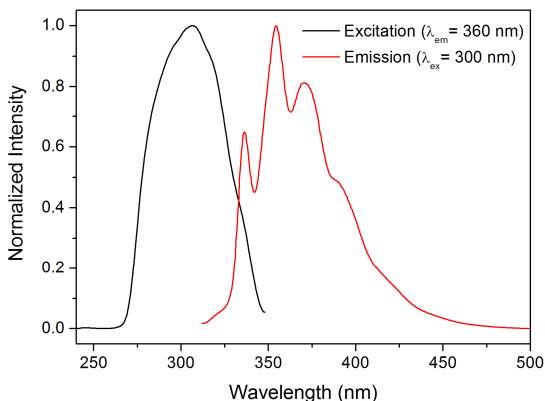


Figure II. 8. Excitation and emission spectrum of the PPO molecule in chloroform.

### 2.2.2 Lumogen Violet

BASF Lumogen F Violet 570 (LV) is the secondary dye used in this work. As already mentioned, originally it was employed as dye in photovoltaic applications. It has good efficiency, close to 85% [BASF\_LV] and it has been already reported to be a very promising secondary solute in plastic scintillators, in combination with PPO [Carturan2011, Hamel2008]. This molecule belongs to the family of 1,8-Naphthalimides (Figure II. 9 left) and has an emission peak centred at 430 nm and an excitation spectrum very well overlapping with the PPO emission (Figure II. 9 right).

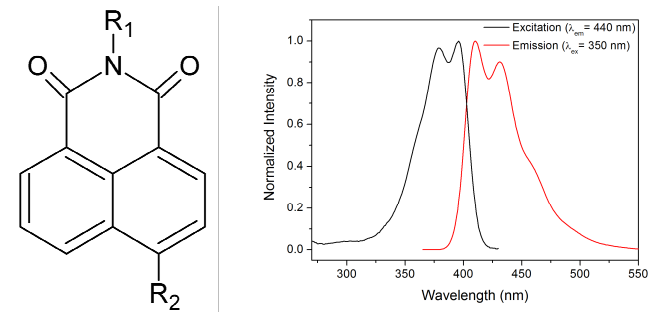


Figure II. 9. (Left) Generic molecular structure of 1,8-Naphthalimide. The substituents R1 and R2 are patented for the LV molecule. (Right) Emission and excitation spectra of the LV molecule in chloroform.

### 2.2.3 Lumogen Red

In the case of quaternary scintillator, a third dye has to be added to the solution. In this work, in order to produce a red emitting polysiloxane material, the chosen dye was BASF Lumogen Red F 305 (LR). This dye belongs to the perylendiimide family (Figure II. 10) and it also has been developed for solar energy applications. It has very high efficiency (over 90% [BASF\_LR]) and very good solubility in many media including polysiloxane. Furthermore, this dye has a good stability, crucial also for solar applications [Baumberg2001] and a good radiation resistance [Keivanidis2008]. All these characteristics, together with long emission wavelength, at 610 nm, make this dye suitable to be employed as wavelength shifter in plastic scintillators. Its absorption spectrum, even if having its maximum at 570 nm, shows a secondary peak at 450 nm (Figure II. 11), well matching the emission of LV, and thus being suitable to be excited by the secondary dye used in this work (Figure II. 12).

Both LR and LV dyes used for this thesis were kindly offered by Colorflex (Mannheim, Germany).

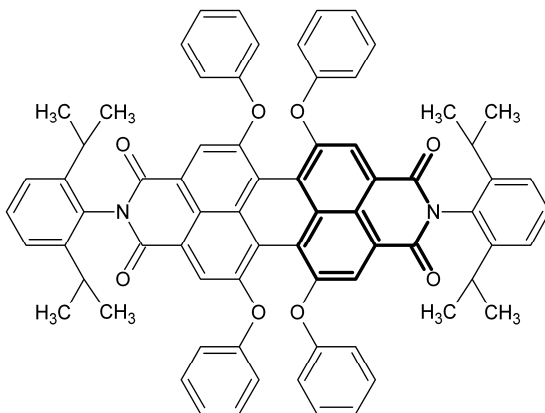


Figure II. 10. Molecular structure of the LR molecule [Balaban2014].

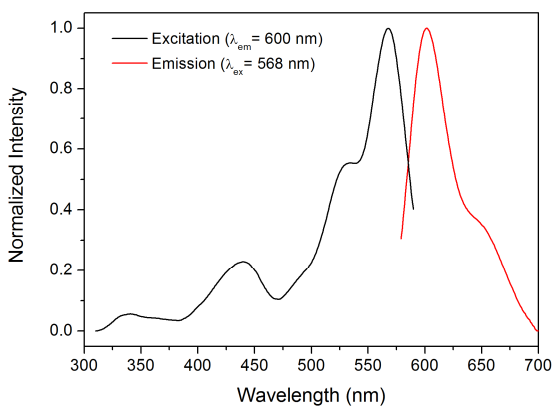


Figure II. 11. LR emission and excitation spectra in acetone.

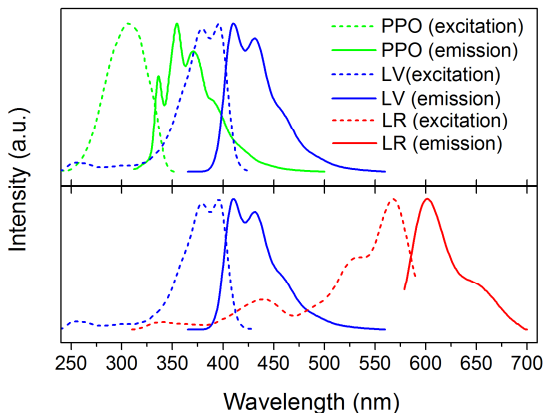


Figure II. 12. Overlap between the different dyes emission and excitation spectra.

## 2.3 Samples preparation

### 2.3.1 Polysiloxane plastic scintillators

The production of polysiloxane plastic scintillators occurs through different steps. A first step is represented by the dissolution of the desired amount of dyes in the A resin, by stirring the mixtures for some hours at about 50 °C. It is worth to note that all concentrations reported in this work refers to weight percentage of dye with respect to the only A component. Following this step, the remaining components of the polysiloxane material (Pt complex, cure moderator and B part) are added in the proper quantities, depending on the type of A resin employed, and the resulting mixture is stirred for some more minutes at room temperature. After this, the mixture is poured in the mould having the desired dimensions and the samples are degassed in low vacuum, in order to remove gas and bubbles produced during the stirring process and to reduce the concentration of dissolved oxygen that could reduce the efficiency of the scintillation process [Birks1964]. After the deaeration the mould are put in an oven overnight at 60°C to accelerate the cross-linking reaction. The so produced samples have 2 cm or 3 cm diameters and a thickness of 1 mm for the larger samples and 3 mm to 7 mm for the smaller ones. In the following tables, the specific recipes for the two different resins employed are reported. All the samples having diameter 3 cm are made by 22PDPS polysiloxane, while the smaller one are produced using both resins.

Table II. 3. Typical formulation of 22PDPS based polysiloxane matrix.

Component	Chemical name	Quantity
A part	Poly(22-25mol% diphenylsiloxane-co-dimethylsiloxane) vinyl terminated	1 g
B part (cross-linker)	Poly(45-50mol% methylhydrosiloxane-co-methylphenylsiloxane) hydride terminated	74,8 $\mu$ l
Cure moderator	1,3,5,7-Tetravinyl-1,3,5,7-Tetramethyl-cyclotetrasiloxane	5 $\mu$ l
Catalyst	Platinum-Divinyltetramethyldisiloxane complex in xylene	0.8 $\mu$ l

Table II. 4. Typical formulation of 100PMPS based polysiloxane matrix.

Component	Chemical name	Quantity
A part	Poly(phenylmethylsiloxane) vinyl terminated	1 g
B part (cross-linker)	Poly(45-50mol% methylhydrosiloxane-co-methylphenylsiloxane) hydride terminated	0.15 g
Cure moderator	1,3,5,7-Tetravinyl-1,3,5,7-Tetramethyl-cyclotetrasiloxane	5 $\mu$ l
Catalyst	Platinum-Divinyltetramethyldisiloxane complex in xylene	1 $\mu$ l

### 2.3.2 Polysiloxane liquid scintillators

In case of polysiloxane liquid scintillators, no chemical reaction is occurring during the preparation of the samples. The steps for the production of solutions however are similar to those employed for plastic scintillators: after the addition of the dyes to the polysiloxane liquid, the mixtures are stirred at 60°C for some hours in order to allow their complete dissolution. The solutions are then deaerated in low vacuum for the removal of bubbles and dissolved oxygen. After this step the liquid is poured in the quartz cuvette used for the measurement, before a final quick further deaeration step, needed to remove the gases introduced in the cuvette during the pouring.

## **2.4 Characterization techniques**

### **2.4.1 Optical measurements**

Both liquid and plastic scintillators have been optically characterized before their test with radiations. Optical measurements involved UV-Vis spectroscopy, steady state fluorescence spectroscopy and time resolved fluorescence spectroscopy.

#### **2.4.1.1 UV-Vis spectroscopy**

Absorption measurements have been performed by using a Jasco V-570 double beam spectrophotometer, equipped with a deuterium lamp, covering the range from 190 nm to 350 nm, and a halogen lamp, covering the range 330 nm- 2500nm. Direct absorption measurements have been performed in case of solid sample, while in case of liquid mixtures, the solutions have been analyzed in quartz cuvettes having 10 mm optical path. A special cuvette, with reduced 2 mm optical path has been instead employed to measure the absorption spectrum of the undoped polysiloxane liquids in tetrahydrofuran (THF) solution, in order to reduce saturation effects due to the strong absorption in the UV range of the materials.

#### **2.4.1.2 Steady state fluorescence spectroscopy**

Steady state fluorescence measurements have been performed using a Jasco FP-6300 spectrofluorometer, equipped with Xe lamp. The fluorescence emission and excitation spectra for plastic samples have been measured both in front-face and in transmission geometry (Figure II. 13). The first type of measurements allows to reduce the distortions due to inner filter effects in the samples, the latter is a configuration similar to the scintillation measurements, and allows to understand the effect of self absorptions in the scintillation process.

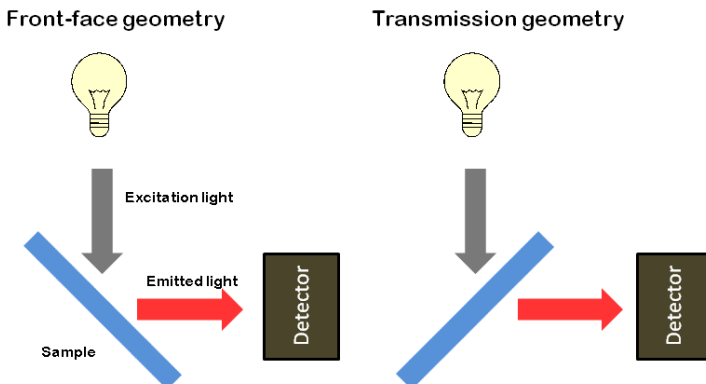


Figure II. 13. Schematic representation of the front-face and transmission geometry employed in the fluorescence measurements of solid samples.

Fluorescence measurements on liquid samples have been performed in right angle geometry, using 10 mm optical path quartz cuvette. Also in this case, the analysis of the undoped polysiloxane liquids has been performed using a 2 mm optical path cuvette in front face geometry, in order to reduce the distortions coming from the strong absorption of the phenyl groups in the UV range, and for the same reason, measurements have been done on 1 g/l diluted THF solutions. All spectra are presented as recorded, without any correction for the instrumental response, with the exception of the spectra reported in the chapter regarding red emitting scintillators. In that case, since the emission of the sample was occurring also above 600 nm, a correction for the spectrofluorometer response curve was needed, and therefore, all the spectra showing red emitting samples have been previously corrected.

#### 2.4.1.3 *Fluorescence lifetime measurements*

Time resolved spectrofluorimetry has been performed at the Fluorescence Lab of the University of Verona, Department of Computer Science. The used instrument is a Horiba® Nanolog spectrofluorometer, and exciting the samples with 280 nm and 375 nm pulsed Horiba LED (pulse width smaller than 1.2 ns). The fitting of the decay, was performed directly by the instrument software, and the reported uncertainties are the fitting errors given by the software itself. The measurements are performed using a quartz cuvette with 10 mm optical path in right angle geometry.

The employed fitting function is a multi-exponential decay where the rise time is modelled as an exponential function with negative pre-exponential term.

$$I(t) = Ae^{-\frac{t}{\tau_A}} - De^{-\frac{t}{\tau_D}} \quad (17)$$

Where  $\tau_A^0$  is the decay time of the acceptor (LV in this case), whereas  $\tau_D$  is the one of the donor (PPO in this case) in presence of energy transfer and represents the rise time of the system [Birks1968, Valeur2001].

In some cases, it has been necessary to introduce a further exponential term, according the equation

$$I(t) = Ae^{-\frac{t}{\tau_1}} + Be^{-\frac{t}{\tau_2}} - De^{-\frac{t}{\tau_R}} \quad (18)$$

Being  $\tau_R$  the rise time and  $\tau_1, \tau_2$  the decay times of the system. In that case, the fractional intensity of the fast and slow components was calculated as [Valeur2001]:

$$A\% = \frac{A \tau_1}{A \tau_1 + B \tau_2} \cdot 100 \quad (19)$$

$$B\% = \frac{B \tau_2}{A \tau_1 + B \tau_2} \cdot 100 \quad (20)$$

## 2.4.2 Scintillation light yield measurements

### 2.4.2.1 Plastic scintillators

Table II. 5. Main characteristics of the photodetectors used for this work.

Detector	Hamamatsu R1450	Hamamatsu R2228	RMD S0814
Sensitivity range [nm]	300-650	300-900	400-1050
Maximum sensitivity [nm]	420	600	950
Applied Voltage [V]	-1500	-1200	+1810
Gain	1.7 10 <sup>6</sup>	7.5 10 <sup>5</sup>	10 <sup>3</sup>

The scintillation performances of polysiloxane plastic scintillators have been tested with alpha particles and  $\gamma$ -rays. For the characterization with  $\alpha$  particles,  $^{241}\text{Am}$  a source (5.486 MeV) has been used, while  $^{60}\text{Co}$  (activity 370 kBq, energy 1.17 MeV and 1.33 MeV) and  $^{137}\text{Cs}$  (activity 370 kBq, 0.662 MeV) sources have been used for  $\gamma$  rays. Depending from the sample, tests have been performed using as photodetector either a Hamamatsu R2228 red enhanced photomultiplier tube (PMT), a RMD S0814 avalanche photodiode (APD) or a fast response Hamamatsu R1450 PMT, all of them fed by Ortec 556H High-Voltage Power Supply, with voltages reported in (Table II. 4).

The red enhanced PMT and the APD, having higher efficiency at longer wavelength were used to test red emitting polysiloxane scintillators. In all cases, the scintillator was placed directly in contact with the detector window, with no need for optical grease since the polysiloxane was perfectly adhering on the detector surface, and the addition of optical couplant was not improving the performances of the apparatus (Figure II. 14). This can be regarded as a further advantage of polysiloxane scintillators, since, as visible in Figure II. 15, the same is not true for standard plastic scintillators.

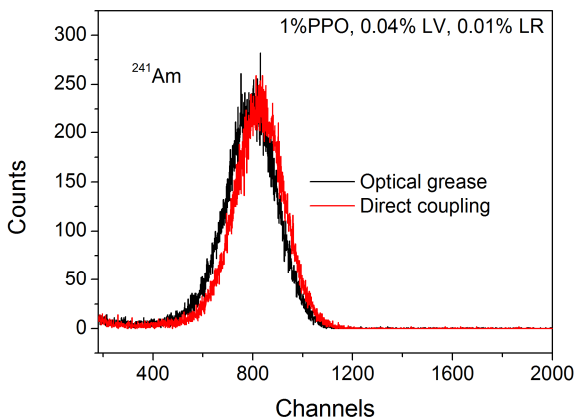


Figure II. 14. Comparison of a  $^{241}\text{Am}$  scintillation spectrum collected by a polysiloxane scintillator with or without optical couplant.

The system was then wrapped on the front face with 10  $\mu\text{m}$  aluminated Mylar tape, and on the sides with white Teflon tape, with the aim of reducing the scintillation light losses without stopping the  $\alpha$  particles. In order to minimize the ambient light during the measurement, the system was placed in a completely darkened scattering chamber. When performing  $\alpha$  particle tests, the source was placed directly in contact with the sample, while in case of  $\gamma$  measurements, the sources were kept at about 1 cm from the scintillator. In case of red emitting materials, in order to evaluate the contribution coming from the red part of the visible spectrum, some measurements were also performed using a 515 nm long-pass filter (Thorlabs), interposed between the scintillator and the PMT window. In this case, the optical coupling between the detector and the filter was guaranteed by the application of a droplet of A resin between the two components.

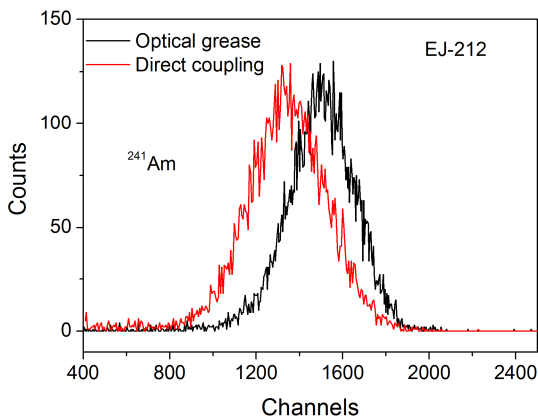


Figure II. 15. Comparison of a  $^{241}\text{Am}$  scintillation spectrum collected by EJ-212 plastic scintillator with or without optical couplant.

Signals from the PMTs have been directly amplified by a Canberra 2021 Spectroscopy Amplifier, with a shaping time of  $0.25\ \mu\text{s}$  and a gain of 30. When using the APD instead, a preamplification stage was added before sending the signal to the amplifier, the preamplifier having a gain of  $45\ \text{mV/MeV}$ . The Spectroscopy Amplifier produces Gaussian signals having amplitude proportional to the integral of the scintillation pulse. The signal is then converted by an analog to digital converter (ADC) and a channel, proportional to the Gaussian amplitude, is assigned to each signal. In this way the scintillation spectrum is recorded as a histogram showing the number of counts for each channel, the higher is the intensity of the scintillation pulse, the higher is the channels number of the signal.

In order to compare different materials the scintillation yields were evaluated in terms of relative light output in comparison to EJ-212 (Eljen Technology) commercial plastic scintillator with the same dimensions of the tested samples. In case of alpha particles, the relative light yield has been evaluated by comparing the positions of the centroids of the peaks in the scintillation spectra. In case of gamma rays, this evaluation is not so straightforward, since the scintillation spectrum is not a single Gaussian peak. In this case, the scintillation light yield has been calculated from the position of the so called Compton edge, and in case of thin samples, when this was also not clearly distinguishable, from the position of the Compton end point.

#### 2.4.2.2 Liquid scintillators

The scintillation yield of polysiloxane liquid scintillators have been evaluated with gamma rays from  $^{60}\text{Co}$  and  $^{137}\text{Cs}$  (and also  $^{22}\text{Na}$  in some cases) sources and

compared with a commercial EJ-309 (Eljen Technology) low toxicity liquid scintillator.  $^{60}\text{Co}$  and  $^{137}\text{Cs}$  sources were the same used also for the characterization of plastic scintillators, while for liquid scintillators also  $^{22}\text{Na}$  source has been used in some cases, emitting  $\gamma$ -rays at two different energies, 511 keV and 1277 MeV. The scintillating solutions have been tested in cylindrical quartz cells (Hellma Optics) with 50 mm optical path and 25 mm diameter flat parallel faces, using a Hamamatsu R1450 PMT as photodetector. The optical coupling between the PMT window and the cell face has been achieved using silicon based optical grease (Dow Corning). The quartz cuvette has been wrapped in white Teflon tape in order to minimize light losses, and the  $\gamma$  source was placed in front of the cell, at a distance of 1 cm from the other face of the cylindrical vessel Figure II. 14.

The electronic chain employed for the measurements is the same described in the previous section, with the only difference that the bias of the PMT was set in this case to -1300 V and the Spectroscopy Amplifier is a Canberra 2024. Also in this case the relative scintillation yields have been evaluated on the base of the position of the Compton edge in scintillation spectra, calculated through the fitting of the Compton peak with a Gaussian function. For each sample, tests were repeated several times in order to optimize the light collection and to acquire enough data to allow a determination of the spread in the results. This spread resulted to be around 10%, in well agreement with literature data [Haas2008].

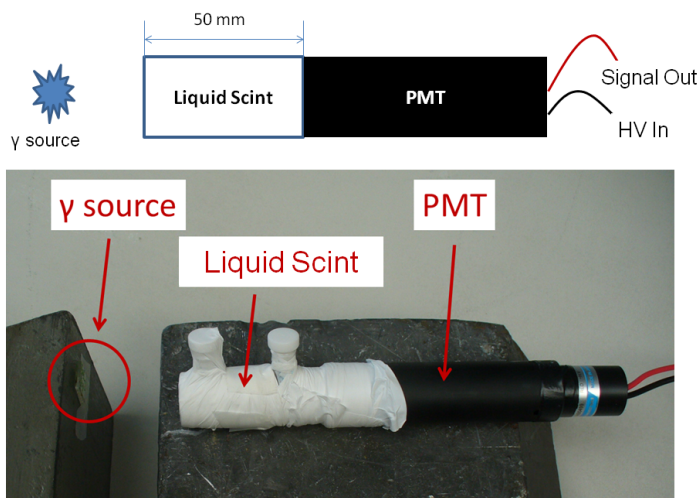


Figure II. 16. Schematic representation and picture of the measurement geometry.

### 2.4.3 Pulse shape analysis

Pulse shapes of polysiloxane liquids were analysed using a pulsed neutron beam at the "CN" Van de Graaff accelerator at the INFN-Legnaro National Laboratories. The neutron flux was produced exploiting the  ${}^7\text{Li}(p,n){}^7\text{Be}$  reaction produced by the collision of 4 MeV protons on a LiF target, with the emission of 2.32 MeV neutrons in forward direction. The pulsed proton beam had a repetition rate of 3 MHz, with 2 ns width pulses.

The quartz cells containing the scintillators were mounted on the PMTs as described in the previous section, and the assemblies were placed at a distance of 60 cm from the target, in forward direction. With this configuration, the neutron flux at the samples was of the order of  $10^2$  neutrons  $\text{cm}^{-2} \text{s}^{-1}$ . Every single pulse produced by the PMT was recorded directly by 250 MS/s, 12 bit CAEN V1720 digitizer, and the single waveforms were analyzed offline. Time of Flight (ToF) discrimination technique was used in order to distinguish the signals produced by neutrons to the signals coming from gamma rays, also produced during the  ${}^7\text{Li}(p,n){}^7\text{Be}$  reaction. With this aim, the signal coming from an inductive pickup placed immediately before the LiF target was also collected and used as time reference.

In the post-processing the average pulse shapes produced by neutrons and gammas were obtained by summing up all the normalized pulses, labelled as neutrons or gammas using the ToF technique and with the zero position on the timescale corresponding to the position of the maximum. The waveforms were fitted using the OriginPro 8.5 software. The reported errors for the fitting parameters are the sum of the fitting errors given by the software itself and an estimation of the uncertainties of the experimental setup, whose main contribution comes from the PMT transit time spread (0.76 ns at the FWHM).

Also in this case the curves were fitted with a multi-exponential decay, but in this case, the introduction of a second decay term was always necessary in order to achieve a good fitting, and the employed fitting function was therefore always in according to Eq. 18, Eq. 19 and Eq. 20.

#### 2.4.3.1 Pulse shape discrimination

Pulse shape discrimination performances of polysiloxane liquids were evaluated by using the so called *charge comparison method*, described for the first time by Brooks [Brooks1959] and still largely used with liquids [Pawelczak2013, Comrie2015, Luo2014, Söderström2008] and even plastic scintillators [Pozzi2013]. In this method, every pulse is integrated over two different periods, a fast one, including the first part of the decay, and a second longer one, integrating the slower part. The ratio between these values depends on the shape of the scintillation signal, and allows to distinguish the events produced by different particles. In this work, the fast interval was set from -8 ns to 50 ns, while the slow integral was calculated from 50 ns to 800

ns. After obtaining these two values, a PSD value was assigned to each pulse, calculated as:

$$PSD = \frac{10 \cdot \text{slow integral}}{\text{fast integral} + \text{slow integral}} \quad (21)$$

And a PSD frequency distribution was consequently derived for each set of data, typically showing two Gaussian-like peaks, corresponding to neutrons and gammas signals. From these histograms, the so called *figure of merit*, FoM, has been derived, allowing to compare the pulse shape discrimination capability of different scintillating mixtures. The FoM is conventionally defined as [Annand1987]:

$$FoM = \frac{\langle n \rangle - \langle \gamma \rangle}{FWHM_n + FWHM_\gamma} \quad (22)$$

Where  $\langle n \rangle$  and  $\langle \gamma \rangle$  are respectively the centroids of neutron and gamma distributions, and  $FWHM_n$  and  $FWHM_\gamma$ , their full width at half maximum.

Following this procedure, the FoM was derived for different energies, after dividing the pulses in 200 keVee bins, on the basis of the pulse amplitude, and after calibration of the scintillator with  $\gamma$ -rays. The calibration was performed assigning to each channel the energy of the electrons producing a signal with the corresponding amplitude, and for this reason, the energy scale used for in the graphs is electron equivalent keV (keVee).

#### 2.4.4 Time resolved ion beam induced luminescence (TRIBIL)

Time resolved ion beam induced luminescence measurements were performed at the INFN-LABEC laboratory in Sesto Fiorentino. These measurements allow to record the signal emitted by the samples when irradiated with a pulsed ion beam. For the measurements, 10 MeV  $C^{3+}$ , 10 MeV  $O^{3+}$  and 3 MeV  $H^+$  ions were used.

The light emitted from the samples was collected by Hamamatsu R3478 fast PMT, biased with -1700 V, and the signal from the PMT was directly acquired by a 250 MS/s CAEN V1720 digitizer. The pulsed beam had a frequency of 20 Hz, with 4 ns pulses. Acquisition from the PMT was set in coincidence with the beam pulses, using as a time reference the signal of the beam deflector. Also TRIBIL pulses were fitted using Eq. 18, Eq. 19 and Eq. 20 in order to compare the signals produced by different ions on different samples.

Measurements were performed in high vacuum, placing both samples and PMT in the measurement chamber at about  $10^{-7}$  bar.

# Chapter III

## Polysiloxane liquid scintillators

*Part of this chapter has been published in:*

M. Dalla Palma, S. M. Carturan, M. Degerlier, T. Marchi, M. Cinausero, F. Gramegna, A. Quaranta

**“Non-toxic liquid scintillators with high light output based on phenyl-substituted siloxanes”**,

*Opt. Mater*, Vol. 42 (2015) pag. 111-117.

### 3.1 Introduction

As already mentioned in the first chapter, liquid scintillators are widely used in many applications, ranging from nuclear physics [Leo1987] to homeland security [Joyce2012], materials analysis [Vartsky2003], medicine [Kirov2005] and fusion science [Kaschuck2000]. In large-scale scientific facilities, liquid scintillators are largely employed, and will be even more used in future experiments, in extremely large volumes (Table III. 1) [Bellini2013, Araki2005, Zhan2013, Kraus2006, Wurm2012]. The choice of liquid scintillators is unavoidable in these cases since they represent the only reasonable possibility to achieve extremely large detection volumes with good efficiency, and relatively low costs. Furthermore, as it will be extensively treated in the next chapter, they are the preferred solution in fast neutron detection whenever neutron-gamma discrimination is needed, thanks to their superior PSD capability.

Table III. 1. Volumes of liquid scintillators employed in some important large-scale facilities (foreseen or in operation).

Experiment	Liquid scintillator volume [l]
Borexino (LNGS)	300 000
Daya Bay (CN)	320 000
SNO+ (CAN)	800 000
KamLAND (JP)	1 000 000

There are however some drawbacks in the use of these materials. Most efficient and most used liquid scintillators present indeed problems connected with their toxicity, their flammability, their volatility and with their high sensitivity to oxygen. These issues are mainly due to the aromatic solvents used in the scintillating mixtures (e.g.

xylene), and for his reason in the last years, much work was done on the investigation of the scintillation performances of new aromatic solvents [Chang2015, Joyce2012, OKeefe2011, Bentoumi2013]. Thanks to these new researches on the topic, new interesting scintillation solvents were discovered, having lower toxicity and lower volatility. Among the number of these new scintillators, it is worth to mention LAB (linear alkyl benzene) [Marrodan2009, Lombardi2013], di-isopropilnaphthalene (DIN) [Lombardi2013] or phenyl-o-xylylene (PXE) [Marrodan2009, Back2008], all of them having a lower volatility (lower than  $10^{-2}$  torr) and higher flash point (above  $140^{\circ}\text{C}$ ) than the traditional aromatic solvents. In this framework, also commercial liquid scintillators are following the need for less harmful materials, with the new EJ-309 liquid scintillator, characterized by low toxicity, high flash point, good light yield and good PSD performances [EJ-309ds, Enqvist2013, Tomanin2014], even if without reaching the performances of xylene based EJ-301 or the equivalent BC-501A [Pawelczak2013, Stevanato2012].

The improved characteristics of PXE or LAB based scintillators are the reason for their use in new large-scale facilities like Double Chooz [Aberle2012] and SNO+ [Kraus2006] and in future large scale detectors [Oberauer2013].

Polysiloxane liquids could also play a role in this research for new, less hazardous solvent, given their very good chemical stability, their excellent thermal stability, very low toxicity, low flammability, low volatility (lower than  $10^{-4}$  torr at room temperature) and high flash point (more than  $200^{\circ}\text{C}$ ) [GelestMSDS]. There is an extremely large variety of possible polysiloxane liquid scintillators, having different content and distribution of phenyl groups, different molecular weight, and different viscosity. This chapter reports the analysis of several liquid polysiloxanes, with the aim of finding the best solvent in terms of optical properties and light output.

### **3.2 Experimental part**

In order to compare the performances of different polysiloxane liquids as solvents for liquid scintillators, 1 wt% PPO and 0.02 wt% LV were added to all solvents (see Chapter II for solvents structure and properties). The mixtures were then tested by UV-Vis spectroscopy and by fluorescence spectroscopy in order to analyze the optical properties and to evaluate the differences in energy transfer between solvent and dyes and between different dyes. The pure solvents were also analysed with the same techniques, in order to determine the differences in the photophysical properties and to correlate them with the molecular structure. Aiming at reducing the self-absorption effects, the measurements were performed in a reduced optical path (2mm) quartz cuvette and the materials were diluted in tetrahydrofuran (THF) in 1g/l concentration; furthermore, fluorescence measurements were performed in front face geometry. The dilution of 1g/l was chosen as the one allowing the best compromise between maximum intensity and minimum inner filter effect. This is clear when

looking at Figure III. 1: when increasing the dilution factor, from undiluted material to 1 g/l the intensity is strongly reducing, but the shape of the spectrum is also changing, the component at lower wavelength becoming increasingly more important due to the reduction of the self-absorption in that region.

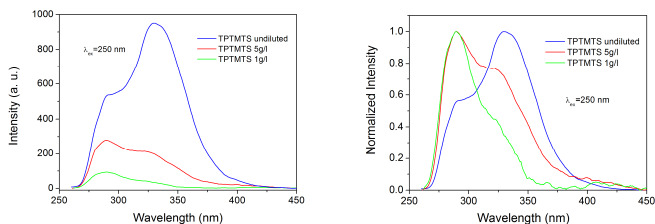


Figure III. 1. Comparison between the emission spectra of TPTMTS in THF solution at different dilutions. Spectra are shown with (right) and without (left) normalization.

Scintillation yields of the samples were measured using  $^{60}\text{Co}$  and  $^{137}\text{Cs}$  gamma sources, relatively to EJ-309. The position of the Compton edge was used for the comparison of the different samples, and in order to have a precise estimation of this position, the last part of the spectrum was fitted with a Gaussian function (Figure III. 2).

A detailed description of the experimental setup is reported in the Chapter II.

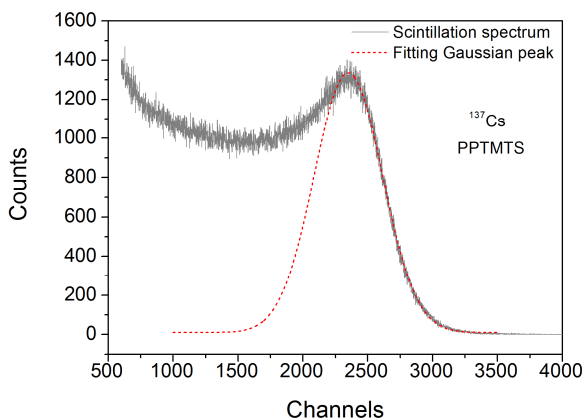


Figure III. 2. Typical  $^{137}\text{Cs}$  scintillation spectrum, with the fitting function used to evaluate the position of the Compton Edge.

### 3.3 Optical properties of polysiloxane liquids

#### 3.3.1 Absorption spectra

##### 3.3.1.1 Absorption spectra of polysiloxane liquids

A first characterization of polysiloxane liquids involved the analysis of their optical absorption, performed in diluted solutions in order to distinguish the shape of the absorption spectra and avoid saturation effects. This analysis allowed to have a confirmation of the phenyl content and to ensure that no other strongly absorbing contaminant was present in the material, causing a possible reduction of the final light output. In Figure III. 3, the absorption spectra of the diluted solutions are shown. It has to be noted that no absorption peak occurs above 300 nm, in the region where PPO and LV emits, meaning that all these materials are suitable for hosting the fluorophores in liquid scintillating cocktails. As regarding the absorption peak at 260 nm, it is important to observe that the peak position is the same for all liquids. This peak corresponds to the  $\pi \rightarrow \pi^*$  transition of the phenyl rings [Itoh2001, Horta1991], and its intensity therefore depends on the amount of phenyl rings in the solution. A confirmation of this can be found in Figure III. 4, showing the linear correlation existing between the peak absorbance at 260 nm and the content of phenyl moieties in the material. The large error bars on the figure are due to the difficulty in measuring precisely small quantities of undiluted resins, due to their viscosity. This results on errors larger than 10% in the solution concentrations that affect also the absorption measurements. This estimation was obtained by repeated measurement on different nominally identical samples.

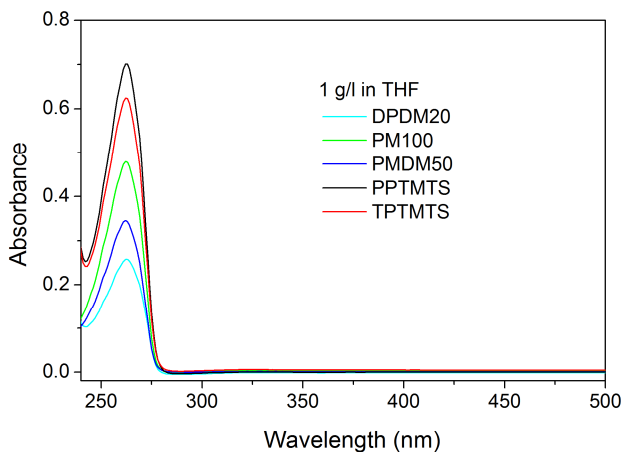


Figure III. 3. Absorption spectra of 1 g/l diluted solutions of different polysiloxane liquids.

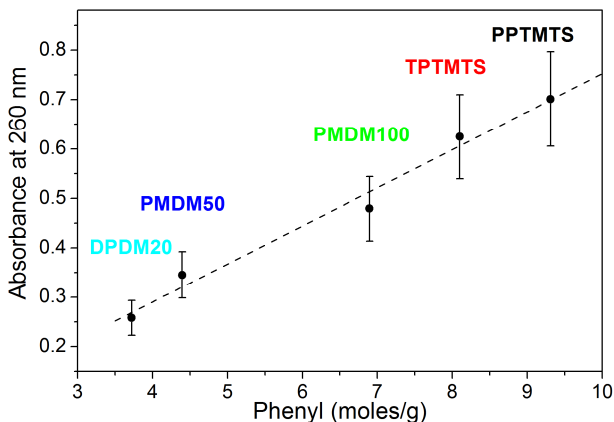


Figure III. 4. Linear correlation between the amplitude of the absorption peak and the amount of phenyl groups in the different polysiloxane liquids.

It is worth noting that the shape of the absorption peak is unchanged for different materials, this allows to exclude that stable non-fluorescent intramolecular dimers are formed. If this occurred, the shape of the absorption spectrum would be different or would not follow the observed linear dependence with the concentration of phenyl groups [Birks1964]. In fact, the chemical interaction between two chromophores, or between a chromophore and a different species, affects also the electronic levels of the chromophore and appears as a shift or a secondary shoulder in the absorption spectrum.

### 3.3.1.2 Absorption spectra of scintillating solutions

Absorption spectra have been measured also for polysiloxane liquids doped with 1% PPO and 0.02% LV. Given the large difference in the concentration of the two dyes, it was not possible to detect the absorption spectra of both, because of PPO saturation occurring in undiluted samples and too low LV absorption occurring in diluted ones. For this reason, two different measurements were needed in order to analyse the absorbance of both dyes. Therefore, PPO absorption was analyzed by studying the materials in 5 g/l THF solutions (Figure III. 5), while LV was studied in undiluted solutions (Figure III. 6).

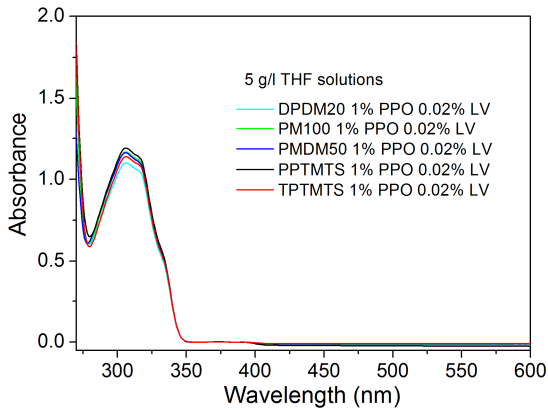


Figure III. 5. Absorption spectrum of polysiloxane liquids doped with 1% PPO and 0.02% LV in 5 g/l THF solutions. PPO absorption peak is visible between 280 nm and 350 nm.

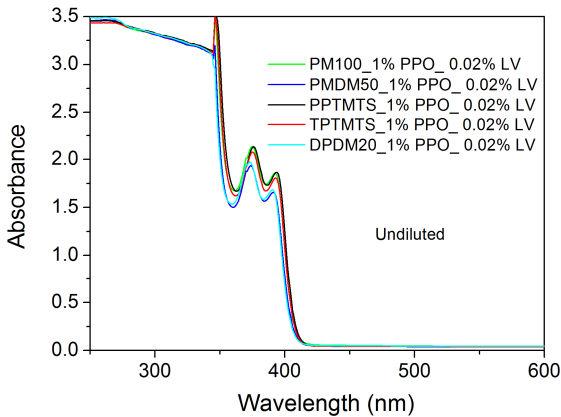


Figure III. 6. Absorption spectrum of undiluted polysiloxane liquids. LV absorption band is visible between 360 nm and 410 nm. Below 350 nm the signal is saturating due to the strong PPO absorption.

In both cases, as expected, all the spectra are very similar, since the hosting solutions have very similar chemical properties. The differences in the absorbance are due to errors in the weightings of the dyes. These errors are higher for LV due to the much smaller quantities to be measured, but in any case they are smaller than 10%. In Figure III. 6, it can be noticed how the signal of PPO, due to its high

concentration in undiluted liquids, is not distinguishable anymore due to absorbance saturation.

### 3.3.2 Fluorescence spectra

#### 3.3.2.1 Fluorescence of polysiloxane liquids

The emission spectrum of polysiloxane liquids in THF solution was measured by exciting the materials at 260 nm, corresponding to their absorption peak (Figure III. 5). All spectra showed two main peaks, with relative intensities varying according to the material. In most cases, the longer wavelength peak, at around 320 nm, represented the most intense emission, with the exception of TPTMTS, having the main emission at 290 nm and only a secondary shoulder at 320 nm. The origin of these two features can be found again in the presence of the phenyl moieties attached to the main siloxanes backbone: the shorter wavelength component (290 nm) represent the emission of the single aromatic unit, while the one at longer wavelength (320 nm) comes from the emission of excimers, formed by the interaction of an excited state phenyl unit with a ground state one [Itoh2001, Hirayama1965, Hamanishi1993].

The formation of intramolecular excimers, which is affecting the photophysical properties of the solutions, strongly depends on the molecular structure of the material. In carbon based compounds, excimers form only when the aromatic groups are positioned along the main chain at a distance of three carbon atoms (Ph-C-C-C-Ph) [Hirayama1965]. Given the rigid tetrahedral structure of the organic bonds, with the fixed bond angle of  $109.5^\circ$ , this configuration is the only one allowing a face-to-face configuration with a reciprocal distance of 0.254 nm, needed for the interaction to occur. In polysiloxane materials, instead, the Si-O-Si bonds have a lower rigidity, allowing the molecule to assume configurations that are not possible in carbon based materials. For this reason, in aromatic polysiloxanes, excimers can form much more easily, not only with a separation of three atoms (Ph-Si-O-Si-Ph) but also with an intramolecular distance of five atoms (Ph-Si-O-Si-O-Si-Ph) [Itoh2001, Horta1991]. These considerations are consistent with what observed in the fluorescence measurements, where the molecules formed by longer chains (DPDM20, PM100, PMDM50), having at least the 20% of phenyl siloxane units, show a strong excimer band, as confirmed also by other authors reporting similar values for the excimer to monomer intensity ratio ( $I_E/I_M$ ) [Itoh2001, Salom1989, Salom1991, Itoh1996]. In particular, PM100, the solvent having the highest phenyl content among the long polymers, is the material showing the highest  $I_E/I_M$  ratio, in good agreement with theoretical observations (Table III. 2).

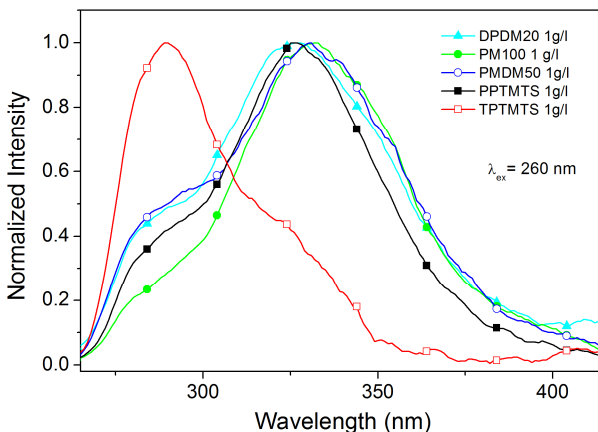


Figure III. 7. Fluorescence emission spectra for different liquid polysiloxane in 1g/l THF solution. Excitation wavelength was fixed at 260 nm for all samples.

As regarding shorter molecular weight compounds, TPTMTS and PPTMTS, it is interesting to notice how, despite the very similar molecular structure, their fluorescence emission is totally different. The spectrum of PPTMTS is not too dissimilar from the ones of the previously observed molecules, while TPTMTS is instead the only material showing a much stronger monomer emission than excimer emission [Itoh2001]. This indicates that, at least at room temperature, the formation of excimers is somehow hindered for this compound, probably due to the presence of the methyl group between the phenyl units, and to the larger distance existing between close chromophores. The replacement of a central methyl group with an aromatic moiety in PPTMTS, strongly favours the reciprocal interaction, leading to a high excimer formation probability.

Table III. 2. Excimer to monomer intensity ratio for the different polysiloxane liquids in 1g/l THF solutions and undiluted.

Sample	$I_E/I_M$ Diluted	$I_E/I_M$ Undiluted
PPTMTS	2.4	3.4
TPTMTS	0.34	1.4
PM100	3.6	5.4
PMDM50	2.0	2.7
DPDM20	2.1	4.6

The fluorescence spectra of the undiluted polysiloxanes were also measured (Figure III. 8). TPTMTS is still the compound showing the highest monomer relative intensity, as it can be observed from the comparison in Figure III. 9, but in this case there is an apparent increase in the excimer to monomer intensity ratio for all the samples. This phenomenon can be mostly ascribed to the inner filter effect due to the strong absorption occurring below 290 nm. To a certain extent, part of this effect can also be due to the increased viscosity of the system as an effect of the reduced dilution, but the influence of the viscosity in the excimer formation process is reported to be very small in linear polysiloxane compounds [Salom1991]. Another reason could also be the formation of intermolecular excimers, formed by the interaction between aromatic groups of different molecules, much more probable in highly concentrated or undiluted solutions. In any case, other authors already reported a similar effect for diphenyl and triphenyl alkenes at different concentrations [Hirayama1965].

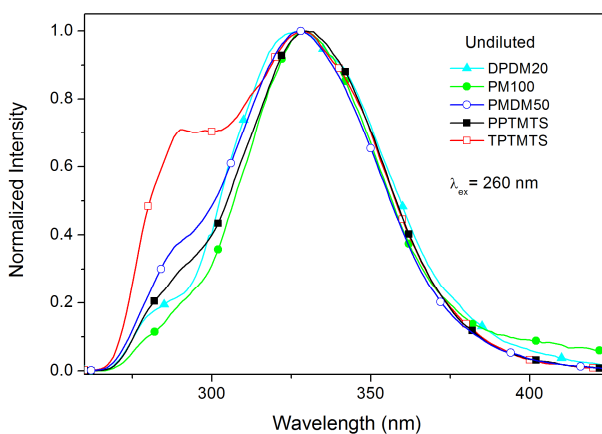


Figure III. 8. Emission spectra of undiluted polysiloxane liquids excited at 260 nm.

### 3.3.2.2 Fluorescence of scintillating mixtures

In liquid or plastic scintillators, the efficiency of the energy transfer from the solvent to the primary dye and from the primary dye to the secondary dye is crucial for the final performances of the material. As explained in Eq. 13, one of the key factors in order to have a good energy transfer is the spectral overlap between solvent emission and primary dye absorption. Experimentally it appears that the process reaches the best efficiency when the energy levels of the donor are slightly higher than those of the acceptor (0.5 eV – 1 eV) [Birks1964]. In these terms, the single monomer emission appears to be favoured over the excimer emission for the energy transfer to PPO.

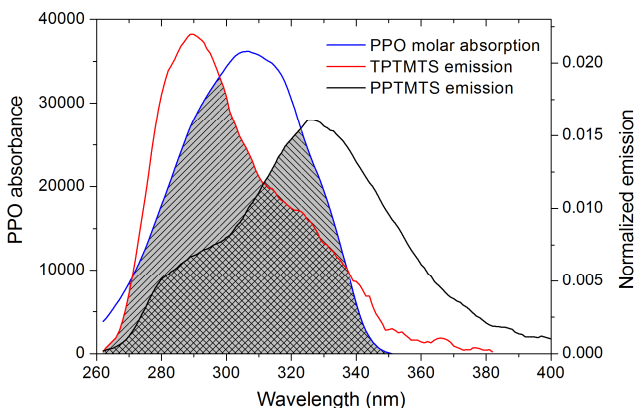


Figure III. 9. PPTMTS and TPMTS emission spectra overlapped to PPO molar absorption. Emission spectra are normalized over the area. Grey areas represent the overlap integral (equation(13)).

Furthermore, Figure III. 9 shows the overlap between TPTMTS (mainly monomer emission) and PPTMTS (mostly excimer emission) emissions, with peak areas normalized to unity, and PPO absorptivity. The grey areas represent the overlap integral used in the calculation of the Förster radius, needed to derive the energy transfer efficiency. As it can be seen, for both liquids there is a good degree of spectral overlap with the acceptor absorption, but the overlap is larger for TPTMTS, showing the highest monomer emission. The value for the overlap integral calculated following the expression in Eq. 13 is reported in Table III. 3.

Table III. 3. Calculated value of the overlap integral for PPO in liquid polysiloxanes.

Sample	Overlap integral [cm <sup>6</sup> ]
PPTMTS	1.72 E-11
TPTMTS	2.08 E-11
PM100	1.48 E-11
PMDM50	1.51 E-11
DPDM20	1.60 E-11

In order to evaluate the energy transfer efficiency from the solvents to the primary dye, PPO excitation spectra were also measured. Figure III. 10 reports the

normalized spectra recorded at 360 nm for the different polysiloxane liquids with 1% PPO concentration. The range from 240 nm to 290 nm is shown in the large image, while the full spectra are reported in the inset. The spectra are very similar, but small differences in the intensity can be noticed at 270 nm (corresponding to the solvent absorption wavelength). Due to the very strong excitation of PPO also at those wavelengths, to the uncertainties in dye concentrations and to the inner filter effect distorting the spectra, a precise evaluation of the energy transfer in this way is very difficult. The trend seems however to be similar to the one shown by the overlap integral, with the best performances shown by TPTMTS (25% higher intensity than DPD20), followed by PPTMTS. For a more precise evaluation, the values of the excitation intensity at 270 nm are reported below (Table III. 4).

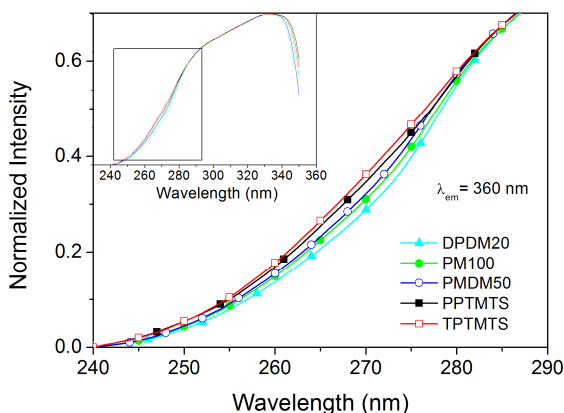


Figure III. 10. Normalized PPO excitation spectrum, measured at 360 nm, for different polysiloxane samples with 1% PPO.

Table III. 4. Normalized intensity measured a 360 nm with excitation at 270 nm for the different polysiloxane samples with 1% PPO.

Sample	Normalized intensity ( $\lambda_{ex}=270nm$ $\lambda_{em}=360nm$ )
PPTMTS	0.347
TPTMTS	0.362
PM100	0.311
PMDM50	0.322
DPDM20	0.289

In addition, energy transfer from PPO to LV was also studied. Figure III. 11 reports, as an example, the emission spectra of PM100 with 1% PPO concentration, with and without the addition of LV. As it can be observed, the addition of LV, leads to the obvious appearance of the LV peak at 430 nm, but also to a decrease in the PPO emission intensity. This reduction is due to energy transfer occurring between the two dyes. Furthermore, the shape of PPO emission, almost unchanged after the addition of secondary dye, indicates that the type of energy transfer is mainly the non-radiative one [Valeur2001]. This observation is in good agreement with other works also in plastic polysiloxane scintillators [DallaPalma2014].

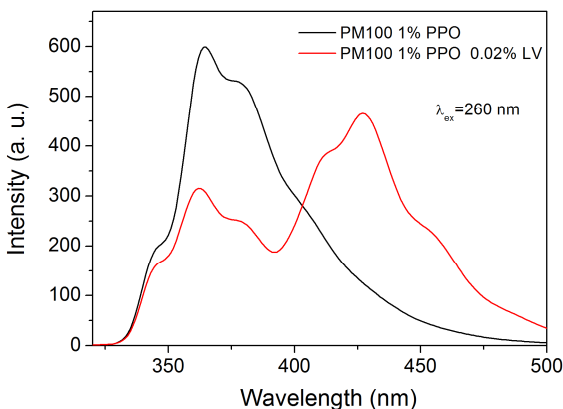


Figure III. 11. Emission spectra of PM100 doped with 1% PPO and with 1% PPO and 0.02% LV, excited at 260 nm.

In order to monitor the differences in the behaviour between the different polysiloxanes, the ratio between the emission at 360 nm (PPO emission peak) and the emission at 430 nm (LV emission peak) was calculated. As it can be seen from Figure III. 12, this ratio is unchanged, within the errors, for all the solutions, giving a first indication that the solvent is not strongly influencing the energy transfer from the primary dye to the secondary one. Error bars were calculated from the differences between nominally identical solutions, and are mainly due to errors in the dye amounts.

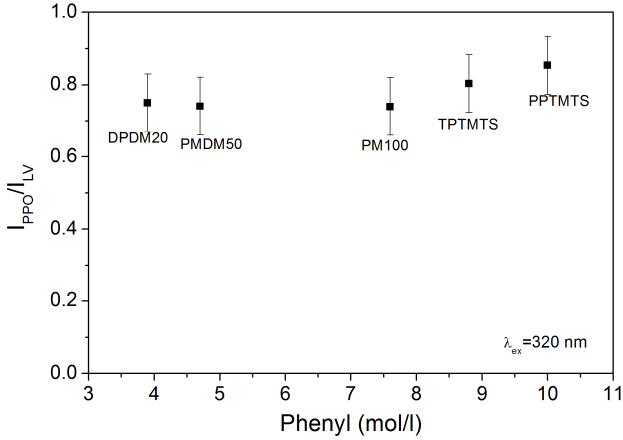


Figure III. 12. Ratio between PPO and LV emission, for different polysiloxane solutions, excited at 320 nm.

The energy transfer efficiency can be evaluated as [Valeur2001]:

$$\Phi_T = 1 - \frac{A_D^0(\lambda_{ex}) I_D(\lambda_{ex}, \lambda_{em}^D)}{A_D(\lambda_{ex}) I_D^0(\lambda_{ex}, \lambda_{em}^D)} \quad (23)$$

Where  $A_D^0(\lambda_{ex})$  and  $A_D(\lambda_{ex})$  are the donor absorbance at the excitation wavelength respectively in absence and presence of acceptor, while  $I_D^0(\lambda_{ex}, \lambda_{em}^D)$  and  $I_D(\lambda_{ex}, \lambda_{em}^D)$  are the donor emission, in absence and presence of acceptor, measured at the donor emission wavelength. For the polysiloxane solutions used in this work, due to the very high concentration of PPO employed, the ratio  $\frac{A_D^0(\lambda_{ex})}{A_D(\lambda_{ex})}$  is very close to one, since the contribution of LV absorption to the total absorption is negligible. Eq. 23 thus reduces to

$$\Phi_T = 1 - \frac{I_D(\lambda_{ex}, \lambda_{em}^D)}{I_D^0(\lambda_{ex}, \lambda_{em}^D)} \quad (24)$$

An accurate quantitative calculation of the energy transfer efficiency,  $\Phi_T$ , is however not straightforward in the present case, due to the high dye concentration involved that leads to non negligible distortions due to inner filter effect. On the other side, a more accurate study with less concentrated solutions would be meaningless for the aim of this work, given the strong dependence of the energy transfer efficiency to the dye concentrations [Valeur2001]. These distortions however do not depend on the polysiloxane materials employed, that are all transparent at the considered wavelengths (see Figure III. 3), and for this reason, even if a quantitative accurate description is not possible, a comparison of the PPO-LV energy transfer efficiency in the different materials can still be done on the basis of Eq. 24.

The estimation of the transfer efficiency is therefore shown in Figure III. 13. The graph still confirms that there is no difference as regarding the energy transfer efficiency from PPO to LV between the different solutions. This is not an obvious outcome, because different properties of the liquids like viscosity, phenyl content or different dye solubility could have some influence on the molecular interaction. This certifies that, at these high concentrations, energy migration and diffusion, strongly dependent on the solvent, have only a minor role in the energy transfer from primary to secondary dye, as already noticed also by other authors [Malimath1997].

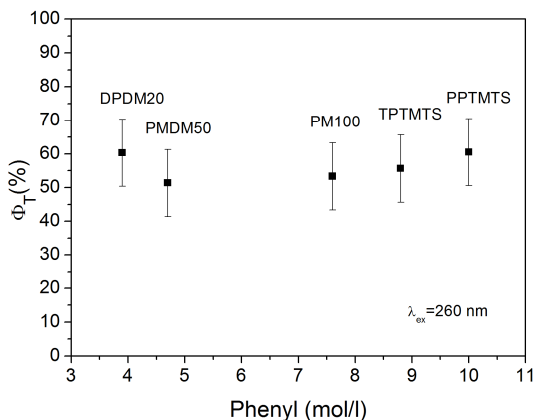


Figure III. 13. Estimation for non-radiative energy transfer efficiency.

### 3.4 Scintillation response of polysiloxane liquids

The scintillation response of the different mixtures and of EJ-309 liquid scintillator was measured with  $^{60}\text{Co}$  (Figure III. 14) and  $^{137}\text{Cs}$  (Figure III. 15)  $\gamma$ -rays. In all cases the typical Compton spectra produced by gamma rays in organic scintillators was observed. Since these materials are composed by light elements, at the involved energies only Compton scattering occurs, allowing the detection of gamma rays thanks to the scattering of electrons in the material. An accurate comparison of the spectra produced by the two sources shows a slight difference in the shape of the spectra. This difference is due to the fact that  $^{137}\text{Cs}$  emits only gamma rays at 0.662 MeV, while  $^{60}\text{Co}$  emits with equal probability gamma rays at two different energies 1.17 MeV and 1.33 MeV. For his reason, in Figure III. 14 a shoulder appears immediately after the main Compton peak, due to the higher energy photons. It is interesting to notice that the peak in Figure III. 14 occurs at about twice the channels of the peak from  $^{137}\text{Cs}$ . This is in very good agreement with the energies of the emitted gamma rays,  $^{60}\text{Co}$  emitting photons at an average energy of 1.25 MeV, about double the energy of  $^{137}\text{Cs}$ .

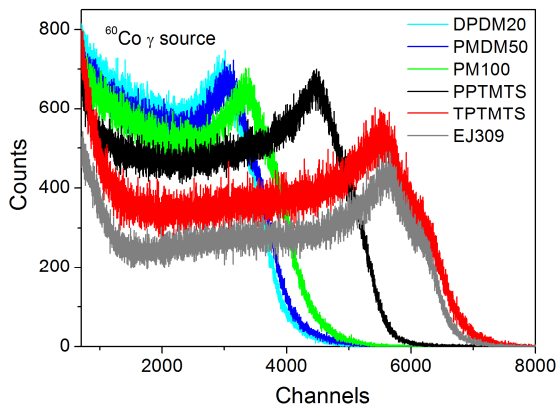


Figure III. 14. Scintillation spectra of polysiloxane based liquid scintillators measured with  $^{60}\text{Co}$   $\gamma$ -source. Spectrum of EJ-309 is also shown for comparison.

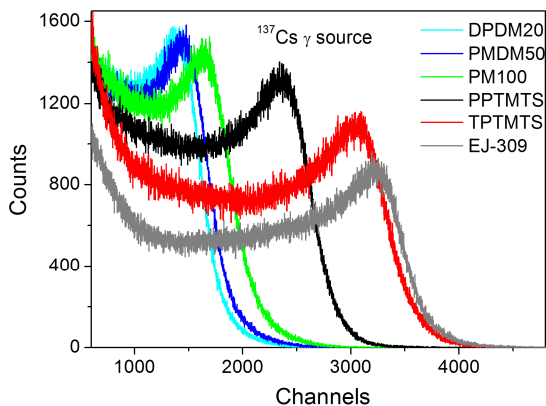


Figure III. 15. Scintillation spectra of polysiloxane based liquid scintillators and EJ-309 measured with  $^{137}\text{Cs}$   $\gamma$ -source. Spectrum of EJ-309 is also shown for comparison.

Figure III. 16, shows the scintillation light yields of the different samples, as a function of the phenyl concentration, expressed in percentage of EJ-309. It clearly appears that the scintillation light output increases with the concentration of phenyl groups in the solvents, with the only exception of TPTMTS, having the best performances despite a lower amount of phenyl moieties than PPTMTS. The observed dependence from the phenyl concentration can be explained by the increased energy migration rate within the solvent, leading to an increased energy

transfer probability to PPO. As regarding TPTMTS, instead, its different behaviour can be linked to the different excimer to monomer ratio (Figure III. 7).

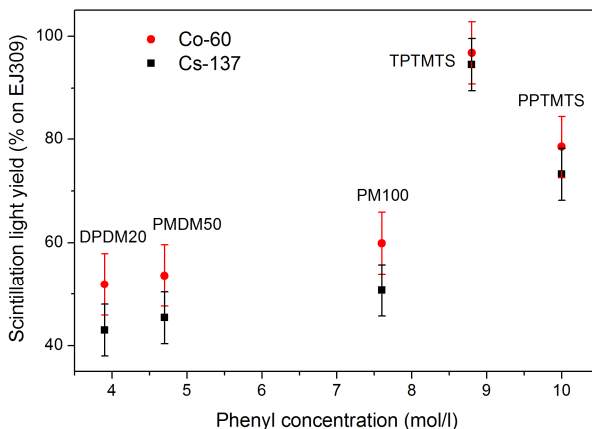


Figure III. 16. Scintillation light yields for different polysiloxane liquid scintillators, relative to EJ-309, as a function of the phenyl concentration.

This difference indeed influences not only the emission spectrum of the solvent, but also its fluorescence quantum yield and the energy migration rate.

As already reported in the previous section, the spectral overlap between solvent emission and PPO absorption is higher for TPTMTS, due to the stronger monomer emission (Table III. 3), and this affects also the scintillation light yield. A proof of that can be found in Figure III. 17, where the existence of a certain correlation between spectral overlap and scintillation light yield can be clearly noticed, especially for the highest phenyl amounts, while at lower phenyl concentrations this correlation is poorer since the effect of a worse energy migration rate is more important than a better spectral overlap.

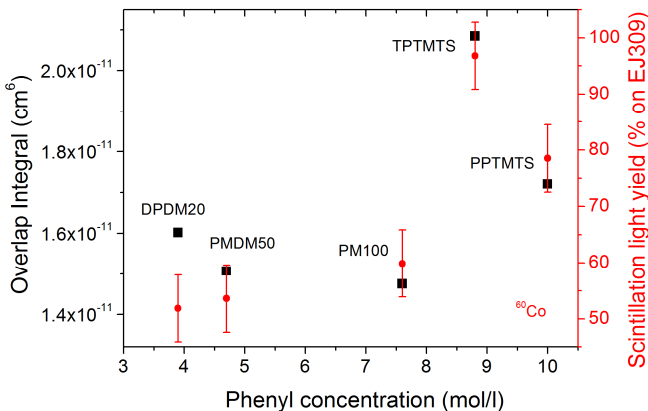


Figure III. 17. Trend comparison between scintillation light yield (from  $^{60}\text{Co}$ ) and overlap integral for different polysiloxane liquids.

Even if it seems to be the most important, this effect is not the only possible advantage of TPTMTS. It has to be recalled that monomer emission, diversely from excimer, is occurring at slightly higher energies than PPO absorption, which is also an advantage for an efficient energy transfer. Furthermore, as it can be seen from Eq. 1212 and Eq. 13, the rate of non-radiative transfer depends also on the donor quantum efficiency. Since data from literature [Hirayama1965, Hamanishi1993, Adadurov2011, Itoh2002] report that monomers have higher efficiency than excimers, this could be another aspect influencing the behaviour of the material. Finally, when comparing TPTMTS with the other solvents, the energy migration has also to be taken into account. One of the most accepted theories about energy migration in solvents suggests that this process occurs by migration of excited states through Coulombic interactions between neighbouring aromatic moieties [Voltz1963, Hirayama1968, Mathad1986], following the scheme:



Being  $M_1$  and  $M_2$  phenyl groups of two different molecules, and the star indicating the excited state.

Another approach [Birks1966, Birks1970b, Horrocks1974] suggests that the migration process occurs by consecutive formations and dissociations of intermolecular excimers, following the process:



Where  $(M_1M_2)^*$  is the intermolecular excimer formed between aromatic groups of different molecules.

In any case, whatever being the real process, the formation of intramolecular excimers seems to reduce the efficiency of the energy migration in the solvent. In the first case, excimers can be regarded as excitation traps, thus decreasing the efficiency of the solvent-solvent energy transfer [Hallam1978]. In the second case, intramolecular excimers hinder the formation of the intermolecular ones, and therefore, according to the proposed transfer mechanism, they affect the solvent-solvent energy transfer efficiency.

The correlation between energy transfer efficiency and scintillation light yield is confirmed by the PPO excitation spectrum shown in Figure III. 10, reporting a trend similar to the one observed for scintillation in the region corresponding to the phenyl group excitation (260 nm-270 nm). It has however to be recalled that this comparison is not completely explaining the results achieved in the scintillation light yield, since the differences observed between samples with fluorescence measurements are much smaller than the one reported for the scintillation output. These discrepancies between fluorescence and scintillation were already reported by other authors [Birks1964, Hirayama1968, Ott1956, Lipsky1956, Bertman1961a, Furst1956] and can be ascribed partly to the different geometries of the measurement setups, partly to the different excitation and the different importance of the energy migration process between light excitation and radiation excitation.

### **3.5 Conclusions**

In this chapter, the development of new non-toxic polysiloxane liquid scintillators has been described. Various polysiloxane liquids, characterized by different phenyl concentrations and distribution were analyzed in terms of optical properties by means of UV-Vis spectroscopy and fluorescence emission spectroscopy. The analysis was performed both on undoped materials and on liquids containing 1 wt% PPO and 0.02 wt% LV, and the results were correlated with the molecular structure and the concentration of aromatic species. In particular, the fluorescence analysis on diluted polysiloxane revealed that the predominant emission was due to the formation of intramolecular excimers in most of the materials, except 1,1,5,5-tetraphenyl-1,3,3,5-tetramethyltrisiloxane (TPTMTS), showing mainly the typical emission of unbounded phenyl units.

The results of the optical characterization were employed to explain the behaviour observed in the scintillation measurements performed with  $^{60}\text{Co}$  and  $^{137}\text{Cs}$  gamma sources. The best spectral overlap between solvent emission and PPO absorption, the higher quantum efficiency of monomer emission, the different position excited state energy levels relatively to PPO absorption and the better expected energy migration rate allowed to explain the better performances shown by TPTMTS in terms of scintillation light output. When compared to EJ-309 liquid scintillator, this material reached relative scintillation light yields of over 95%, resulting by far the best polysiloxane liquid. In the following chapter, the time performances of TPTMTS

liquid scintillators will be investigated in order to evaluate its pulse shape discrimination capability and in turn its suitability to be used as liquid scintillator for neutrons.



# Chapter IV

## Pulse shape discrimination in polysiloxane liquid scintillators

*Part of this chapter has been published in:*

M. Dalla Palma, T. Marchi, S. Carturan, C. Checchia, G. Collazuol, F. Gramegna, N. Daldosso, V. Paterlini, A. Quaranta, M. Cinausero, M. Degerlier,  
**“Pulse shape discrimination in polysiloxane based liquid scintillator”**  
*IEEE Trans. Nucl. Sci.*, article in press.

### 4.1 Introduction

$^3\text{He}$  is at present the most used material for neutron detection, due its very high efficiency and low gamma sensitivity [Kouzes2011], especially in systems exploiting its very high capture cross-section of slow neutrons obtained after fast neutron moderation [Hall-Wilson2012, ASTM1807]. After September 2001, however, the increase in the demand for this gas due to homeland security reasons and the contemporary decrease in its production following non-proliferation treaties reduced the availability of this material, consequently increasing its price [CRSreport2010, Hurd2014]. This fact triggered the research for valid  $^3\text{He}$  alternatives [Kouzes2010] and a number of new systems with interesting characteristics was recently developed employing fast neutron elastic scattering or thermal neutron capture reactions (see Chapter I).

As regarding the detection of fast neutrons, liquid scintillators are one of the most used solutions since their pulse shape discrimination (PSD) capability allows achieving very good gamma rejection. Best performing liquid scintillators, based on xylene have however some drawbacks connected with their high toxicity, high volatility, and high flammability as already seen in the previous chapter. The obvious solution to overcome these problems is the replacement of toxic solvents with less harmful ones, but this is not so easy and newly developed low-toxicity liquids [Back2008, Bentoumi2013, Marrodan2009, Lombardi2013] at the moment do not equal the performances of xylene based scintillators [Pawelczak2013, Hamel2014]. Polysiloxane materials, thanks to their low toxicity and inertness could be a promising candidate in this field. On the basis of the good results in terms of light yield reported for polysiloxane liquid scintillators (see previous chapter), the time response of the best performing polysiloxane liquid, 1,1,5,5-tetraphenyl-1,3,3,5-tetramethyltrisiloxane (TPTMTS) was investigated in order to characterize the pulse shape discrimination capability of this material. In particular different solutions of

TPTMTS at different PPO concentrations were investigated, with UV excitation, neutrons and  $\gamma$ -rays and the results were connected with their PSD capability.

## 4.2 Experimental part

TPTMTS samples were produced with four different concentrations of PPO (0.5 wt%, 1 wt%, 2 wt% and 4 wt%) and with 0.02 wt% fixed concentration of LV, following the procedure described in Chapter II. The optical properties of the scintillators were then tested by steady state and time resolved fluorescence spectroscopy, in 10 mm optical path quartz cuvette, using right angle geometry. The scintillation response of the material was tested by  $^{22}\text{Na}$ ,  $^{60}\text{Co}$  and by  $^{137}\text{Cs}$   $\gamma$ -rays. The scintillation pulses instead were investigated using a 2.3 MeV pulsed neutron beam at the “CN” accelerator in INFN-Legnaro National Laboratories. The PSD capability of the material was finally evaluated using the charge comparison method, as described in Chapter II. All the results were compared with commercial low-toxicity liquid scintillator EJ-309, recently developed by Eljen Technology. In Table IV. 1 the most important physical properties of TPTMTS are reported and compared to EJ-309 and to one of the best performing liquid scintillators in terms of PSD, EJ-301.

Table IV. 1. Main physical properties of TPTMTS, EJ-309 and EJ-301 liquid scintillators.

Product	TPTMTS	EJ-309	EJ-301
Viscosity [cSt]	38	<10	0.7
Density [g/cm <sup>3</sup> ]	1.07	0.96	0.87
Refractive Index	1.551	1.57	1.50
Flash Point [°C]	220	140	26
Boiling Point [°C]	233 (0.5 mm Hg)	290-300	141
Vapor pressure [mm Hg]	<0.001 (25 °C)	0.002 (20 °C)	18 (37.7 °C)
HMIS	1,1,0	1,1,0	2,3,0

## 4.3 Fluorescence analysis

The fluorescence response as a function of PPO concentration was measured for the various PPO samples. In right angle geometry, inner filter effect is so strong that PPO is not visible, since it is completely absorbed by the secondary dye. This effect can be seen in Figure IV. 1, showing the emission spectra of the same sample

(TPTMTS 1% PPO 0.02% LV) recorded in 2 mm thin optical path cell with front-face geometry and in 10 mm thin cell in right angle geometry. It is clear that the reduction in the emitted intensity below 400 nm is due to inner filter effect. This effect is even more important in case of scintillation measurements, where the optical path is longer, and for this reason, in order to study the final time response of polysiloxane materials as liquid scintillators, the fluorescence lifetime measurements were performed in right-angle geometry.

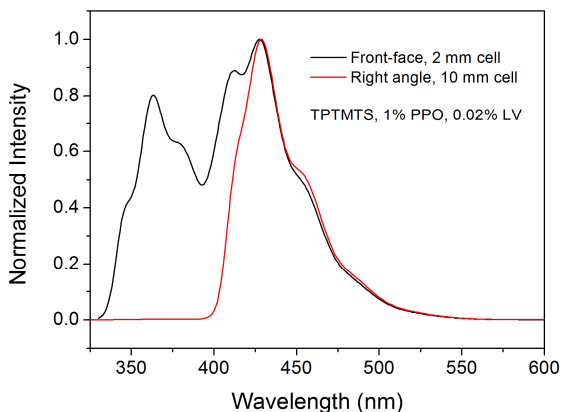


Figure IV. 1. Comparison between emission spectra of TPTMTS with 1% PPO and 0.02% LV, measured with right angle geometry in 10 mm optical path cell and with front face geometry in 2 mm thin optical path cell.

Figure IV. 2 shows the normalized emission spectra measured in right angle geometry, and, for comparison, the emission spectrum of a sample without LV. It clearly appears that normalized spectra are all very similar, indicating that PPO concentration has no effect on the LV emission and that all the light emitted by the primary dye, even at 4% concentration is almost entirely transferred to LV. From the combination of the observations done in the previous chapter, and the distortions due to inner filter effect, it can be inferred that the energy transfer in these samples occurs both radiatively and non-radiatively, in good accordance also with what already reported also for polysiloxane plastic scintillators [DallaPalma2014].

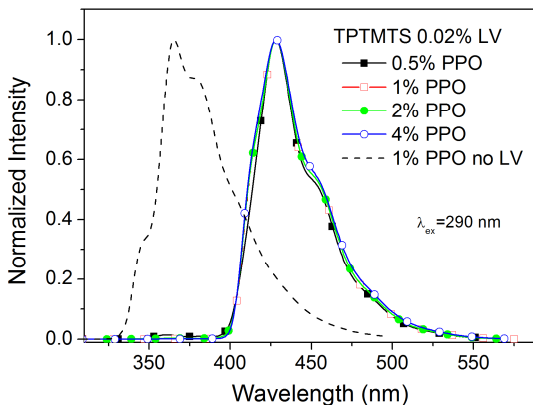


Figure IV. 2. Normalized fluorescence emission spectra at different PPO concentrations. The emission spectrum of a sample without LV is also shown for comparison.

#### 4.4 Fluorescence lifetime analysis

Fluorescence lifetimes of the samples were measured by exciting the solutions at 280 nm (PPO excitation) and at 375 nm (LV excitation), and recording the emission at 427 nm, corresponding to LV emission. Due to the spectra shown in Figure IV. 2 however, these curves are representative for the entire emission of the samples, occurring almost completely from the secondary dye.

Figure IV. 3 and Figure IV. 4 report the fluorescence decay at 427 nm for the investigated samples. In case of LV excitation (375 nm) the curves represent LV decay, and are a further confirmation that different concentrations of PPO are not affecting at all the emission of LV. The three curves are indeed completely overlapping and their fit gave very similar values.

On the other side, Figure IV. 4 shows the decay curves of the same samples when exciting the primary dye. There are some evident differences in this case, with the lifetime clearly increasing with PPO concentration.

In

Table IV. 2 the fluorescence lifetime values are reported in the two cases. It is worth noting that the values measured with PPO excitation are not only different between the samples, but they are also constantly higher than in case of direct LV excitation. These differences can be ascribed to the energy transfer from PPO to LV, which is responsible for the increase in the fluorescence lifetime and for the clear increase in the rise-time.

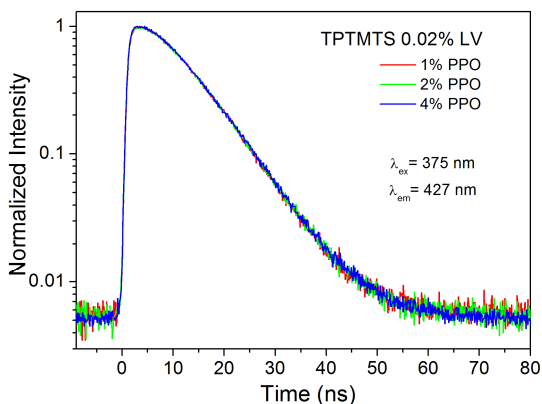


Figure IV. 3. Fluorescence decay spectra for TPTMTS with different concentrations of PPO and 0.02% LV, measured by excitation at 375 nm and emission at 427 nm.

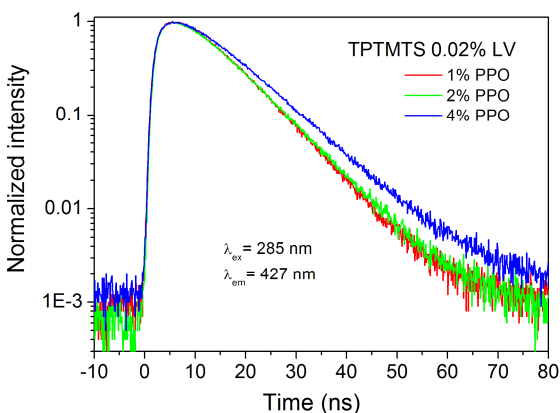


Figure IV. 4. Fluorescence decay spectra for TPTMTS with different concentrations of PPO and 0.02% LV, measured by excitation at 280 nm and emission at 427 nm.

Figure IV. 6 and Figure IV. 7 show a comparison of the LV decay curves at the two different excitation wavelengths for a sample with 1 % PPO and a sample with 4% PPO. In both cases, there is a clear difference between the rise-time at the two excitation wavelength that is always visibly longer in case of PPO excitation. This effect is due to the occurrence of energy transfer between PPO and LV, with the rise time, of about 3.5 ns, corresponding to the lifetime of the donor in presence of

acceptor [Birks1968, Valeur2001]. The lack of energy transfer in case of direct LV excitation didn't allow determining a value for the rise time, since in that case the rise time would be corresponding to the excitation pulse width that has been however deconvolved from the measured curve before the fitting.

Table IV. 2. Fluorescence lifetime fitting values as a function of PPO concentration for PPO and LV excitation. Measurements were performed at 427 nm.

PPO	$\lambda_{\text{ex}}=375 \text{ nm}$	$\lambda_{\text{ex}}=280 \text{ nm}$	
	$\tau$ [ns]	$\tau$ [ns]	$\tau_R$ [ns]
1%	$7.6 \pm 0.1$	$7.9 \pm 0.1$	$3.7 \pm 0.6$
2%	$7.6 \pm 0.1$	$8.1 \pm 0.1$	$3.2 \pm 0.6$
4%	$7.6 \pm 0.1$	$9.0 \pm 0.1$	$3.4 \pm 0.6$

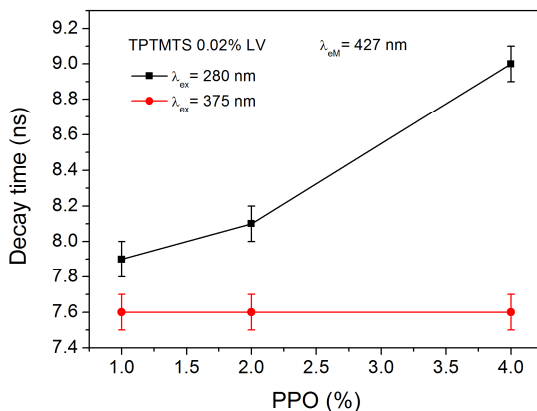


Figure IV. 5. Fluorescence decay time as a function of PPO concentration at the two different excitation wavelengths.

The clear increase in the decay time with dye concentration (Figure IV. 5) can be ascribed either to self-absorption effects, or to the formation of excimers [Yguerabide1962] between excited and ground state PPO molecules. It is known that their formation is characterized by longer emission wavelength (410 nm-430 nm), similarly to what already reported for phenyl groups in the previous chapter, and by longer decay times [Berlman1961b, Weinreb1962, Birks1967]. This phenomenon was already observed in liquid solutions [Marrodan2009, Berlman1961b] and also in polysiloxane plastic scintillators, as reported in Chapter VI.

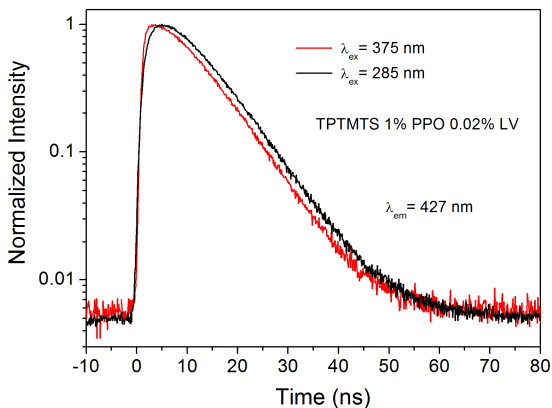


Figure IV. 6. Fluorescence decay for a sample with 1% PPO excited at 280 nm and at 375 nm.

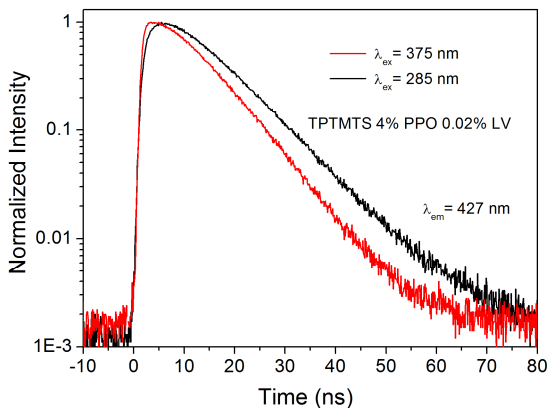


Figure IV. 7. Fluorescence decay for a sample with 4% PPO excited at 280 nm and at 375 nm.

#### 4.5 Scintillation lifetime analysis

As mentioned in Chapter II, in case of scintillation pulses, in order to achieve a good fit of the curves, a second decay term was needed, corresponding to the slow component of the scintillation signals. Measurements were performed using both  $\gamma$  and neutron excitation and the fitting parameters are reported respectively in Table IV. 3 and Table IV. 4.

Table IV. 3. Fitting parameters for  $\gamma$  induced scintillation pulses in TPTMTS samples at different PPO concentrations and 0.02% LV.

<b>PPO [%]</b>	<b>0.5 %</b>	<b>1 %</b>	<b>2 %</b>	<b>4 %</b>	<b>EJ-309</b>
$\tau_1$ (ns)	$8.2 \pm 0.4$	$8.5 \pm 0.4$	$9.2 \pm 0.4$	$10.7 \pm 0.4$	$5.0 \pm 0.4$
$\tau_2$ (ns)	$70 \pm 5$	$74 \pm 3$	$68 \pm 3$	$67 \pm 2$	$62 \pm 10$
$\tau_R$ (ns)	$3.7 \pm 0.4$	$3.1 \pm 0.4$	$2.7 \pm 0.4$	$1.9 \pm 0.4$	$2.9 \pm 0.4$
A	$1.62 \pm$	$1.39 \pm$	$1.21 \pm$	$1.03 \pm$	$1.80 \pm$
	0.06	0.03	0.01	0.01	0.01
B	$0.046 \pm$	$0.062 \pm$	$0.075 \pm$	$0.088 \pm$	$0.039 \pm$
	0.004	0.003	0.004	0.004	0.006
A%	$81 \pm 4$	$72 \pm 2$	$68 \pm 1$	$65 \pm 1$	$80 \pm 1$
B%	$20 \pm 2$	$28 \pm 2$	$32 \pm 2$	$35 \pm 2$	$20 \pm 5$

Table IV. 4. Fitting parameters for neutron induced scintillation pulses in TPTMTS samples at different PPO concentrations and 0.02% LV.

<b>PPO [%]</b>	<b>0.5 %</b>	<b>1 %</b>	<b>2 %</b>	<b>4 %</b>	<b>EJ-309</b>
$\tau_1$ (ns)	$8.6 \pm 0.4$	$8.7 \pm 0.4$	$9.0 \pm 0.4$	$9.8 \pm 0.4$	$5.4 \pm 0.4$
$\tau_2$ (ns)	$91 \pm 3$	$96 \pm 2$	$88 \pm 2$	$84 \pm 2$	$58 \pm 2$
$\tau_R$ (ns)	$3.4 \pm 0.4$	$2.8 \pm 0.4$	$2.5 \pm 0.4$	$1.5 \pm 0.4$	$3.2 \pm 0.4$
A	$1.45 \pm$	$1.23 \pm$	$1.13 \pm$	$0.92 \pm$	$1.87 \pm$
	0.03	0.02	0.01	0.01	0.01
B	$0.063 \pm$	$0.092 \pm$	$0.122 \pm$	$0.148 \pm$	$0.135 \pm$
	0.002	0.002	0.003	0.003	0.005
A%	$69 \pm 2$	$54.7 \pm 0.9$	$48.5 \pm 0.9$	$42.2 \pm 0.6$	$56.4 \pm 0.6$
B%	$31 \pm 2$	$45 \pm 1$	$51 \pm 1$	$58 \pm 2$	$44 \pm 2$

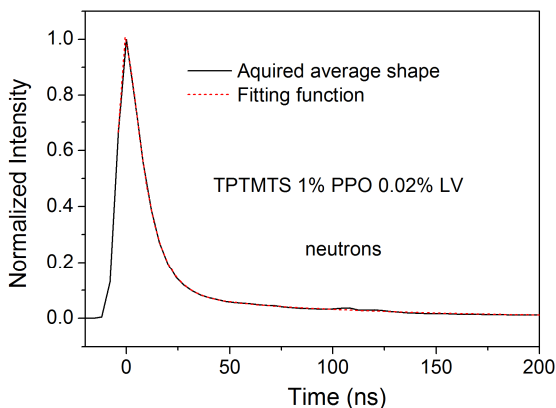


Figure IV. 8. Comparison between measured average pulse shape and fitting function employed to extract the fitting parameters reported in Table IV. 3 and Table IV. 4.

As an example, in Figure IV. 8 The comparison between the fitting function and the measured average shape is reported, showing the good agreement between the two.

As it can be seen, in this case, the fast component  $\tau_1$  is a bit higher than in case of fluorescence lifetimes measurements, probably due to the different geometry of the experimental setup [Moszynski1979] and to the different timing properties of the electronic setup.

Also in this case, similarly to what observed for PPO excitation, the decay time is increasing with the concentration of primary dye, as a result of excimer formation (Figure IV. 9, Figure IV. 10).

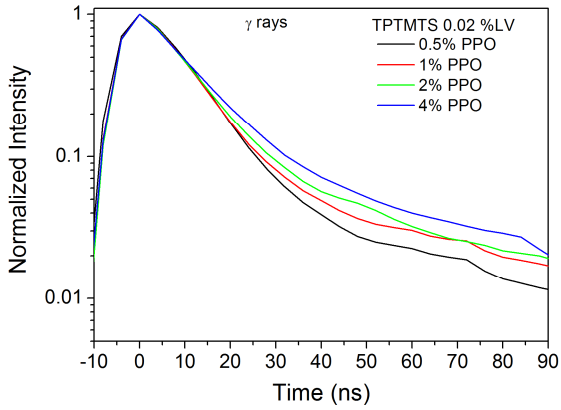


Figure IV. 9. Averaged  $\gamma$ -rays scintillation pulse shapes for TPTMTS at different PPO concentrations.

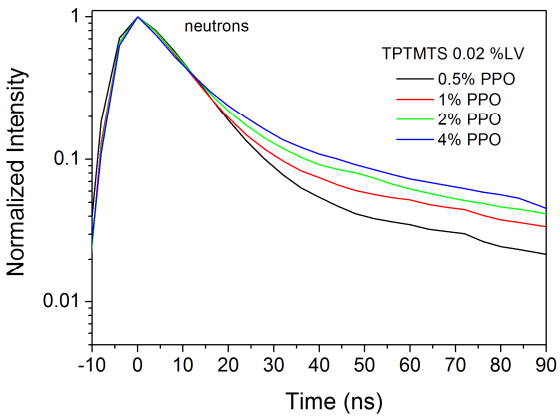


Figure IV. 10. Averaged neutrons scintillation pulse shapes for TPTMTS at different PPO concentrations.

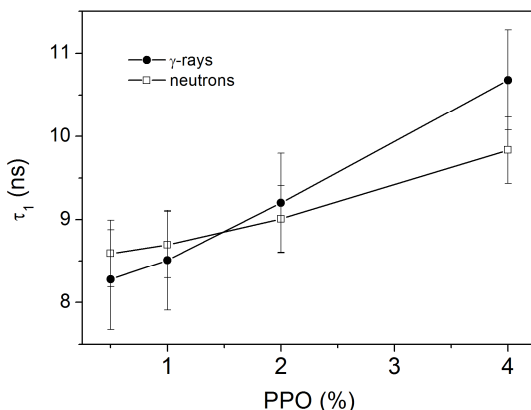


Figure IV. 11. Fast decay time fitting value as a function of PPO concentration in case of neutrons and gamma irradiation.

The increasing rate however is not the same for the two types of radiation (Figure IV. 11), and the explanation for this phenomenon can be connected with a different sensitivity of excimers to ionization quenching, which is stronger for neutrons than for  $\gamma$ -rays [Berlman1961a, Berlman1973].

As visible from the fitting data and from Figure IV. 12, the rise time,  $\tau_R$ , seems also to be slightly correlated to the PPO concentration, changing from 3.7 ns at the lowest concentration to 1.9 ns with 4% PPO. Such behaviour can be explained with an improvement in the solvent to PPO energy transfer, consequently leading to a faster overall transfer to LV. A similar behaviour was observed in the reduction of the fast PPO decay time in binary solution, both with radiation excitation and with UV excitation at 267 nm [Lombardi2013], in agreement also with other reported measurements on similar systems [Marrodan2009, Ranucci1998]. It is worth noting that in this work no significant change was observed in the rise time when 280 nm excitation was employed, probably because at this wavelength mainly PPO direct excitation occurs, and the effect of solvent-solute energy transfer is hidden. Since the rise time of acceptor emission is associated to the donor lifetime (Chapter I), the effect of a rise time reduction can be also linked to a decrease of PPO lifetime. This decrease, observed even without acceptor, can be also partially regarded as a further proof of the formation of excimers leading to a decrease of the fast single molecule emission lifetime, and to an increase of the slower excimer emission intensity [Valeur2001].

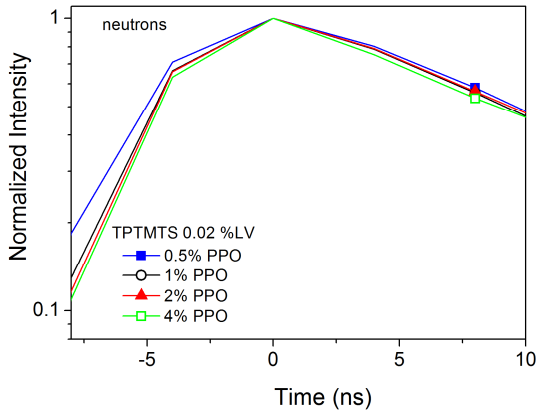


Figure IV. 12. Detail of the neutron induced scintillation pulses, showing the difference in the rise time at the various PPO concentrations.

For the purpose of this work, however, the most important effect is the variation of the second component,  $\tau_2$ , with the primary dye concentration. This slower emission is connected with the delayed fluorescence, responsible for the PSD capability. In fact, it has to be noticed that this component was not observed in photoluminescence measurements, but only with neutrons or  $\gamma$ -rays excitation. As already mentioned in Chapter I, this term is due to the triplet-triplet annihilation process, which in turns depends on the ionization density produced by the particle in the material [Birks1964, Brooks1979]. Triplet states are formed with higher probability when the ionizing particle produces a high density of ionized states, since their formation is principally connected to the capture of an electron by ionized species. For this reason neutron scattered protons and gamma induced Compton electrons are expected to produce different triplet states densities and therefore to have different delayed fluorescence intensities. This expectation is confirmed in Figure IV. 13, showing the average pulse shapes at the four tested concentrations for neutrons and for gamma rays coming from two different sources ( ${}^7\text{Li}(p, n){}^7\text{Be}$  reaction and  ${}^{60}\text{Co}$ ). There is a good agreement between the two different gamma signals, while the pulses produced by neutrons show a much more intense delayed fluorescence. The small differences between gamma induced pulses have to be ascribed to the difference in energy between the two types of photon.

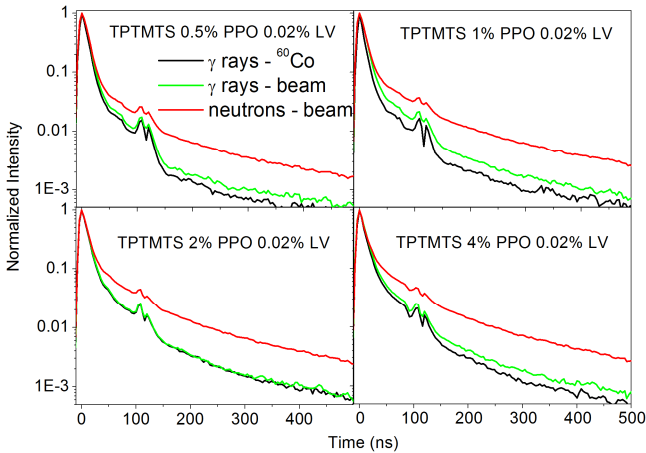


Figure IV. 13. Average pulse shapes for TPTMTS at different PPO concentrations. Each graph shows the comparison between neutrons and gamma rays produced by two different sources.

The difference between the various samples is quantitatively shown in Figure IV. 14, reporting the fractional amplitude of the slow component pre-exponential term as function of the primary dye concentration. As expected, it can be seen that for neutron induced scintillation pulses the intensity of this component is always stronger. Furthermore, as already visible also in Figure IV. 9 and Figure IV. 10, it clearly appears that its intensity is also dependent on the PPO concentration for both kinds of radiation: higher dye concentrations lead to higher triplet-triplet interaction probabilities, and in turns to higher delayed component intensities. It is worth noting that the increasing trend is not the same for neutrons and gammas, but the neutron induced pulse shapes have a higher increasing rate, so that the maximum LV difference in the intensity of the slow emission between neutrons and gammas occurs with the highest PPO concentration (4%). This behaviour seems to be related to solvent employed for the liquid scintillators, since it was not observed with PPO in linear alkylbenzene (LAB) or di-isopropylnaphtalene (DIN) [Lombardi2013], but it was reported, at smaller concentrations in p-xylene and in plastic scintillators [Zaitseva2012]. This is reasonably due to the slightly higher TPTMTS viscosity that, reducing molecular diffusion, is also reducing dye molecules interactions and therefore requires higher dye concentrations to allow an optimal triplet states interaction. A high primary dye concentration is indeed increasing the non-radiative energy migration probability allowing to compensate for the reduced molecular mobility [Valeur2001, Birks1970a].

The small signals at about 110 ns are due to spurious effects in the PMT. These effects are called after-pulses and can be due to two main different reasons. A first one is the elastic scattering of electrons on the first dynode, another possible reason is the ionization of residual gases inside the tube. The positive ions are accelerated

to the cathode where they cause the late emission of electrons. Different gases having different molecular masses are accelerated in different ways by the voltage, giving rise to different after-pulses. The presence of two peaks can then be explained as the ionization of two different gases [HammamatsuPMT]. Examples of similar effects have already been reported in literature [Abbasi2010].

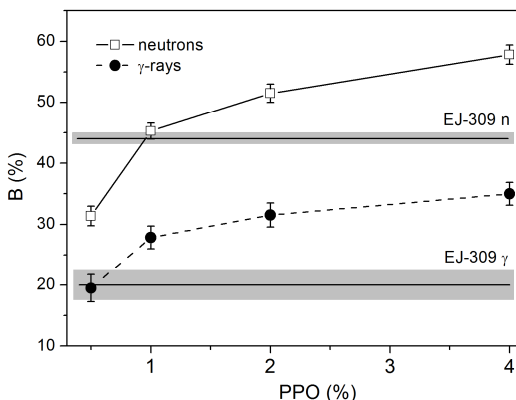


Figure IV. 14. Slow component intensity for neutrons and gamma shapes as a function of PPO concentration.

#### 4.6 Scintillation light yield

$^{60}\text{Co}$  and  $^{137}\text{Cs}$   $\gamma$ -sources were used to investigate the scintillation light yield as a function of PPO concentration during the beam tests. The best concentration, as regarding the light output, resulted to be the one with 2% PPO concentration, as visible in Figure IV. 15, with a relative light yield reaching 80% of EJ-309. The worst mixture instead resulted to be TPTMTS with 4% PPO. The performances the samples however were quite similar, so that these results could be influenced not only by the material itself, but also by small errors in the weightings of LV and by imperfect coupling with PMT. In order to perform a more accurate estimation of the light yield of the materials, a series of measurements has been repeated using  $^{60}\text{Co}$ ,  $^{137}\text{Cs}$  and  $^{22}\text{Na}$   $\gamma$ -sources (Figure IV. 16). Also in this case the relative scintillation light yields were about 80%-90% of EJ-309, with small differences between the various concentrations. The best mixture resulted to be the one with 1% PPO, and, similarly to the evaluation performed at the beam test, the worst was the one with 4% PPO. Once again, it is worth recalling that the differences between samples fall within the experimental errors, even if repeated measurements, seems to confirm a decrease in the light yield for concentrations above 2% PPO. This could be linked to

a concentration quenching phenomenon, which is a side effect of the increased dye molecules interaction.

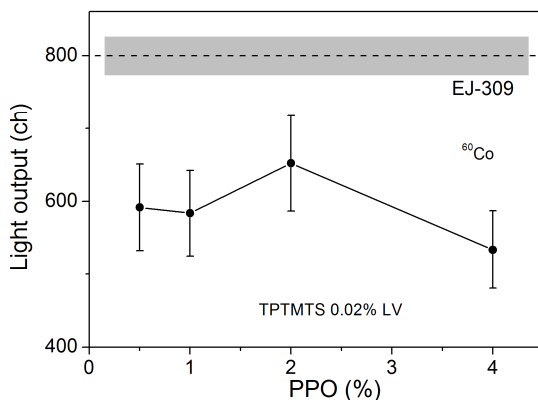


Figure IV. 15. Scintillation light output as a function of PPO concentration with  $^{60}\text{Co}$   $\gamma$ -rays.

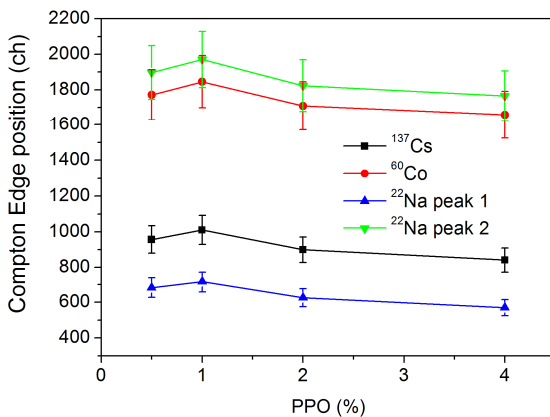


Figure IV. 16. Compton Edge position as a function of PPO concentration evaluated for the different gamma sources.

#### 4.7 Pulse shape discrimination capability

As described in Chapter II, the PSD parameter distribution was drawn for the different TPTMTS samples (Figure IV. 17) and for EJ-309 liquid scintillator (Figure IV. 18). In all cases, two peaks corresponding to neutrons and gammas signal could be distinguished. In order to set the Figure of Merit for each distribution, the two

peaks were fitted by a Gaussian function, and the fitting parameters (i.e. peak centre and peak width) were used to calculate the FoM.

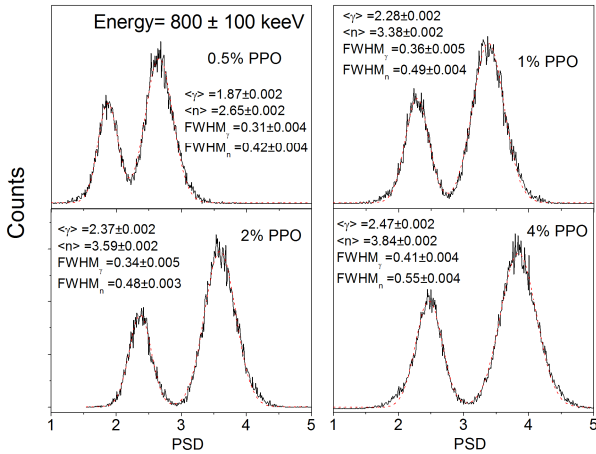


Figure IV. 17. PSD distribution for different TPTMTS solutions with 0.02% LV and variable PPO amount, shown for energy of 800 keVee (keV electron equivalent). Dashed red lines represent the fit used to determine the FoM. Corresponding fitting parameters are also reported.

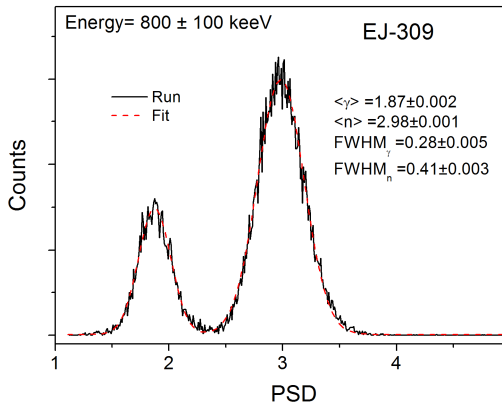


Figure IV. 18. PSD distribution for EJ-309 liquid scintillator, shown for energy of 800 keVee. Dashed red lines represent the fit used to determine the FoM, and the relative fitting parameters.

In this way, the FoM could be calculated for each sample at different energies. As an example, in Figure IV. 19, FoM is reported for three different energies as a function of PPO concentration. As clearly visible, the trend shown by this parameter is

different at high or low energies. In the latter case, it reaches a maximum with 2% PPO before decreasing at higher concentrations; at high energies instead it increases monotonically.

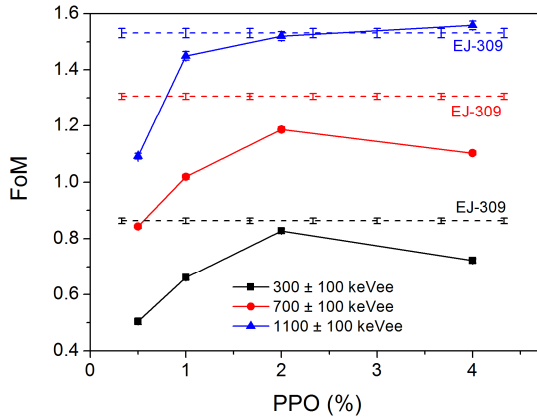


Figure IV. 19. FoM as a function of PPO concentration for TPTMTS with 0.02% LV, at three different energies. FoM of EJ-309 is also shown for comparison.

This behaviour is due to two different effects, acting in contrast one to each other. FoM is the ratio between the peak centroids separation and their FWHM, and these two terms depends on the PPO concentration in different ways. The former is constantly increasing with the quantity of dye dissolved in the material, as shown in Figure IV. 20, due to the increased difference in the delayed component intensity between neutron and gammas (Figure IV. 14). The higher is the difference in the intensity of the delayed component, the larger is the peak separation in the PSD distribution.

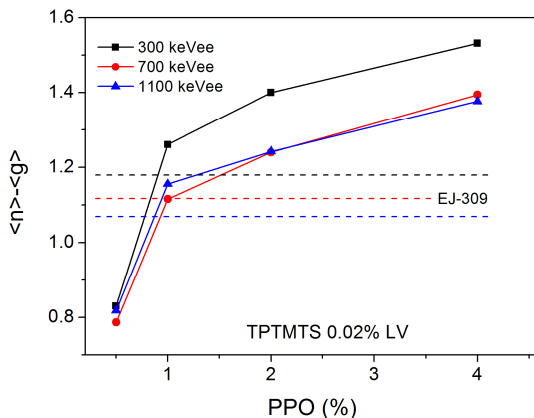


Figure IV. 20. Peak centroids separation as a function of PPO concentration at three different energies. Values for EJ-309 are also shown.

The latter term influencing FoM is the sum of the FWHMs, that is also affected by the PPO amount. Among other things, it depends from the scintillation light output, because the better is the light output, the better is the signal to noise ratio and the narrower is the PSD distribution [Zaitseva2012]. This means that at low energies, when the light yield is small and the signal is close to the identification threshold, the best solution is the one with the most intense light output, that is EJ-309 overall and TPTMTS with 2% PPO and 0.02% LV among the polysiloxane solutions. At high energies instead, the signal to noise ratio is good enough for all samples and the PSD distribution is consequently narrow. In this situation the best FoM is achieved by the material showing the largest peak separation, corresponding to the highest PPO concentration (Figure IV. 20) that shows a FoM even slightly better than EJ-309 (Figure IV. 19). This trend is well shown in Figure IV. 21, where FoM is reported as function of the radiation energy. It has to be observed how, the solution with 4% PPO has one of the worst performances at low energies, since it is the one showing the least intense light output, but, thanks to the larger peak separation (largest difference in the neutron and gamma slow component intensity), its increasing trend is higher than the other solutions, and above 900 keVee, it becomes the best performing solution, reaching a FoM which is even slightly better than EJ-309.

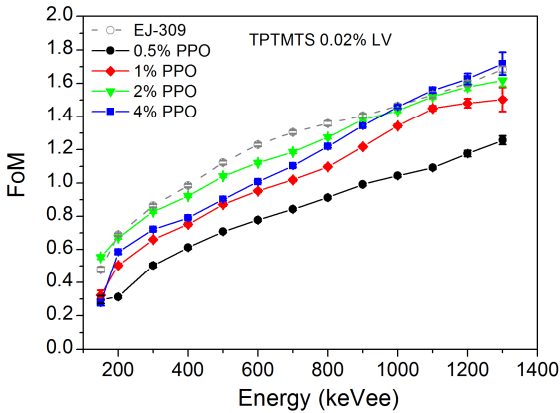


Figure IV. 21. FoM as a function of energy for the different TPTMTS samples and for EJ-309.

On Figure IV. 22 the PSD-Energy distribution is shown. This plot allows to have a more complete overview over the pulse shape discrimination capability of the materials. Understanding which is the energy threshold allowing reasonable neutron gamma discrimination. It is again clear that at lower energies, the performances of the scintillators in terms of light output are affected by the width of the PSD distribution, becoming narrower at higher energies.

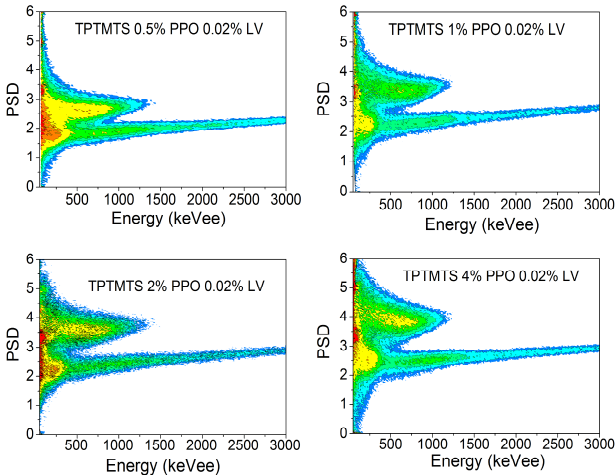


Figure IV. 22. PSD parameter-energy 3D plot for the different TPTMTS mixtures.

## **4.8 Conclusions**

This part of the work dealt with the analysis of the time response of different 1,1,5,5-Tetraphenyl-1,3,3,5-Tetramethyltrisiloxane (TPTMTS) samples, doped with variable concentrations of PPO and 0.02% LV. The final goal was the investigation of the pulse shape discrimination (PSD) capabilities of these newly developed liquid scintillators. In particular, the effect of PPO concentration was studied by various techniques. Fluorescence lifetime analysis showed that higher primary dye concentration leads to a longer fluorescence lifetime in case of PPO excitation at 280 nm. This behaviour, not observed for direct LV excitation at 375 nm, was connected with the formation of excimers between PPO molecules. The analysis performed on the samples using radiation excitation (neutrons and  $\gamma$ -rays), revealed the appearance of a second slower component in the samples emission. This component was ascribed to the delayed fluorescence induced in the scintillator by the particles ionization. The intensity of this component depends on the type of impinging radiation and can be exploited to distinguish neutrons from gamma rays using PSD techniques. The intensity of this slower component was also increasing with the PPO concentration thanks to the improved dye molecules interaction, but at different increasing trends between neutron and gammas, so that the difference between the two shapes was larger with the highest amount of dyes. The variation of the FoM of the process as a function of the energy was also studied for the different samples and for the reference EJ-309 liquid scintillator. From this investigation it was observed that at low energies, the light output is the most important parameter also as regarding PSD. At higher energies instead, the most important aspect is the difference in the slow component intensity between neutrons and gammas, which is increasing with the amount of PPO. Thanks to this, above 900 keVee, TPTMTS 4% PPO 0.02% LV was the best solution, showing an even slightly better FoM than EJ-309. These results confirms the suitability of this material to be used as solvent for polysiloxane based liquid scintillators, having performances comparable to the commercial products, with the advantages of lower harmfulness and better handiness.

# Chapter V

## Time response of polysiloxane plastic scintillators

*Part of this chapter has been published in:*

*M. Dalla Palma, T. Marchi, S. Carturan, A. Quaranta, F. Gramegna, G. Collazuol, M. Cinausero, N. Daldosso, V. Peterlini*

**“Fluorescence Lifetimes in Polysiloxane Based Scintillators: Effects of Primary Dye Concentration”**,

*LNL-INFN Annal Reprt 2013.*

*T. Marchi, M. Dalla Palma, S. Carturan, A. Quaranta, F. Gramegna, G. Collazuol, M. Degerlier, M. Cinausero*

**Low Cost, Eco-Friendly Siloxane-Based Scintillators with Neutron/Alpha/Gamma Discrimination Capabilities**

*LNL-INFN Annal Reprt 2012.*

### **5.1 Introduction**

The use of plastic scintillators for fast neutron detection, at present, is mainly hindered by their very poor pulse shape discrimination performances. In order to overcome this problem, many attempts have been done in the last decade [Bertrand2015], but for most of them the effectiveness and the efficiency were quite poor and also a newly commercialized plastic scintillator with PSD capability is still under evaluation. The reason for this behaviour is that in rigid matrixes, molecular mobility is strongly hindered and as a consequence also triplet-triplet interactions, crucial for pulse shape discrimination is less probable [Bertrand2015]. For this reason, at the moment, the only reasonable PSD in plastic scintillators has been achieved through the dissolution in the matrix of extremely high amounts of PPO, up to 30 wt% [Zaitseva2012, VanLoef2014], with inherent stability problems connected to the high concentration. Beside the already mentioned advantages (Chapter II) polysiloxane materials may be favoured also in this respect. In the last years they have been successfully tested as plastic scintillators, displaying reasonable light yield and very good radiation hardness [Quaranta2010a, Quaranta2010c, Carturan2011, Quaranta2013, Bell2004, Harmon1991].

It has been reported [Chu1990] that for viscosity ( $\eta$ ) above 50 cP, the mobility of small organic molecules in PDMS is not controlled by system viscosity, but by the micro-viscosity. The former, called also macro-viscosity, depends on the movement of the entire solvent molecules; the latter, called also local viscosity instead, depends on the movement of segments or side groups of the macromolecule. It has been estimated that in polysiloxane rubbers the micro-viscosity can be as low as 10 cP, in

materials with macro-viscosity of  $10^6$  cP. This unique properties of polysiloxanes are connected with free volume fraction, in turn depending on their higher chain mobility [Jones2013], already described in Chapter II. For the same reason, PDMS is also one of the polymers with the highest gas permeability [Robb1968]. The very low micro-viscosity is also at the basis of the observed dependence of the solute interaction rate from the viscosity of the solvent, which becomes almost independent from  $\eta$  for values above 50 cP [Chu1990]. The low micro-viscosity could increase the triplet-triplet interaction probability, thus allowing to achieve an efficient PSD at lower PPO concentrations and consequently reduce the related long term stability issues. In order to investigate the possibility to achieve pulse shape discrimination with polysiloxane plastic scintillators, their time response has been investigated using time resolved spectrofluorimetry, time resolved ion induced luminescence (TRIBIL) at the INFN-LABEC in Sesto Fiorentino, and the pulsed neutron beam at the INFN-LNL in Legnaro. Tests were performed at different PPO concentrations ranging from 1 wt% to 8 wt% with and without LV.

## **5.2 Experimental part**

Since the PPO concentration to be added to the polysiloxane matrix in this case was higher than the usual one, in order to achieve the maximum dye solubility a higher amount of phenyl groups was needed in the base resin, because it was not possible to dissolve 8 % PPO in Poly(22-25mol% diphenylsiloxane-co-dimethylsiloxane) (22PDPS). To achieve this goal, the employed A part was an homopolymer composed by only phenylmethylsiloxane units: Poly(phenylmethylsiloxane) (100PMPS), allowing a better dye solubility at the price of a small reduction in the optical transparency. The synthesis procedure for this material was very similar to the one employed for 22PDPS, and it is extensively described in Chapter II, together with the precise mixture formulation. All the tests were performed on small samples, produced with 1.5 grams of A component resin, having 5 mm thickness and 20 mm diameter. In order to evaluate the effect of the high dye amount on the photophysical properties, fluorescence studies (both steady state and time resolved) were performed on the samples with and without LV. Furthermore, for a better comprehension of the dye concentration effect on the fluorescence spectra, different solutions of PPO in toluene were also analyzed.

## **5.3 Fluorescence emission analysis**

Fluorescence emission spectra for 100PMPS samples at different PPO concentration are shown in Figure V. 1 and Figure V. 2. In both figures, the appearance of a long wavelength tail at high PPO concentrations can be clearly noticed, and its presence was connected with the formation of excimers between an excited state and a ground state PPO molecule. At high dye concentrations, the molecules interaction probability is increasing, and this can be of great advantage for

delayed fluorescence and pulse shape discrimination, but this has also the unavoidable effect of excimer formation and concentration quenching. The latter can be clearly noticed from the non-normalized spectra in Figure V. 2, where the overall emission intensity decreases at increasing PPO concentration. The same effect was observed also for PPO in toluene solutions, in the same range of concentrations (Figure V. 3) and a very similar phenomenon was also observed by Berlman [Berlman1961b] in xylene solutions at 100 g/l.

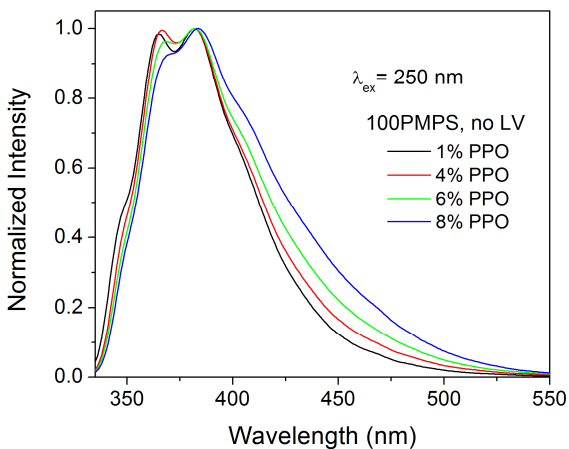


Figure V. 1. Normalized fluorescence emission spectra of polysiloxane samples at different PPO concentrations without LV, recorded with 250 nm excitation.

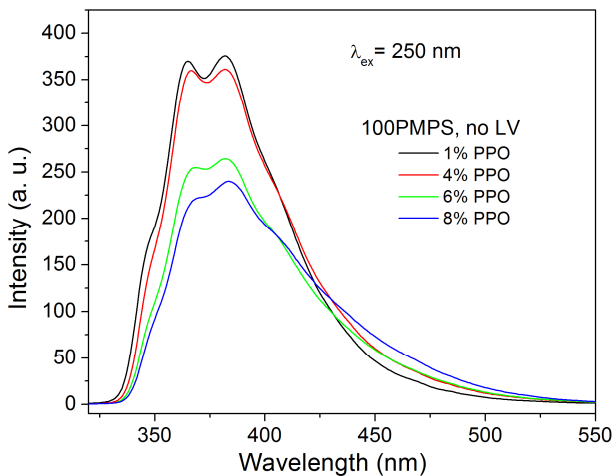


Figure V. 2. Non-normalized fluorescence emission spectra of polysiloxane samples at different PPO concentrations without LV, recorded with 250 nm excitation.

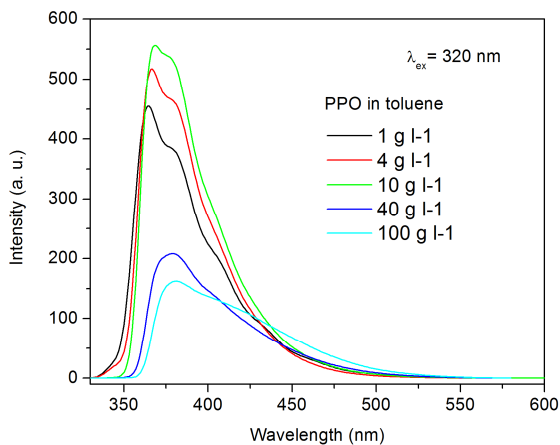


Figure V. 3. Fluorescence emission with excitation at 320 nm different PPO concentrations in toluene.

In order to confirm the attribution of the tail to excimer formation, a deeper investigation was performed as a function the excitation wavelength. As visible from Figure V. 4, for excitation wavelength longer than 360 ns a secondary peak arises at

higher wavelength. The intensity of this peak is again dependent from the PPO concentration, as it can be observed in Figure V. 5, and can be regarded as a further indication of the formation for excimers between PPO molecules.

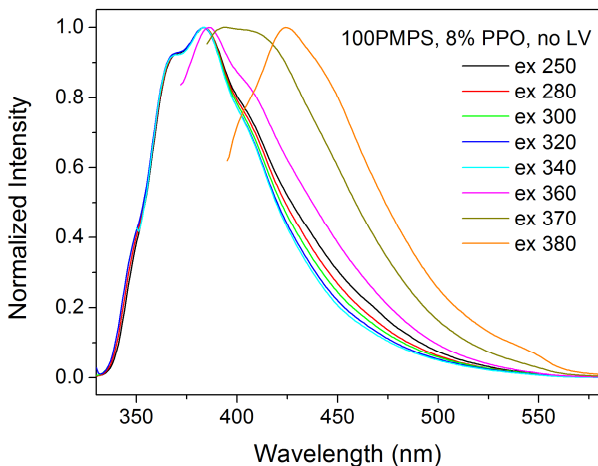


Figure V. 4. Fluorescence emission at different excitation wavelength for a polysiloxane samples with 8% PPO and no LV.

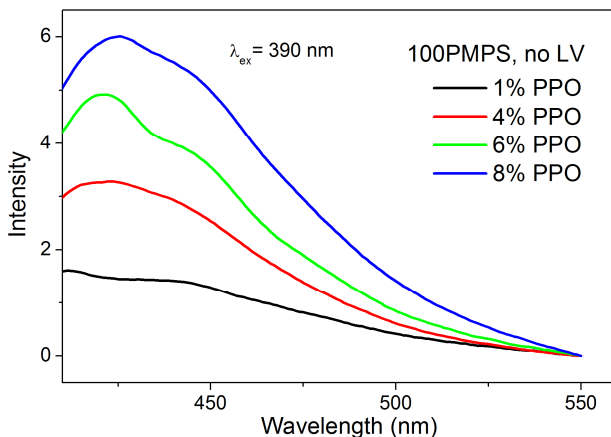


Figure V. 5. Fluorescence emission spectra of different polysiloxane samples, without LV, at different PPO concentrations, excited at 390 nm.

Fluorescence analysis was performed also on the samples doped with 0.02% LV, and the relative emission spectra are shown in Figure V. 6 and Figure V. 7. There

seems to be a reduction in the overall emission intensity at the highest PPO concentrations, but a quantitative analysis of this decrease is not straightforward since many external parameters, including small differences in the measurement geometry and in the quality of the samples could greatly affect the recorded intensity. It is however worth noticing that despite the large variation in PPO concentration, the relative intensity of the LV and PPO peaks shows little changes (Figure V. 7), with only a small reduction of the PPO/LV emission ratio. This effect could be due to a slight improvement in the energy transfer to LV due to the improved energy migration between PPO molecules that allows excitation to reach closer distances from the acceptor molecules. This improvement is however balanced by a reduction in the overall intensity due to concentration quenching effects, whose effect is more important, and is the reason for the decrease observed in Figure V. 6.

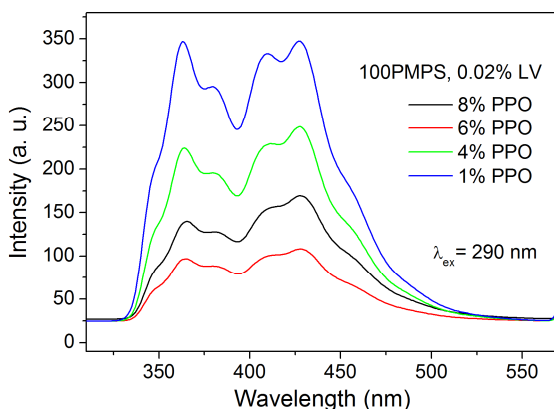


Figure V. 6. As recorded fluorescence emission excited at 290 nm for 100PMPS samples with 0.02% LV and various PPO concentrations.

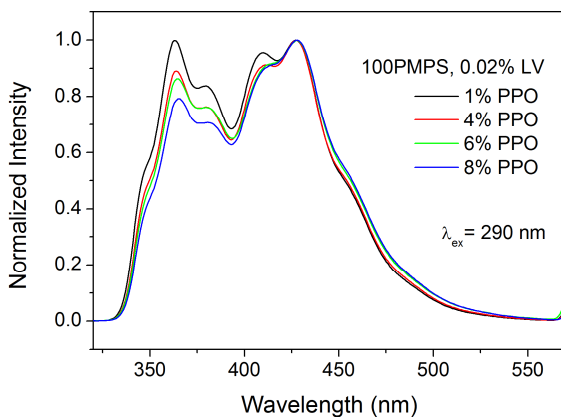


Figure V. 7. Normalized fluorescence emission excited at 290 nm for 100PMPs samples with 0.02% LV and various PPO concentrations.

#### 5.4 Fluorescence lifetime analysis

The fluorescence decay of the polysiloxane samples was investigated for the different PPO concentrations, with and without LV. As clearly visible in Figure V. 8, when recording PPO emission ( $\lambda_{\text{em}} = 385 \text{ nm}$ ) after excitation at 280 nm, the decay curves show a clear multi exponential decay. In order to perform the fit of the curves, a tri-exponential function has been used, showing a fast lifetime of about 1-2 ns, a second one in the range from 7 to 15 ns and a third decay time higher than 25 ns. These components are generally ascribed respectively to the regular singlet-singlet transition [Birks1964, Berlman1973], to excimer formation [Berlman1961b] and, even if with some uncertainty, to triplet-triplet interactions [Marrodan2009, Berlman1973] and their values are in good agreement with other data previously reported for PPO liquid solutions [O'Keeffe2011, Marrodan2009]. The relative intensity of the slow components appears to increase with the concentration of dye (Figure V. 9), and this increase can be associated once again with the formation of excimers [Berlman1961b, Weinreb1962, Birks1967], as already reported also in polysiloxane liquid scintillators.

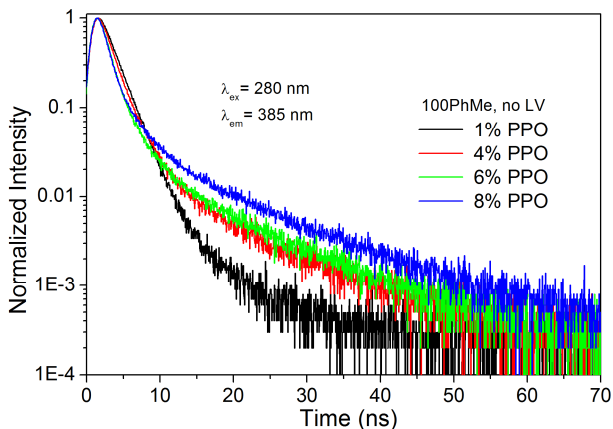


Figure V. 8. Fluorescence lifetime at different PPO concentrations for samples without LV. Excitation wavelength at 280 nm and emission at 385 nm (PPO emission) have been employed for the measurements.

Furthermore, as shown in Figure V. 10 and Figure V. 11, the intensity of the slower component is also increasing with the emission wavelength, and this is a further confirmation that it can be ascribed to excimers, whose emission is more intense at higher wavelengths (Figure V. 1 and Figure V. 2)

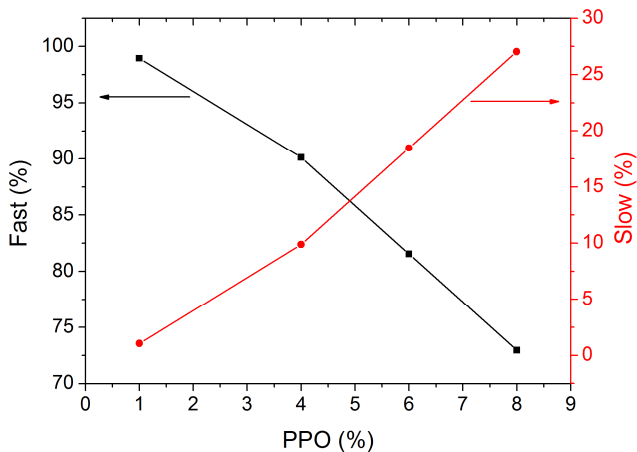


Figure V. 9. Fast and slow component relative intensities, as derived from the fittings of the decay curves, as a function of PPO concentration.

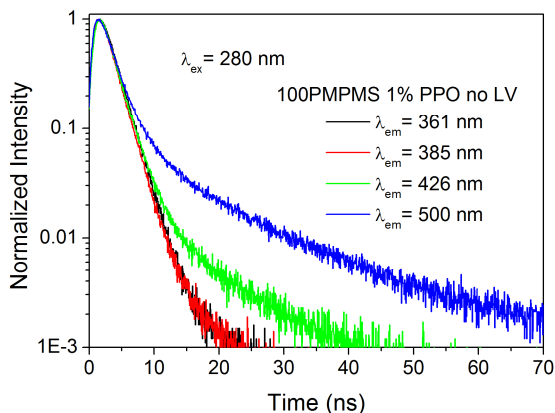


Figure V. 10. Fluorescence decay for a sample with 1% PPO concentration at different wavelengths, excited at 280 nm.

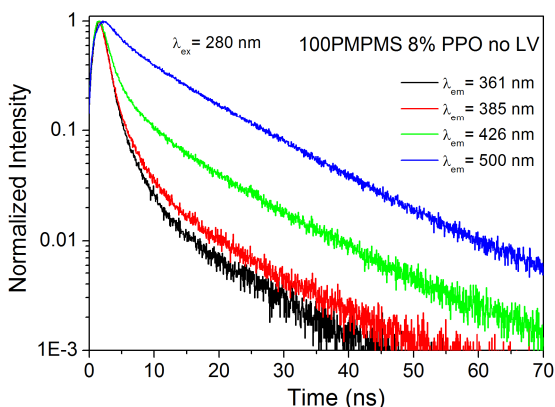


Figure V. 11. Fluorescence decay for a sample with 8% PPO concentration at different wavelengths excited at 280 nm.

As already noticed for liquid polysiloxane scintillators, this phenomenon affects also LV emission lifetime, exhibiting dependence from PPO concentration, as shown in Figure V. 12 and Figure V. 13. In case of LV emission however, the fitting of the decay curve was well performed by a single exponential decay, with lifetimes dependent on the PPO concentration, ranging from 7.2 ns to 9.3 ns, which are in well agreement with the values observed in similar solution of TPTMTS (Chapter IV).

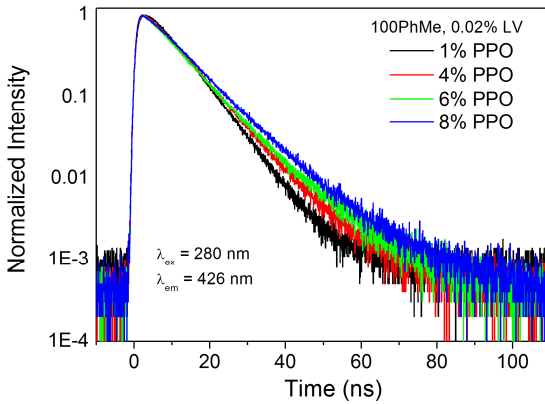


Figure V. 12. Fluorescence lifetime at different PPO concentrations for samples without LV. Excitation wavelength at 280 nm and emission wavelength at 426 nm (LV emission) have been employed for the measurements.

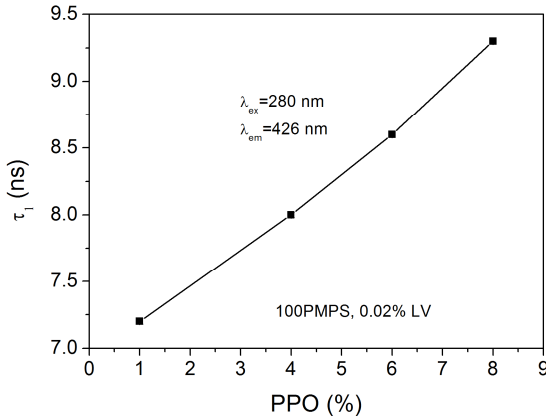


Figure V. 13. Fluorescence lifetime as a function of PPO concentration for polysiloxane scintillators. Emission was recorded at LV emission peak (426 nm) excited at 280 nm.

### 5.5 Time resolved ion beam luminescence (TRIBIL)

100PMPS samples were also analyzed by TRIBIL technique at the INFN-LABEC laboratory, in order to evaluate the change in the light pulse shape with the different ions. The ions employed for the analysis are listed in Table V. 1, together with their main characteristics and the most important interaction parameters in 100PMPS

matrix. Projected range and stopping power values were calculated using the SRIM software [SRIM].

Table V. 1. Main parameters for the ions employed in TRIBIL analysis and their interaction with 100PMPS matrix.

Ion	Mass [amu]	Energy [MeV]	Projected range [ $\mu\text{m}$ ]	$\frac{dE}{dx}$ [ $\frac{\text{keV}}{\mu\text{m}}$ ]
H <sup>+</sup>	1	3	154	12.3
C <sup>3+</sup>	12	10	15.3	775
O <sup>3+</sup>	16	10	12.2	1169

TRIBIL spectra for the different type of ions are shown in Figure V. 14, Figure V. 15 and Figure V. 16. In case of carbon ions (Figure V. 14) and protons (Figure V. 15), a small difference was observed between samples, with the arising of a faint slow component, whose intensity was increasing with the concentration of PPO, as already observed in fluorescence emission for both plastic and liquid scintillators. In case of oxygen ions instead, the difference between samples was negligible.

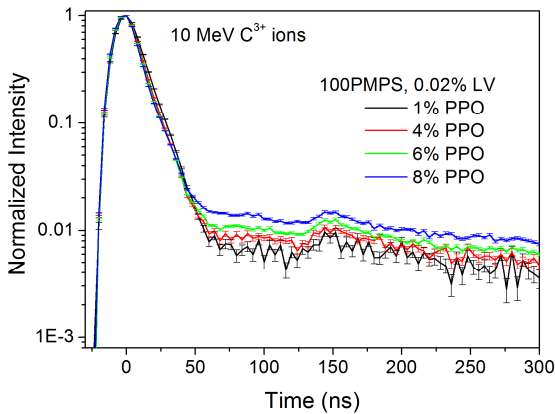


Figure V. 14. 10 MeV C<sup>3+</sup> beam TRIBIL curves at different PPO concentration.

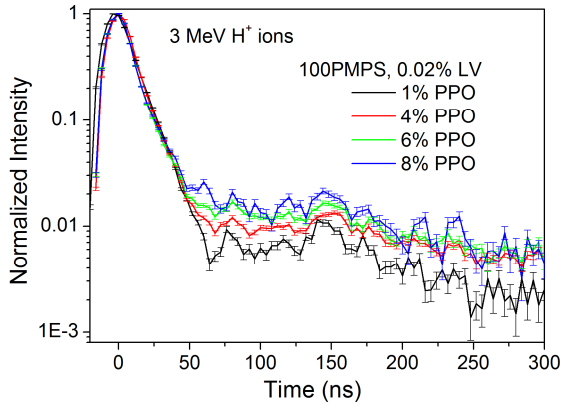


Figure V. 15. 3 MeV proton beam TRIBIL curves at different PPO concentration.

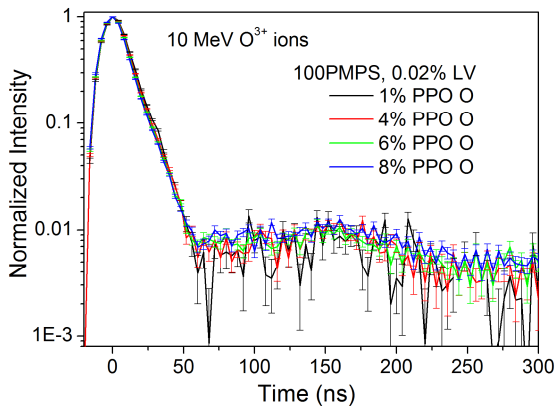


Figure V. 16. 10 MeV  $O^{3+}$  beam TRIBIL curves at different PPO concentration.

Also in this case the fit was performed using a bi-exponential decay function. The faster decay-time ranges between 9 ns and 11 ns, for all the different measurements, which is in quite good agreement with fluorescence lifetime measurements. In order to have a quantitative comparison between the intensities of the slow component in the different cases, the fractional amplitude of the slow term (B%) has been plotted as a function of PPO (Figure V. 18). It clearly appears that in case of protons and carbon ions, B% increases with the PPO concentration even if with different trends, while in case of oxygen ions the differences are within the error bars.

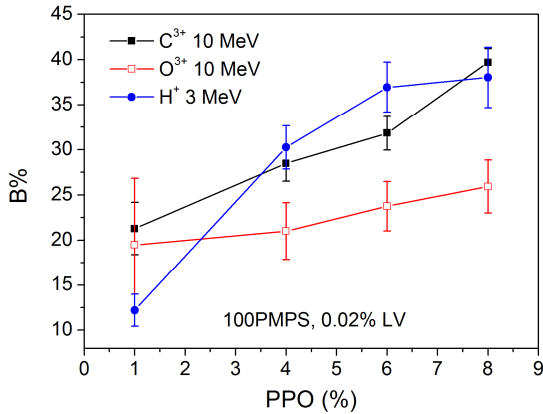


Figure V. 17. Slow decay fractional intensity as a function of PPO concentration measured for carbon ions, oxygen ions and protons.

This unexpected behaviour is most likely due to the change in the concentration of PPO during the measurement session. Carbon and oxygen irradiation were performed on different spots of the same samples, in two consecutive days, and between the two measurements the samples were left overnight in high vacuum. This, combined with the high dye mobility in polysiloxane might have resulted in sublimation of PPO, with a consequent dye depletion of the first layer of the samples, where ion interaction occurs.

As a result, the light intensity of carbon and oxygen light pulses resulted to be almost 30 times larger for carbon ions, while the theoretical difference in the light output, due to the different ionization quenching of the particles, was expected to be linearly dependent with the particles range [Birks1964], and thus only about 20% (see Table V. 1).

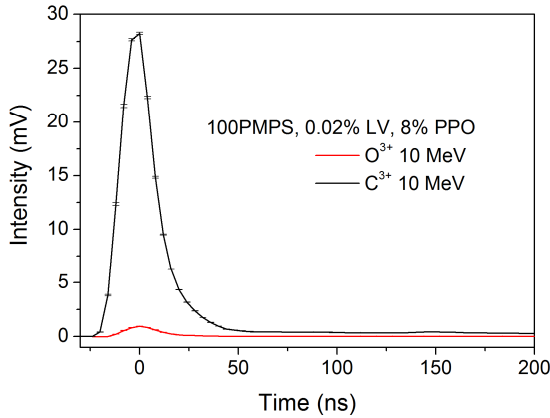


Figure V. 18. Comparison between carbon and oxygen average pulses in a sample with 8% PPO.

On this basis, the comparison between the intensity of the light pulses produced by the different ions becomes difficult, and so the comparison between pulses of different ions, since samples with identical nominal composition might have different PPO concentrations.

Tests with proton beam, instead, were performed on new samples, in order to allow a better comparison with the results achieved with carbon ions. The comparison between pulse shapes didn't show any significant difference between protons and carbon ions (Figure V. 18). Also this comparison however is not straightforward because it was not possible to control the time spent by the samples in the vacuum chamber, and therefore it was not possible to compare with precision two samples with the same nominal composition.

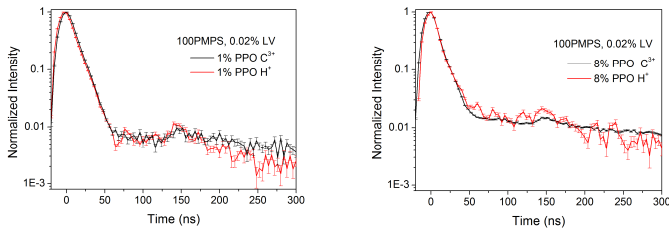


Figure V. 19. Comparison of proton and carbon induced TRIBIL pulses for a sample with 8% PPO concentration.

The comparison of the fluorescence emission of irradiated samples with that of non-irradiated ones showed a strong increase in the fluorescence emission after

irradiation for all the samples except those with 1% PPO, where the difference is negligible (Figure V. 20).

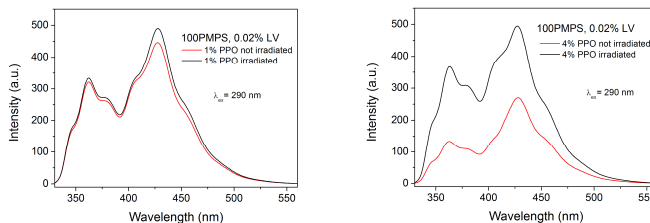


Figure V. 20. Comparison of emission spectra for irradiated and non-irradiated samples with 1% PPO and 4% PPO.

This is a further confirmation of the reduction in the PPO concentration due to the sublimation of PPO in high vacuum. As already shown in Figure V. 6, the intensity of the emission is decreasing with the dye concentration, so that a reduction in this quantity results in more intense emission. This instability of PPO in high vacuum could be the reason for the large differences observed in the light outputs in the work of Zaitseva [Zaitseva2012] and in that of Van Loef [VanLoef2014]. The former work observed a maximum in the light yield for concentrations about 1 wt% PPO, and a decrease light output for higher concentrations, similarly to what reported in the next paragraph for polysiloxane scintillators. Van Loef and co-workers instead, observed a steadily increasing trend up to concentrations as high as 30 wt%. This very large difference can be explained by the slightly different production techniques: in the first case, polyvinyltoluene based scintillator was produced, with PPO concentrations up to 30 wt%, by polymerizing the monomer under nitrogen atmosphere, in the second case polystyrene samples with similar nominal concentrations were produced by polymerisation of the monomer in evacuated containers. The much smaller pressure, kept for several days during polymerization in the second work, results in a smaller effective dye concentration that well explains the differences in the observed behaviours.

## 5.6 Scintillation light yield

The scintillation light yield of the samples was also measured with  $^{241}\text{Am}$ , in order to understand the influence of the high PPO concentration on the samples and in all cases a clear  $\alpha$  peak was visible (Figure V. 21). The scintillation light yield resulted to be decreasing with the PPO concentration, as reported in Figure V. 22, showing an important lowering in the scintillation output for the sample with 8% PPO concentration. This is due to the concentration quenching effect, in good agreement with what already reported for fluorescence intensity and similarly to what observed by other authors [Zaitseva2012]. As a consequence, the light yield decreases from

almost 55% of EJ-212 with 1% PPO, to below 40% in case of 100PMPS with 8% PPO and 0.02% LV.

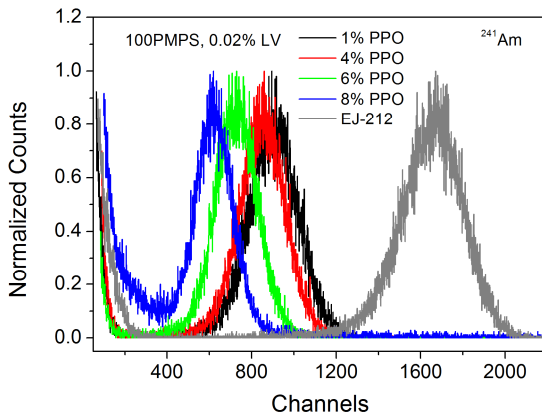


Figure V. 21. Scintillation spectra, measured with  $^{241}\text{Am}$  alpha source at different PPO concentrations. EJ-212 is also shown for comparison.

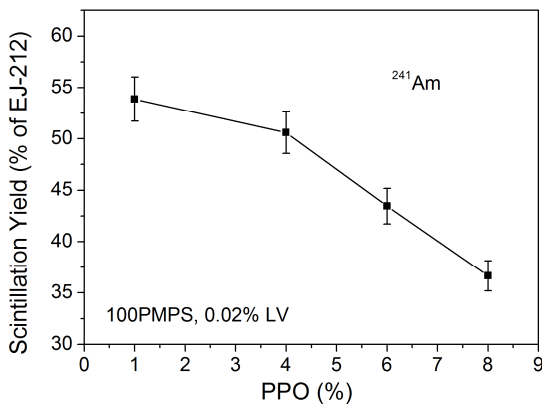


Figure V. 22. Scintillation light yield as function of PPO concentration, measured with  $^{241}\text{Am}$  alpha source.

## 5.7 Scintillation pulses

Scintillation pulse shapes were finally evaluated also for neutron and gammas, using the pulsed neutrons beam at the “CN” accelerator at INFN-LNL, already used also

for polysiloxane liquids. During this test, two samples were compared, having 1% PPO and 8% PPO concentrations and fixed amount of LV (0.02%).

The first important thing, to be noticed from this analysis, is the arising of a slow component, much more intense than in case of TRIBIL measurements. Furthermore, both in case of neutron and gamma rays, there was a clear difference between the signals of the two samples, with a much stronger delayed component in the 8% PPO sample, similarly to what already noticed in polysiloxane liquid samples (Figure V. 23). This effect can be ascribed to increasing dye interaction probability with the PPO concentration, leading to a higher triplet-triplet interaction rate and therefore to a more intense delayed fluorescence.

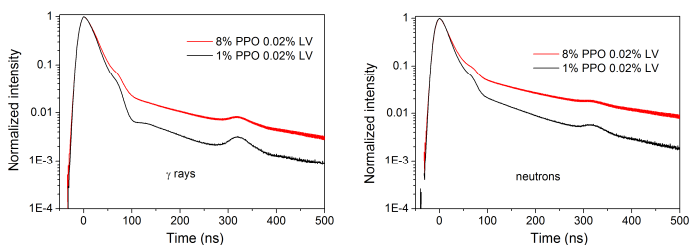


Figure V. 23. Pulse shape comparison between samples with 1% PPO and 8% PPO for neutrons and gamma rays.

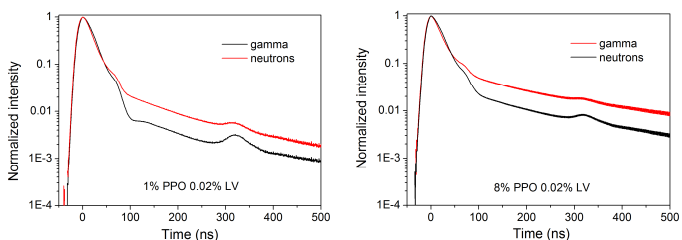


Figure V. 24. Pulse shape comparison between neutron and gamma signals for two different PPO concentrations

Table V. 2. Slow component fractional intensity for neutron and gamma pulses for samples with 1% PPO and 8% PPO.

Sample	B <sub>n</sub> [%]	B <sub>γ</sub> [%]
1% PPO 0.02% LV	23 ± 1	7 ± 4
8% PPO 0.02% LV	41 ± 3	17 ± 4

What is more important however is the clear difference observed between neutron and gamma rays induced pulses even for the sample with only 1% PPO concentration (Figure V. 24). In particular, the difference can be well appreciated in Table V. 2, where the fractional intensities of the slow component in the different cases are reported, showing that the amplitude of the slow component for neutrons is always more than double that of gamma pulses. These results, were never reported before for so low dye concentrations, and confirm the superiority of polysiloxane matrixes in terms of dye mobility.

These data, both as regarding the dependence from the PPO concentration and from the type of radiation of the pulse shapes, do not agree with the TRIBIL measurements results. There are however some main differences between the two types of measurements that could explain this apparent mismatch.

The first difference is that TRIBIL measurements were carried in vacuum, with the result of a decrease in the concentration of PPO in the sample, while scintillation tests were performed at atmospheric pressure. The second notable difference is the type of interaction of heavy ions used in TRIBIL and gamma and neutrons used for this test. As explained in the first chapter, the latter interact randomly with the whole volume of the sample, while the range of the former has a maximum of 155  $\mu\text{m}$  for protons and is ten times smaller for oxygen and carbon ions. As a consequence, TRIBIL measurements are even more sensitive to PPO sublimation, which is affecting much more strongly the surface of the material than the bulk, and is thus influencing TRIBIL measurements much more than neutron or gamma scintillation pulses. In Figure V. 23 the appearance of spurious features between 50 ns and 100 ns and between 300 ns and 350 ns can be noticed. These signals, called "after-pulses" were already described in the previous chapter, and are related to the PMT employed for the measurements.

## **5.8 Conclusions**

In this chapter, an investigation of the response of polysiloxane samples based on poly(methylphenylsiloxane) with different concentrations of PPO and 0.02% LV was reported. The steady state fluorescence measurements, performed also in highly concentrated toluene solutions, showed the arising of a long wavelength tail, corresponding to the formation of excimers between an excited PPO molecule and a ground state one, similarly to what already noticed also in polysiloxane liquid scintillators. This phenomenon is due to the increased dye molecules interaction at high concentrations, leading also, as a side effect, to a decrease in the overall emission intensity due to concentration quenching effects that was confirmed both by fluorescence emission measurements and by scintillation light yield analysis. Fluorescence lifetime measurements, verified the formation of excimers with high dye amounts, showing the arising of a slower decay component in the most

concentrated samples without secondary dye, resulting in an overall lifetime increase in ternary systems.

Time resolved ion beam induce luminescence (TRIBIL) measurements, performed with  $C^{3+}$ ,  $O^{3+}$  and  $H^+$  ions, confirmed once more the arising of a slower component for increasing PPO concentrations, but didn't allow a direct comparison between the signals produced by the different ions, due to the sublimation of PPO in high vacuum, necessary for the measurement. This phenomenon resulted in an uncontrolled decrease in the effective PPO concentration in the first layer of the material, which is also the area of interaction of the impinging ions. The result is however important to be considered in future applications of these materials, showing that these highly doped scintillators are not suitable to be used in high vacuum atmosphere.

The shape in time of neutron and gamma pulses was also analyzed for 1% and 8% PPO concentrations. As already noticed also in polysiloxane liquids and in contrast with TRIBIL measurements, the arising of a slow component was clearly noticed in these measurements, and its intensity was depending both on PPO concentration and on the type of impinging radiation. In particular, due to the higher dye molecules interaction probability, the intensity of the slow decay was increasing with the primary dye concentration, and for the same reason, due to the consequent higher triplet-triplet interaction, there was a clear difference in the pulse shapes between neutrons and gammas. These results are very important, since they were never reported before in plastic scintillators for such low concentrations of primary dye. This seems to indicate that PSD is feasible with polysiloxane based scintillators, even at PPO concentrations as low as 1%. The results are in contrast with what observed during TRIBIL analysis, but the differences can be explained by the different setup employed in the two measurements (especially as regarding the measurements in vacuum) and by the different type of interaction of heavy charged particles in comparison to gamma rays or neutrons. A more detailed analysis needs however to be performed, in order to evaluate the Figure of Merit of the system and also in order to investigate the long term stability of the samples.



# Chapter VI

## Red emitting polysiloxane scintillators

*Part of this chapter has been published in:*

M. Dalla Palma, A. Quaranta, T. Marchi, G. Collazuol, S. Carturan, M. Cinausero, M. Degerlier, F. Gramegna

**“Red Emitting Phenyl-Polysiloxane Based Scintillators for Neutron Detection”**,  
*IEEE Trans. Nucl. Sci.*, vol. 61 n. 4 (2014) pag. 2052-2058 .

M. Dalla Palma, A. Quaranta, S. Carturan, F. Gramegna, T. Marchi, G. Collazuol, M. Cinausero,

**“Red emitting silicones for particles detection: Coupling with APD”**,  
*Proc of Sci.*(2013) 51<sup>st</sup> Intern. Winter Meeting on Nucl. Phys. Bormio, pag. 10.

### 6.1 Introduction

The read-out of a polysiloxane scintillator with an avalanche photodiode would allow combining the promising properties of both components, overcoming the problems connected to the use of PMT, in view of the development of more compact devices, required by several fields of application. One of the main factors limiting the widespread of APD detectors in coupling with scintillators is that the spectral efficiency of these devices is higher in the red part of the visible spectrum, with the maximum responsivity often above 700 nm. Following this consideration, the shifting of the scintillator emission to longer wavelength could allow improving the spectral matching between APD responsivity and scintillator emission [Kalivas2012]. Furthermore, future progresses in microelectronics, with the development of 3D diodes having internal multiplication [DallaBetta2012] could further increase the importance of these considerations, combining direct radiation detection with scintillation detection in a compact, integrated device.

This chapter describes the development of red emitting polysiloxanes plastic scintillators, aimed at improving the optical coupling with APD. In order to achieve this goal, several samples have been produced with different concentrations of secondary dye (LV) and tertiary dye (LR), and their optical properties have been investigated by Uv-Vis and fluorescence spectroscopy optimizing the energy transfer process and maximizing the scintillation light output. These samples have then been tested with  $\alpha$  particles and  $\gamma$  rays, both with PMT and APD readout. The measurements showed a clear improvement in the light output measured by APD in case of red emitting materials in comparison to standard blue emitting ones.

## 6.2 Experimental part

In order to optimize the dye concentration, several samples have been produced using Poly(22-25mol% diphenylsiloxane-co-dimethylsiloxane) based matrix, a fixed concentration of PPO (1 wt%) and different concentrations of LV and LR. PPO concentration was kept fixed on the basis of previous works reported in literature [Quaranta2010c], showing 1 wt% to be the one optimizing the scintillation light yield in polysiloxane plastic scintillators. All the samples were produced with thickness 1 mm and diameter 3 cm.

The optical properties of these samples were tested by fluorescence emission spectroscopy in transmission geometry, in order to reproduce the geometrical configuration of the scintillation process. As explained in the second chapter, in this case, all the reported spectra have been corrected for the spectrofluorometer response curve. Without this precaution, spectra would result distorted at wavelength longer than 600 nm due to the decrease in the instrument detector efficiency. Scintillation light yield of the samples have also been tested with  $^{241}\text{Am}$  and  $^{60}\text{Co}$  using both red emitting PMT and APD. Measurements performed with PMT, were repeated also interposing a 515 nm long pass filter (Figure VI. 1) between the sample and the detector, in order to evaluate the contribution of the red emission to the total emitted intensity.



Figure VI. 1. 515 nm Thorlabs long-pass filter used in this work.

Also red emitting polysiloxane based plastic scintillators were tested for neutron detection at the “CN” accelerator at INFN-Legnaro National Laboratories.

## 6.3 Fluorescence and energy transfer

The first part of the analysis focused on the investigation of the optimal LV concentration in this type of mixture. With this aim, the fluorescence spectra of several polysiloxane scintillators having 1% PPO, 0.02% LR and variable amounts of LV were analyzed and the energy transfer from PPO to LV was studied.

### 6.3.1 Fluorescence emission

Figure VI. 2 reports the emission spectra, excited at 270 nm, normalized on the LV emission peak (425 nm). It is clear that the intensity of the PPO emission (360 nm) decreases at higher concentrations of LV, as an effect of the more efficient energy transfer, so that with 0.04% LV, the energy transfer is almost complete and the relative intensity of PPO is reduced by 10 times. It is also very important to notice that the shape of the PPO emission band is unchanged while decreasing in intensity, meaning that the energy transfer is mainly non-radiative [Valeur2001], and the importance of re-absorption process is small, at least for 1 mm thin samples. For these reasons, 0.04% LV concentration appears to be the one optimizing the energy transfer from the primary dye, and it will be used for the remaining part of the work.

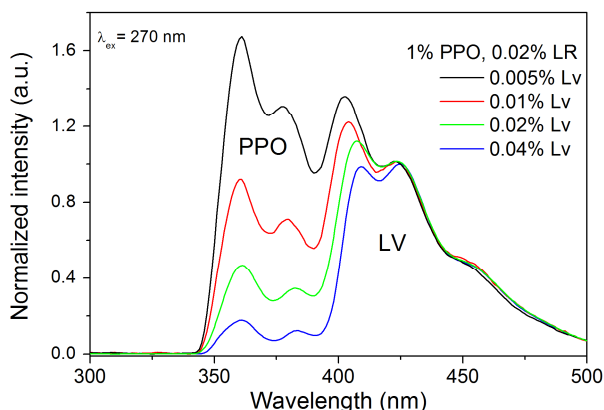


Figure VI. 2. Normalized emission spectra of red emitting polysiloxane samples having 1% PPO, 0.02% LR and different concentrations of LV, excited at 270 nm.

Similarly to LV, also the effect of changing the concentration of LR was analyzed by means of fluorescence measurements. In this case, several samples, with a tertiary dye concentration ranging from 0% to 0.08% were studied, at fixed concentrations of PPO (1%) and LV (0.04%). Once again, the focus of the investigation has been put on the energy transfer between dyes, which is a crucial aspect for the overall scintillation light yield of the material, and is the factor where the dye concentration has the greatest influence.

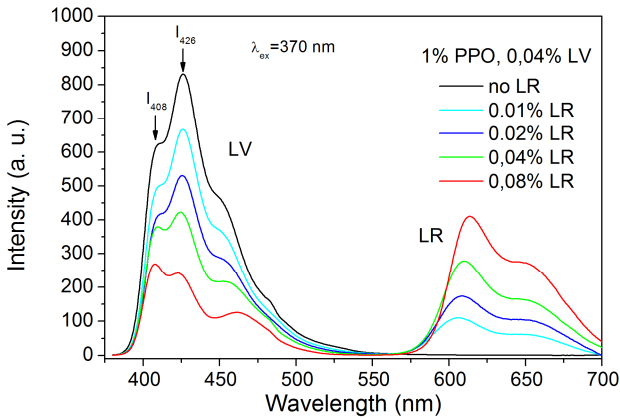


Figure VI. 3. Emission spectra of different samples at fixed 1% PPO and 0.04% LV concentration and with variable amount of LR. Excitation wavelength was fixed at 370 nm.

From Figure VI. 3 it is clear that when increasing concentrations of LR, beside the trivial increase of the emission between 550 nm and 700 nm, there is also a decrease in the LV emission intensity. Differently from what occurring for LV, in this case, the decrease is also followed by a peak distortion, recognisable from the appearance of the local minimum at 450 nm with high LR concentrations, in correspondence to the secondary absorption peak of the dye (Figure VI. 4), and also from the change in the relative intensity between the shoulder at 410 nm and the peak at 425 nm, that is even inverted for the highest LR concentration (Figure VI. 5). The distortion of the LV band is a consequence of the occurrence of radiative energy transfer, and is due to the different absorbance of the dye at the different wavelengths, also called *inner filter effect*. The different type of transfer between primary and secondary dye and secondary and tertiary dye is linked to the lower concentrations involved and to the lower degree of overlap between donor emission and acceptor absorbance, since in the latter case, a secondary absorption peak (450 nm, Figure VI. 4) is involved in the transfer instead of the main one (570 nm) [Valeur2001].

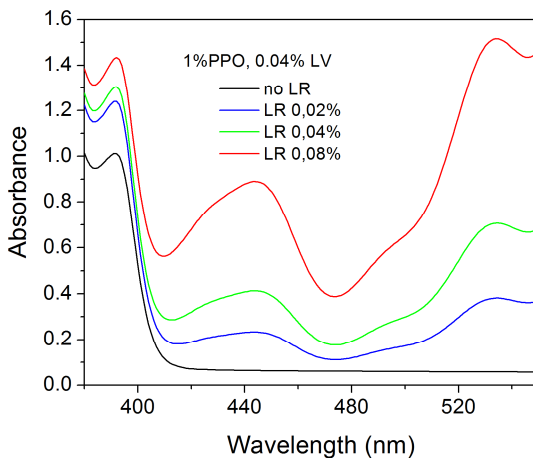


Figure VI. 4. Absorption spectra at different LV concentration, the secondary absorption peak at 450 is clearly visible.

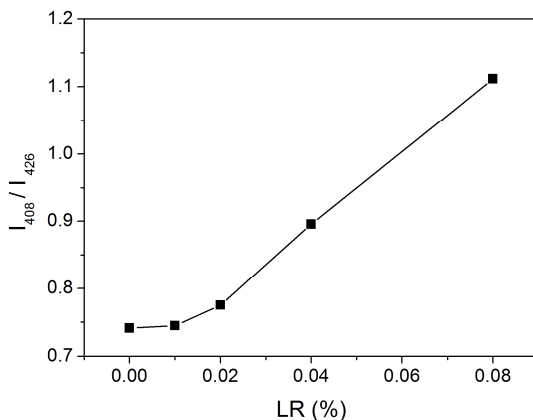


Figure VI. 5. Ratio between the intensity at 408 nm and the intensity at 426 nm as a function of the LR concentration.

A secondary effect to be noticed when increasing the amount of LR dissolved in the polysiloxane is the red shift of its emission peak (Figure VI. 6). This behaviour is due to the self absorption, occurring in the part of the emission band having lower wavelength, due to the partial overlap with its own absorption spectrum. The occurrence of this effect is deleterious for the scintillation light yield of the system since the absorption and re-emission process has efficiency smaller than one, and

the repeating of this process reduces the overall efficiency of the system. For this reason, the maximum concentration of LR has not been increased above 0.08%.

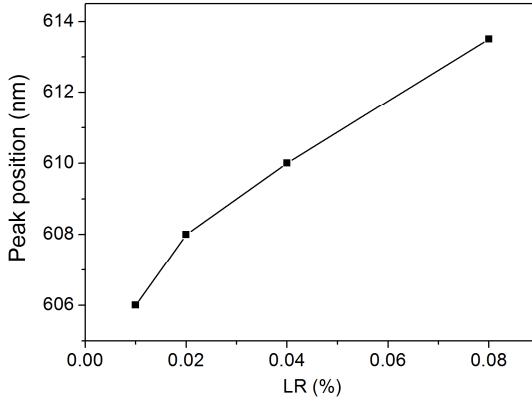


Figure VI. 6. LR peak position as a function of LR concentration.

### 6.3.2 Energy transfer analysis

In order to better understand the effect of LR concentration on the final scintillation light yield, a more accurate study on the energy transfer was performed, for different samples with LR ranging from 0% to 0.08%.

Radiative energy transfer can be quantified through the factor  $a$  (fraction of LV emitted photons absorbed by LR) defined as [Valeur2001]:

$$a = \frac{1}{\Phi_D^0} \int_0^{+\infty} I_{LV}(\lambda) [1 - 10^{-A_{LR}(\lambda)}] d\lambda \quad (27)$$

where  $\Phi_D^0$  is LV fluorescence quantum yield in absence of LR,  $I_{LV}(\lambda)$  is LV fluorescence emission intensity, for a sample without LR, normalized to unity ( $\int_0^{+\infty} I_{LV}(\lambda) d\lambda = 1$ ) and  $A_{LR}(\lambda)$  is LR absorbance at the different dye concentrations calculated using Lambert-Beers law:  $A_{LR}(\lambda) = \varepsilon_{LR}(\lambda) C_{LR} l$ , where  $C_{LR}$  is LR concentration (in g/l),  $l$  is sample thickness in cm and  $\varepsilon_{LR}(\lambda)$  is LR mass absorptivity. Precise thickness values, measured with a micrometer, are listed in Table VI. 1. The absorptivity has been calculated from absorption measurements of LR solutions in acetone with different dye concentrations. Given the linear behaviour of absorbance with concentration,  $\varepsilon_{LR}(\lambda)$  spectrum has been drawn normalizing the absorbance curve of solutions over LR concentration, achieving a very good agreement for the different concentrations used (Figure VI. 7).

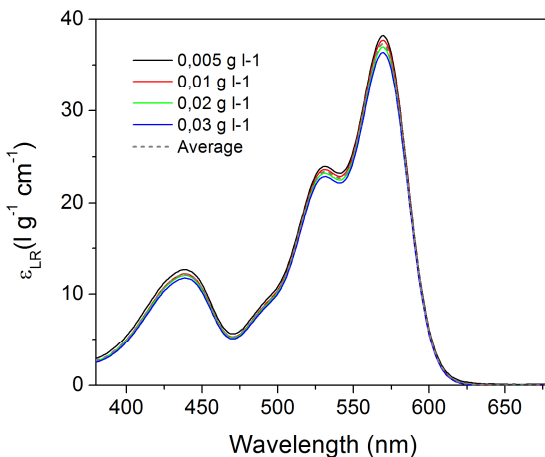


Figure VI. 7. Mass absorptivity as calculated from normalization of measured absorption over concentration.

Table VI. 1. Average sample thickness measured by micrometer.

Sample	Thickness [mm]
1% PPO, 0.04% LV, no LR	$0.69 \pm 0.1$
1% PPO, 0.04% LV, 0.02% LR	$0.74 \pm 0.1$
1% PPO, 0.04% LV, 0.04% LR	$0.77 \pm 0.1$
1% PPO, 0.04% LV, 0.08% LR	$0.76 \pm 0.1$

Factor **a** has been calculated for different percentages of LR dissolved in the matrix, and values are shown in Figure VI. 8. Calculations for those values were done employing either  $A_{LR}(\lambda)$  directly measured from polysiloxane samples, or  $A_{LR}(\lambda)$  calculated from the mass absorptivity measured from acetone solutions, as it can be seen, the agreement between these two values was very good. Factor **a** was consequently used to predict the decrease in LV emission spectrum due to inner filter effect, following the relation  $\frac{I_0}{I} = \frac{1}{1-a}$ , where  $I_0$  is LV emission intensity without LR and  $I$  is the same emission intensity in presence of LR. The so calculated  $\frac{I_0}{I}$  ratio has then been compared with the same ratio achieved from direct measurements of

LV emission intensity, integrated over the range from 390 nm to 550 nm, for different LR concentrations. The comparison of these results is shown in Figure VI. 9.

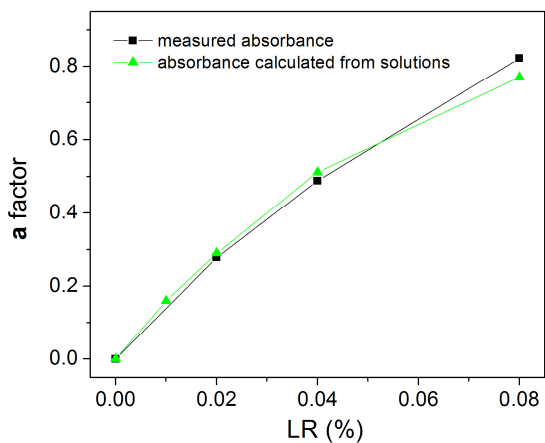


Figure VI. 8. Estimated a factor values.

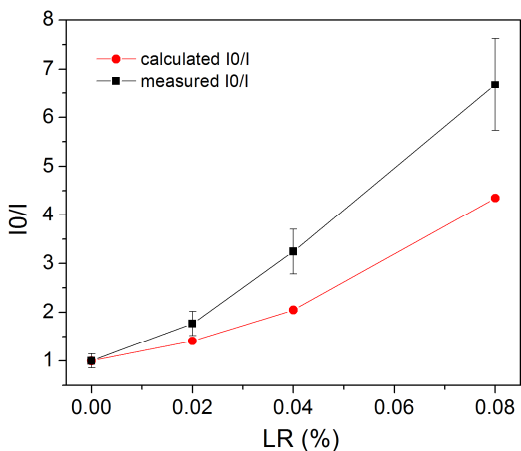


Figure VI. 9. I0/I ratio for different LR concentrations both as measured from fluorescence emission spectra and as calculated from a factor.

As can clearly visible, measured ratio is higher than the expected one, meaning that the emitted intensity decreased more than how expected from radiative energy

transfer. This difference can be explained with the existence of a non radiative energy transfer from LV to LR.

In order to evaluate the importance of this short range transfer, Förster dipole-dipole mechanism has been considered as the leading non-radiative transfer, since the low concentration, and consequently the relatively high intermolecular distance, allows to discard shorter range multipolar columbic interactions or other transitions involving intermolecular orbital overlap (Dexter interaction, charge resonance interaction). These short range mechanisms are indeed effective only for distances below 10 Å while Förster energy transfer can still be operative at much larger distances on the order of 100 Å [Valeur2001, Blasse1994, Lakowicz2006].

In a rigid matrix, with a LR random distribution in the volume of the sample and a dye translational diffusion negligible compared the energy transfer, the following relation can be used to describe the decrease in LV quantum yield due to LR quenching [Valeur2001]:

$$\frac{\Phi_{LV}}{\Phi_{LV}^0} = 1 - \sqrt{\pi} \gamma e^{\gamma^2} [1 - \text{erf}(\gamma)] \quad (28)$$

with

$$\gamma = \frac{\sqrt{\pi}}{2} C_{LR} \frac{4}{3} \pi R_0^3 \quad (29)$$

where  $C_{LR}$  is LR concentration in molecules per Å<sup>3</sup>.

Förster radius  $R_0$ , in cm, can be evaluated using the expression [Lackowitz]:

$$R_0^6 = \frac{9000(\ln 10)\kappa^2\Phi_{LV}^0}{128\pi^5N_A n^4} \int_0^\infty I_{LV}(\lambda)\epsilon_A(\lambda)\lambda^4 d\lambda \quad (30)$$

Where considering for dyes a random orientation, fixed during the lifetime of the excited state, the orientation factor  $\kappa^2$  is assumed to be  $\kappa^2=0.476$ . It has to be remembered however that this value is only an approximation, and errors up to 10% can occur due to the hypothesis of fixed orientation [Lakowicz]. LV quantum efficiency ( $\Phi_{LV}^0$ ) and the matrix refractive index  $n$ , accordingly with suppliers have been taken respectively as  $\Phi_{LV}^0=0.9$  [BASF] and  $n=1.493$  [Gelest] achieving a value for  $R_0$  of about 33.5 Å.

The non radiative transfer efficiency can be consequently evaluated as:

$$\Phi_T = 1 - \frac{\Phi_D}{\Phi_{LV}^0} \quad (31)$$

$\Phi_T$  values for different LR concentrations are shown in Figure VI. 10. As expected, given the low concentration employed, the non radiative transfer efficiency is quite low, as it never goes beyond 10 %.

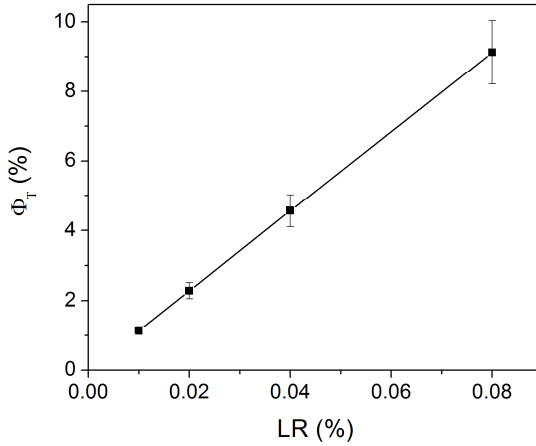


Figure VI. 10. Theoretically calculated resonance energy transfer efficiency from LV to LR at different LR concentrations in samples with 0.04% LV.

Figure VI. 11 shows the relative reduction of LV emission intensity as a function of LR concentration, reporting the measured values and comparing them with a factor alone and with a factor plus non-radiative transfer contribution. From the graph, it is clear that in all cases, the greater contribution to LV intensity decrease comes from the radiative energy transfer, and that the non-radiative transfer efficiency cannot be higher than 20%. Even considering the large variability in the fluorescence measurements there seems to be a certain discrepancy between the measured LV intensity reduction and the one expected from the sum of calculated non-radiative and radiative transfers.

In order to clarify this discrepancy, the non radiative energy transfer efficiency was evaluated also using time resolved fluorescence spectroscopy, according to the equation:

$$\Phi_T = 1 - \frac{\tau_{LV}}{\tau_{LV}^0} \quad (32)$$

Where  $\tau_{LV}$  and  $\tau_{LV}^0$  are respectively the fluorescence lifetime of LV in presence and absence of LR. Figure VI. 12, shows LV decays for different LR concentrations. In all cases, the curves could be fitted by a single exponential decay and as expected, the lifetime is slightly decreasing due to the occurrence of non-radiative energy transfer. The fitting decay times are reported in Table VI. 2 for the different tested samples. Using these data, new values were calculated for the non-radiative transfer efficiency,  $\Phi_T$ , reported in Figure VI. 13.

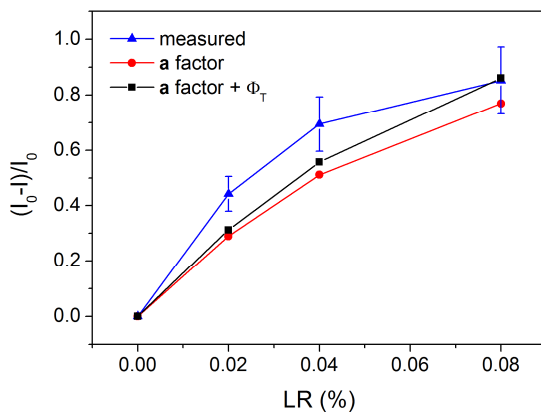


Figure VI. 11. Relative reduction in LV emission intensity as a function of LR concentration. The values are shown as calculated from a factor, from a factor with addition of non radiative transfer and as measured from fluorescence emission.

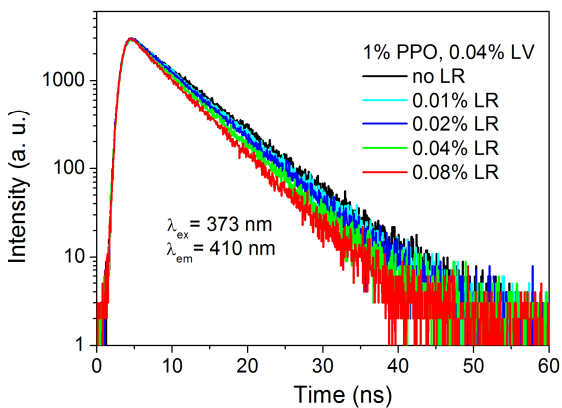


Figure VI. 12. LV fluorescence decays for different LR concentrations.

Table VI. 2. LV decay times, measured at 410 nm for different LR concentrations.

Sample	$\tau_{LV}$ [ns]
1% PPO, 0.04% LV, no LR	$6.42 \pm 0.01$
1% PPO, 0.04% LV, 0.01% LR	$6.04 \pm 0.01$
1% PPO, 0.04% LV, 0.02% LR	$5.81 \pm 0.01$
1% PPO, 0.04% LV, 0.04% LR	$5.46 \pm 0.1$
1% PPO, 0.04% LV, 0.08% LR	$4.99 \pm 0.1$

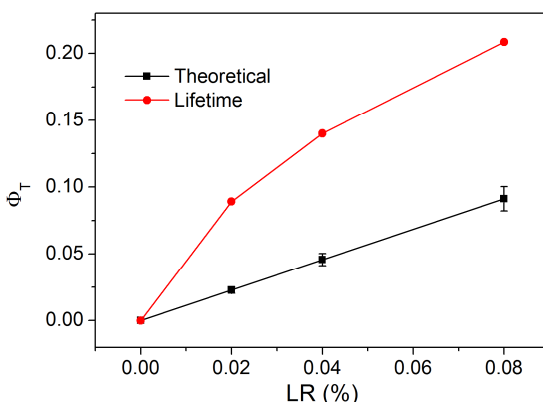


Figure VI. 13. Non-radiative transfer efficiency calculated from LV lifetime decrease. Theoretically calculated values, using Förster theoretical formulation, are also reported for comparison.

The difference between the values calculated theoretically and those measured using the lifetime method, can be at least partially explained with the assumption of a completely rigid matrix, with no molecular diffusion and no molecular rotation. These assumptions are not completely true in the case of polysiloxane matrix due to the higher chain mobility and the higher molecular mobility, and this can be translated into higher energy transfer efficiency. Furthermore, it has to be recalled that all the curves observed were clearly single exponentials, while Förster theory predicts non-exponential decays. This fact was already reported by other authors, and gives an indication of the complexity of the processes involved, and the difficulty to extract precise quantitative description of the system [Birks1968].

Figure VI. 14 shows the comparison between the measured LV emission intensity reduction, due to transfer to LR, and the expected values calculated considering the  $\alpha$  factor and the non-radiative transfer efficiency. As it can be noticed, the best agreement occurs when the non-radiative transfer efficiency calculated with the

lifetime method is considered. This agreement is very good especially up to LR concentrations of 0.04% good, while it is slightly worse at the highest concentration, probably due to non linearity produced by the very high percentage of dye.

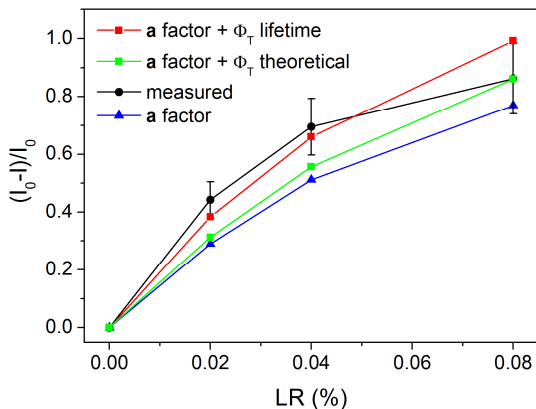


Figure VI. 14. Relative reduction in LV emission intensity as a function of LR concentration. The figure is the same as Figure VI. 11 with the addition of the energy transfer efficiency calculated from the decay times.

Finally, in Figure VI. 15, LR decay curves are shown, recorded at 610 nm, with excitation at 373 nm. From these decays, it clearly appears that LR lifetime is slightly increasing with LR concentration. This phenomenon can be ascribed to inner filter effect, and is a further proof of the occurrence of LR self absorption. This phenomenon has to be minimized in order to achieve the best scintillation light output, since it reduces the overall efficiency of the system.

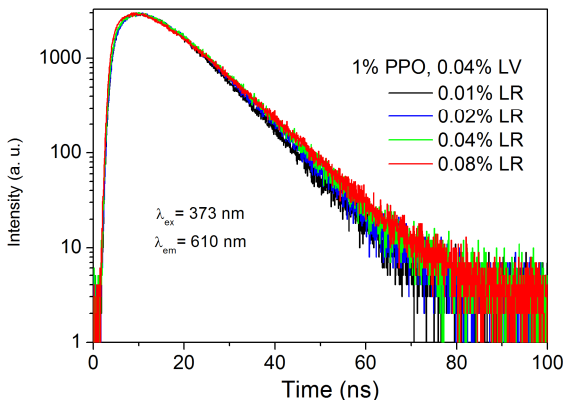


Figure VI. 15. LR emission lifetime at 610 nm with excitation at 373 nm for different LR concentrations

## 6.4 Scintillation light yield analysis

After this preliminary analysis, polysiloxane samples were tested as scintillators, comparing their scintillation light output with that of EJ-212 plastic scintillator.

### 6.4.1 PMT measurements

For a first test, the scintillation light produced by  $^{241}\text{Am}$   $\alpha$  particles was detected using a red enhanced PMT. Measurements were repeated two times, with and without a long-pass filter having its cutting edge at 515 nm, in order to distinguish the contribution of the LR emission to the overall scintillation light. The result of this analysis is shown in Figure VI. 16, where, for comparison, also the spectrum of EJ-212 is shown without filter. No signal could be detected from EJ-212 using the filter since its emission occurs at lower wavelengths, and is completely absorbed by the filter.

As expected, the spectra collected using the filter have a lower light yield, since only part of the emitted light is allowed to reach the detector that has non-zero responsivity in the region of LV emission (Figure VI. 17). It has to be noted how the relative position of the peaks at high and low LR concentrations is inverted. At low concentration (0.01% LR) the overall scintillation light output is slightly more intense than the sample with 0.08% concentration. But once the filter is used, the light yield decreases abruptly, meaning that most of the emitted light comes from LV and has shorter wavelength. With 0.08% LR instead, the light yield decrease observed after using the filter is less important, and the measured scintillation light yield becomes

the highest among polysiloxane scintillators, as a proof of the increased energy transfer, leading to a stronger red emission (see Figure VI. 3 for comparison).

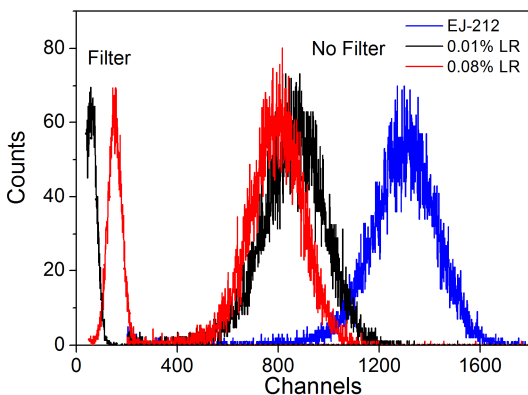


Figure VI. 16. Scintillation spectra, with and without filter, for two samples with 1% PPO, 0.04% LV and two different concentrations of LR (0.01% and 0.08%). EJ-212 is also shown for comparison.

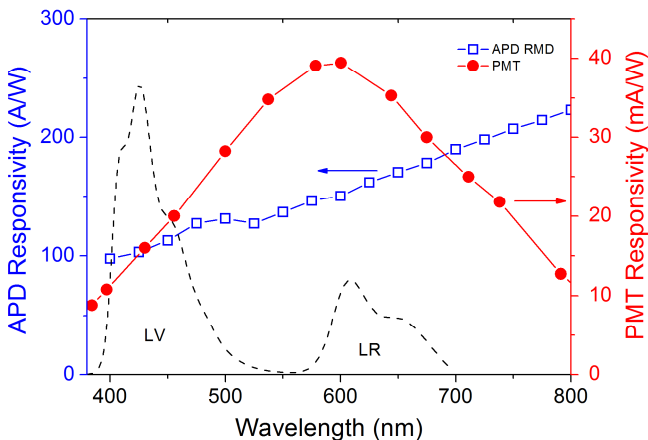


Figure VI. 17. Comparison between the response curve of the red enhanced PMT and APD used in this work. The dashed line shows the typical emission spectrum of red emitting polysiloxane scintillator.

Figure VI. 18 reports the position of the  $\alpha$  scintillation peak, as a function of the LR concentration, expressed relatively to EJ-212, measured with or without filter. It

clearly appears that the total light output is only slightly decreasing for LR concentrations above 0.01%, since the smaller LV emission is almost entirely balanced by the higher red light intensity. The small decrease is related to self absorption effects and to the non-unitary efficiency of the transfer process. It is also worth noting that the overall scintillation light output shows a small increase when going from 0 to 0.01% LR. This can be linked to the improved spectral matching with the PMT response that is balancing the small decrease in the LV emission. The spectra measured with the long-pass filter, instead, show a clear monotonic trend, due to the increased red emission. The non-linearity of this trend is once again connected with self-absorption effects that reduce the light output at elevated concentrations of the dye [Lakowicz2006].

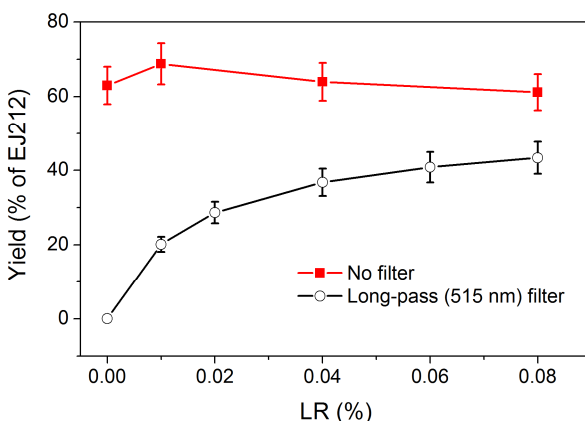


Figure VI. 18. Scintillation light yield, relative to EJ-312, as a function of LR concentration.

#### 6.4.2 APD measurements

Following the measurements with the PMT, polysiloxane scintillators were finally tested using a RMD S0814 APD (see Figure VI. 17 for the spectral response). In this case, tests were performed both with  $^{241}\text{Am}$  and with  $^{60}\text{Co}$ , and the respective scintillation spectra are reported in Figure VI. 19 and Figure VI. 20. As for the PMT, the scintillation light output with  $\alpha$  particles was determined on the basis of the peak centroids positions, in case of gamma rays instead, the position of the Compton shoulder was not easy to be determined, since the reduced thickness of the samples doesn't allow to stop all the recoil electrons produced from the interaction of  $\gamma$  rays within the material. Therefore the scintillation light output was calculated from the end point position of the scintillation spectrum. This was evaluated by fitting the linear part of the spectrum, and by considering the intersection of the fitting line with the abscissa axis. In such a way it was possible to compare the spectra of the

different samples in a reliable way, and to achieve an estimation of relative scintillation yield for  $\gamma$  rays.

From the spectra it clearly appears that the sample with 0.01% LR has a much better scintillation light yield in comparison to the standard polysiloxane scintillator without LR. This phenomenon can be explained by the improvement in the spectral matching factor with concentrations up to 0.01%, which is accompanied by only a small reduction in the overall light yield. For higher concentrations, instead, the reduction in LV emission is more important, and the further improvement in spectral matching is not enough to avoid a decrease in the overall scintillation light yield.

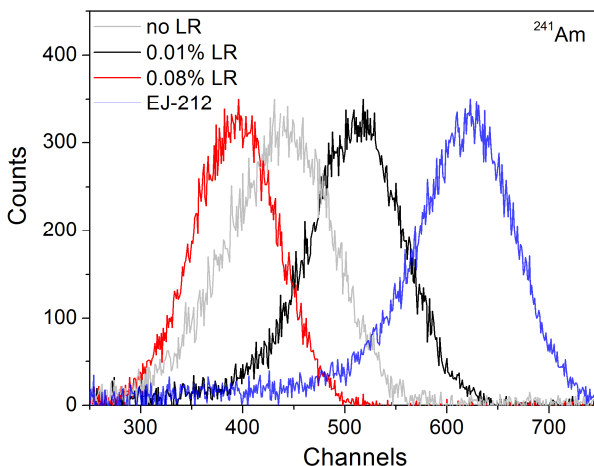


Figure VI. 19. Scintillation spectra produced by  $\alpha$  particles for three polysiloxane samples at different LR concentrations, compared to EJ-212.

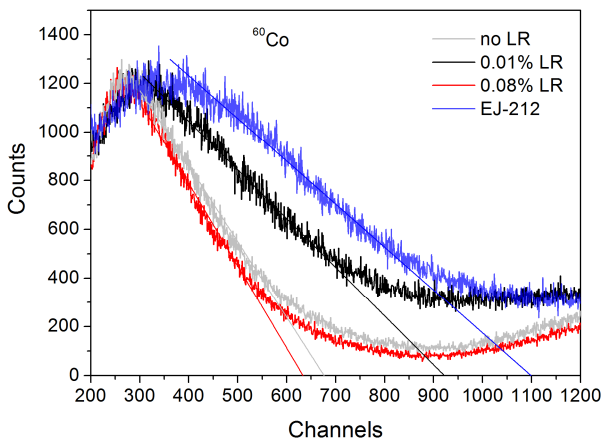


Figure VI. 20.  $^{60}\text{Co}$  gamma rays scintillation spectrum, measured by APD for different LR concentrations. Thin lines represent the linear fit used for the determination of the Compton end point.

The spectra reported in Figure VI. 20 show also an increase in the number of counts at higher channel numbers, roughly over channel 1000. This effect is due to the direct interaction of gamma rays on the APD device, as it can be clearly seen in Figure VI. 21, where the  $^{60}\text{Co}$  spectrum with and without thin polysiloxane scintillator is shown.

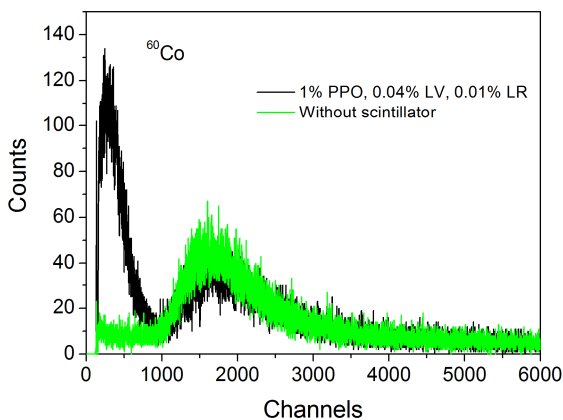


Figure VI. 21. Comparison between the  $^{60}\text{Co}$  gamma spectrum recorded with a red emitting polysiloxane scintillator (0.01% LR) and without scintillator.

The relative scintillation yields measured by APD for  $\alpha$  and  $\gamma$  are summarized in Figure VI. 22 It is worth noting that the trend is very similar for  $^{241}\text{Am}$  and  $^{60}\text{Co}$ , with 0.01% LR being the best performing mixture. In all cases it can be seen that the scintillation light yield increases up to 0.01% LR concentration and then it starts decreasing as an effect of the stronger self absorption and the strong reduction in LV emission. From this analysis it can be observed that the sample with 1% PPO, 0.04% LV and 0.01% LR shows a light output which is, in case of  $\alpha$  particles, 17% higher than the normal blue emitting polysiloxane scintillator without LR, and this improvement is as high as 34% in case of gamma rays, with a relative efficiency about 83% that of EJ-212 commercial scintillator.

The discrepancy in the light yields between  $\alpha$  and  $\gamma$  are due to the different interaction of these particles:  $\alpha$  particles travel only few micrometers in the material, and the emitted light has consequently to travel through the whole thickness;  $\gamma$  rays instead interact more randomly in the whole material, so that, on average, light has to travel a smaller distance, and is therefore less sensitive to self-absorption. This different sensitivity to self-absorption explains the higher light yield reduction shown by the sample with 0.08% LR for  $\alpha$  particles (-7%) in comparison to  $\gamma$  rays (-4%) when compared to the sample without LR.

The overall lower relative light yield of  $\gamma$  rays in comparison to  $\alpha$  particles can be instead explained by the slightly higher thickness of the EJ-212 sample used as reference. This small difference has no effect when comparing the light output from  $^{241}\text{Am}$ , but results in a slightly higher efficiency of EJ-212 to gamma detection and so in a relatively lower light yield in the thinner polysiloxane samples.

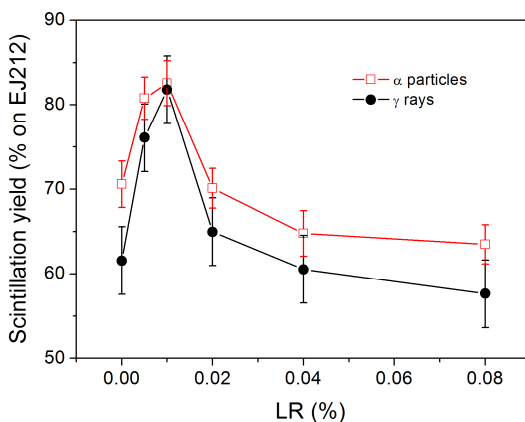


Figure VI. 22. Relative scintillation yield measured by APD for alpha particles and gamma rays as a function of LR concentration.

## 6.5 Neutron response

These samples were finally tested as neutron detectors at the Van de Graaff “CN” accelerator at the INFN-Legnaro National Laboratories, with 2.2 MeV neutron beam. It has to be highlighted that the small thickness of the samples is not the best solution for fast neutron detection, as explained in the first chapter of this thesis. Despite this, the time of flight (ToF) discrimination technique, used to separate the signal induced by neutrons from the signal induced by  $\gamma$  rays, allowed to clearly show the neutron detection capability of these red emitting polysiloxane plastic scintillators. A typical ToF spectrum is shown in Figure VI. 23 for a sample with 0.02% LR concentration. The two peaks represent the signals coming from neutrons and from  $\gamma$  rays. As a proof of that, it is important to notice that the separation between the two peaks is close to 26 ns, which is the foreseen theoretical value in case of  $\gamma$ -rays and 2.2 MeV neutrons travelling a distance of about 60 cm.

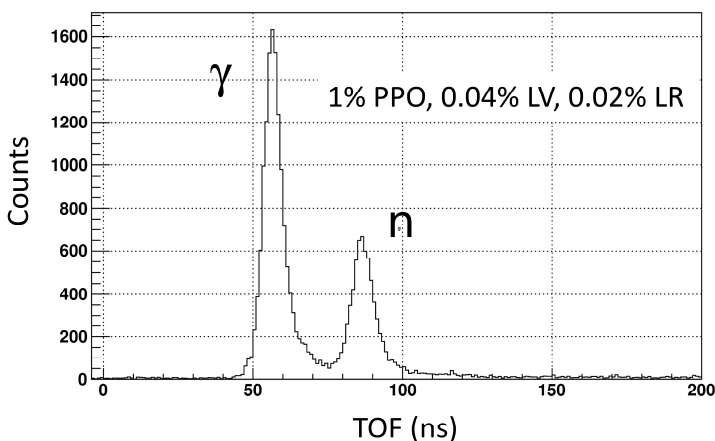


Figure VI. 23. ToF spectrum for a sample with 0.02% LR concentration.

## 6.6 Conclusions

This work showed the development of new red emitting 1 mm thin polysiloxane plastic scintillators, having the aim to improve the spectral matching factor with red sensitive avalanche photodiodes. Beside the primary dye, 2,5-diphenyloxazole, and the secondary dye, Lumogen Violet, already employed in polysiloxane scintillators, a third dye, Lumogen Red, has been added to the polysiloxane matrix, capable of efficiently undergoing energy transfer from the secondary dye. In such a way, the emission of the scintillator was shifted up to over 600 nm. The investigation of the optical properties of the samples at different concentrations, allowed to select 1% PPO, 0.04% LV as the best combination of primary and secondary dye amounts. Fluorescence emission spectra analysis in transmission mode on samples having

1% PPO, 0.04% LV and increasing amounts of LR showed a more intense red emission accompanied by a decrease in the LV intensity, that can be connected energy transfer processes.

From measurements of the scintillation light output performed with a red enhanced PM, with and without 515 nm long-pass optical filter, it could be confirmed that LR contribution increases when going from 0 to 0.08% LR concentration, but they also showed the occurrence of saturation effects at the highest concentrations due to self-absorption. Furthermore, it has been shown that, above 0.01% LR, the decrease in the LV emission is not completely balanced by the red emission, thus resulting in a slight decrease of the overall light yield.

Similar behaviour was observed with an APD detector, both with  $\alpha$  particles and with  $\gamma$  rays. In this case however, an important improvement in the measured scintillation light yield was observed in the sample with 0.01% LR in comparison to blue emitting polysiloxane scintillators without LR. This improvement was of the order of 17% for  $\alpha$  particles and 34% for  $\gamma$  rays, even if the light output relative to EJ-212 was never higher than 83%. Finally, a test with 2.2 fast neutrons using ToF technique, showed the possibility to perform fast neutron detection with this new materials, exploiting the proton recoil process inside the polysiloxane. These results prove that the followed approach is the right strategy toward the development of a compact, efficient and radiation hard detector, coupling red emitting polysiloxanes with APD photodetector.



# Chapter VII

## HYDE experiment

*Part of this chapter has been published in:*

R. Mendicino, M. Boscardin, S. Carturan, G.-F. Dalla Betta, M. Dalla Palma, G. Maggioni, A. Quaranta, S. Ronchin,  
**“Characterization of 3D and planar Si diodes with different neutron converter materials”**,  
*Nucl. Instrum. Meth. A*, 796 (2015), 23-28.

R. Mendicino, M. Boscardin, S. Carturan, M. Cinausero, G. Collazuol, G.-F. Dalla Betta, M. Dalla Palma, F. Gramegna, T. Marchi, E. Perillo, M. Povoli, A. Quaranta, S. Ronchin, N. Zorzi,  
**“Novel 3D silicon sensors for neutron detection”**,  
*J. Inst.*, 9 (2014), C05001.

G.-F. Dalla Betta, M. Boscardin, S. Carturan, M. Cinausero, G. Collazuol, M. Dalla Palma, G. Giacomini, F. Gramegna, C. Granja, T. Marchi, R. Mendicino, E. Perillo, M. Povoli, A. Quaranta, S. Ronchin, T. Slavicek, M. Stefanik, J. Vacik, N. Zorzi,  
**“Hybrid detectors of neutrons based on 3D silicon sensors with PolySiloxane converter”**  
*IEEE NSS/MIC Conf. Rec.* (2013) 106171.

M. Dalla Palma, G. Franco Dalla Betta, G. Collazuol, T. Marchi, M. Povoli, R. Mendicino, M. Boscardin, S. Ronchin, N. Zorzi, G. Giacomini, A. Quaranta, S. Carturan, M. Cinausero, F. Gramegna,  
**“Hybrid detectors for neutrons combining phenyl-polysiloxanes with 3D silicon detectors”**  
*3rd International Conference on Advancements in Nuclear Instrumentation, Measurement Methods and their Applications (ANIMMA), IEEE, 2013, p. 1-9.*

### 7.1 Introduction

As a result of the already mentioned  $^3\text{He}$  shortage [CRSreport2010, Hurd2014], in the last period there has been an increasing attention towards the development of solid state neutron detectors [McGregor2013].

HYDE experiment (HYbrid DETector for neutrons) aims at the development of a pixel hybrid detector for neutrons, by filling the cavities of a 3D silicon diode with a suitable thermal neutron converter. This could allow to produce a new compact detector with good spatial and temporal resolution, capable of interesting neutron imaging performances that could find many application in medical physics [Strobl2009], homeland security [Kouzes2010], forensics [Varga2009], nuclear and high energy physics and others [Caruso2010]. As already explained in Chapter I, direct neutron detection is not possible, also in solid state detectors, and for this reason a neutron converter is needed, which, depending on the energy of incoming neutrons, can be an hydrogen rich material for fast neutrons [Uher2008] or a thermal neutron converter, mostly  $^{10}\text{B}$  or  $^6\text{Li}$ , but also  $^{157}\text{Gd}$  and  $^{113}\text{Cd}$  [McGregor2003, Jakubek2006].

Detector geometry has also a great importance, since it allows enhancing the efficiency of the system by increasing the sensitive area. In this respect 3D sensors represent an advantage over planar sensors. Several different geometries have been proposed, including Si columns surrounded by  ${}^6\text{LiF}$  or  ${}^{10}\text{B}$  converter [McGregor2013, Shao2013], single [Bellinger2012] and double sided Si trenches filled by  ${}^6\text{Li}$  [Fronk2015], sinusoidal trenches [McGrregor2009], and cylindrical holes filled by converter [McGregor2013].  ${}^{10}\text{B}$  as a converter has the advantage of the larger cross section, but it can be fully exploited only with very small dimensions of the neutron converting part. On the other side,  ${}^6\text{Li}$  has the advantage of higher conversion product energies and longer ranges that allow for larger dimensions and higher discrimination thresholds. In this chapter, the preliminary results on the investigation of the performances of a first design of 3D silicon sensors filled with different type of converters for fast and thermal neutrons are reported, and compared with the results of planar silicon diodes.

## 7.2 Experimental part

### 7.2.1 Device structure

3D silicon diodes were produced at FBK, using a single p-type column design, [Piemonte2005], with  $n^+$  3D electrodes and  $p^+$  planar ohmic contacts in the back side,  $n^+$  regions of each cavity were isolated by p-spray thin layer, and all metal contacts were placed on the same side of the device thanks to  $8\ \mu\text{m}$  narrow polysilicon columns (Figure VII. 1). In this first batch, the 3D structure was composed by  $200\ \mu\text{m}$  side cubic cavities, having 8 polysilicon columns on the bottom (Figure VII. 2), with  $400\ \mu\text{m}$  pitch. The thickness of the silicon below the cavities was instead of about  $30\ \mu\text{m}$ .

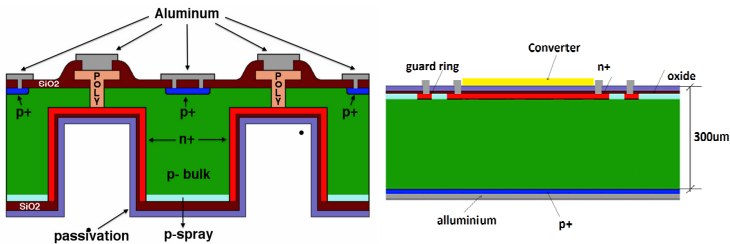


Figure VII. 1. Cross-sectional view of the structure of the HYDE 3D diode (left) and the planar diode used for comparison (right).

For these preliminary tests, all the electrodes were shorted in order to allow a much simpler test procedure and avoid bump bonding process, so that the tested device was finally composed by a sensitive square area with  $5\ \text{mm}$  sides, containing 144 cavities.

## 7.2.2 Polysiloxane deposition

The cavities were filled with different type of materials. In case of fast neutron detection, the converter employed was either Poly(22-25mol% diphenylsiloxane-co-dimethylsiloxane) (22PDPS), already described in Chapter II, or condensation curing polydimethylsiloxane (PDMS), with the latter to be preferred due to its higher hydrogen content (79 mol/l against 71 mol/l for 22PDPS). After mixing of the components and a first quick deaeration step, in order to assure the good adhesion between the converter and the silicon wall, the fluid resin was poured on the surface of the device, and left in low vacuum for some minutes in order to allow the release of the air trapped inside the silicon wells. When restoring the atmospheric pressure, the pressure difference pushes the resin inside the cavities, thus allowing the complete filling. The whole system was finally placed in oven at 60 °C overnight for cross-linking.

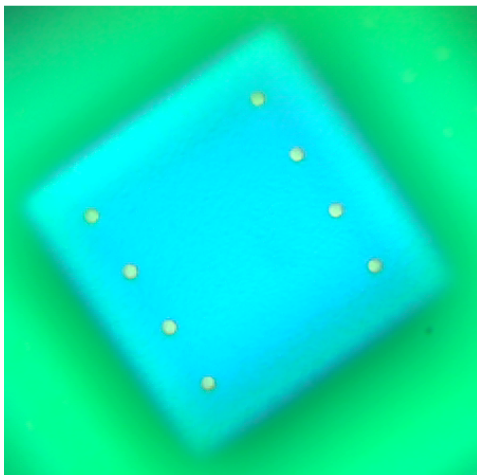


Figure VII. 2. Optical microscope image of the 3D diode, showing the 8 polysilicon columns on the bottom of the cavity.

Figure VII. 3 shows a scanning electron microscope picture of the cross section of a silicon cavity filled by polysiloxane. The very good adhesion between the converter and the diode is visible, confirming the validity of the filling procedure and the good adhesion between silicon and polysiloxane.

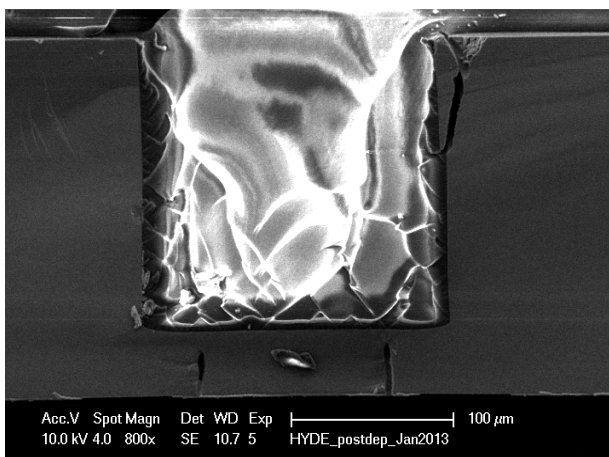


Figure VII. 3. SEM image in cross-section of a silicon cavity filled with polysiloxane.

### 7.2.3 Thermal neutron converters deposition

Table VII. 1. Different type of sample employed in thermal neutron detection tests.

Sample	Material	Converter	Deposition technique
${}^6\text{LiF}$	Enriched sub-micrometric LiF powder	${}^6\text{Li}$	Dry mechanical filling
PDMS carborane	Polydimethylsiloxane doped with 10 wt% o-carborane	${}^{10}\text{B}$	Polysiloxane resin filling
PDMS ${}^{10}\text{B}$	Polydimethylsiloxane doped with 30 wt% enriched B powder	${}^{10}\text{B}$	Polysiloxane resin filling
${}^{10}\text{B}_4\text{C}$ 30 min	Thin enriched $\text{B}_4\text{C}$ layer	${}^{10}\text{B}$	Sputtering 30 min
${}^{10}\text{B}_4\text{C}$ 1h	Thin enriched $\text{B}_4\text{C}$ layer	${}^{10}\text{B}$	Sputtering 1h
${}^{10}\text{B}$	Thin enriched metallic B layer	${}^{10}\text{B}$	Sputtering 1h

In order to perform thermal neutron detection, the filling of the wells with neutron converting materials was needed. With this purpose several different strategies were employed, involving direct mechanical filling of the cavities with enriched sub-micrometer size LiF powder, filling of the cavities with polysiloxane containing  ${}^{10}\text{B}$

rich compounds (o-carborane or metallic  $^{10}\text{B}$  powder), or direct physical vapour deposition of thin layers of metallic  $^{10}\text{B}$  or  $^{10}\text{B}_4\text{C}$  (Table VII. 1).

$\text{LiF}$  filling was performed at the Czech Technical University in Prague, by pressing the enriched  $\text{LiF}$  powder, with average grain size smaller than  $1\ \mu\text{m}$ , inside the wells of the diode. Figure VII. 4 shows the SEM image of a 3D diode filled with  $\text{LiF}$  powder. Thanks to the small dimensions of the powder, the filling was complete and quite homogeneous.

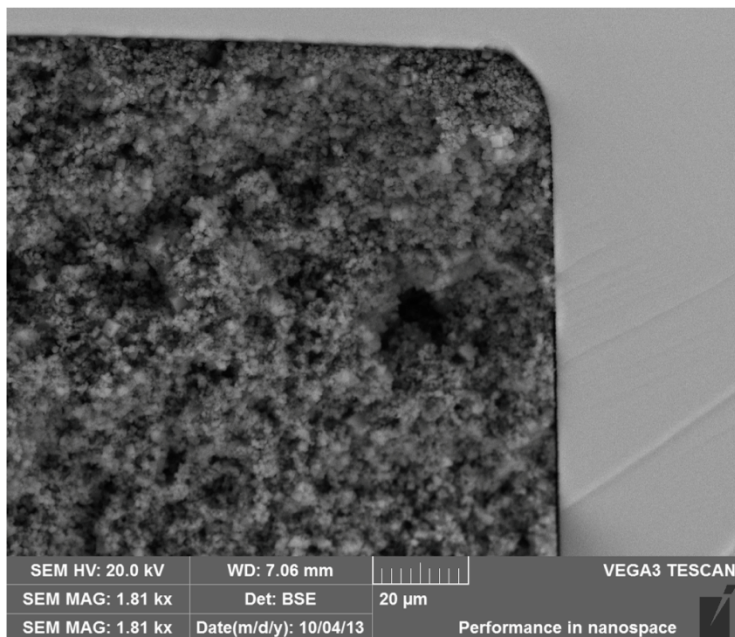


Figure VII. 4. SEM image of the cross-section of a 3D diode filled with  $^6\text{LiF}$  powder.

The samples with PDMS containing 10% o-carborane or 30% metallic  $^{10}\text{B}$  were produced by dispersing the desired quantities of additives in the A part resin. After the dispersion, the remaining components of the resin were also added and the cavities were filled as already described above.

Also in this case, SEM analysis of the filled cavities showed a very good adhesion between the polysiloxane and the silicon wall, even if, in case of metallic boron powder, the large grain size, up to tens of micrometers, didn't allow a homogeneous distribution of the converter inside the material (Figure VII. 5).

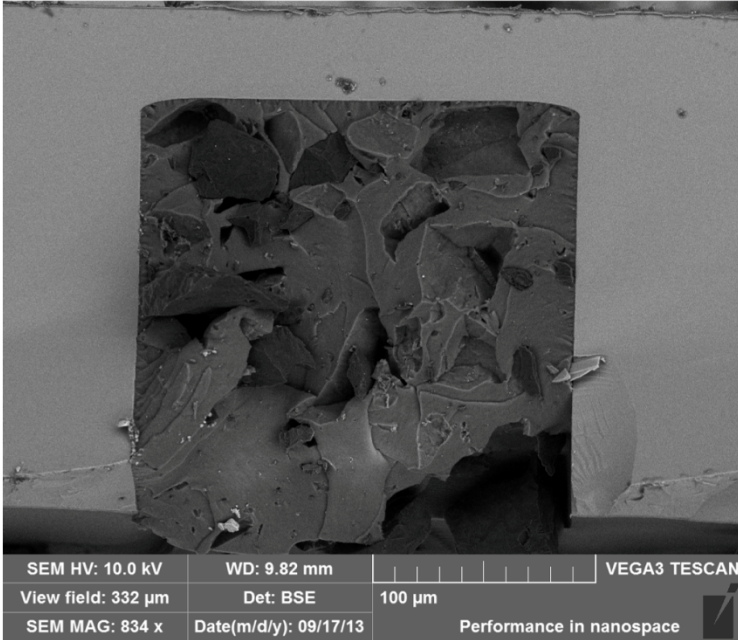


Figure VII. 5. SEM cross-section image of a 3D sensor filled with PDMS containing 30% of metallic  $^{10}\text{B}$  powder.

Thin converter layers were deposited via sputtering, both on planar and 3D sensors. Two different enriched  $\text{B}_4\text{C}$  depositions were performed, with deposition time 30 minutes and 1 h, resulting in a thickness of roughly  $0.5\ \mu\text{m}$  and  $1\ \mu\text{m}$ , while for metallic  $^{10}\text{B}$ , 1 h deposition resulted in a converter layer of about  $0.4\ \mu\text{m}$  (Figure VII. 6). In case of planar sensors, given the presence on the front side of metal contacts, a tape mask was applied before sputtering, in order to avoid the deposition of the converter on the contacts that would have hindered the charge collection. In planar devices therefore, there was a small variability of about 10% in the area of the deposited layer, due to the low reproducibility in the masking process (Table VII. 2).

Table VII. 2. Geometrical parameters of the deposited converter layers on planar Si diodes.

Sample	Thickness [ $\mu\text{m}$ ]	Area ( $\text{mm}^2$ )
$^{10}\text{B}_4\text{C}$ 30 min	$0.4\pm 0.1$	1.45
$^{10}\text{B}_4\text{C}$ 1h	$1.0\pm 0.1$	1.53
$^{10}\text{B}$	$0.5\pm 0.1$	1.46

The thickness of the deposited layers was measured by a profilometer and from SEM images, with a good accordance between the two techniques. The area instead was evaluated from optical microscope images, after a proper calibration.

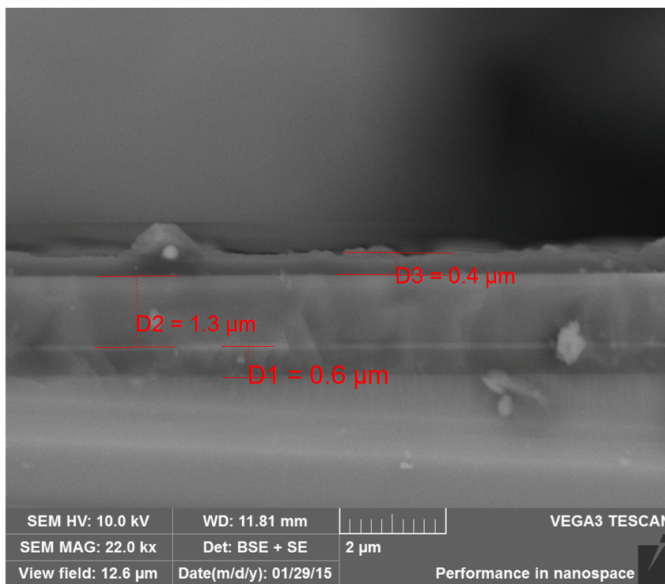


Figure VII. 6. Cross sectional SEM image of a  $^{10}\text{B}$  thin layer deposited on the planar detector surface.  $1.3\ \mu\text{m}$  metal layer and  $0.6\ \mu\text{m}$  oxide layer are also clearly distinguished.

As visible from the comparison of the sputtering time with the layer thickness, the deposition rate for metallic boron was half that of  $\text{B}_4\text{C}$ , but as clearly visible from Figure VII. 7, the quality of the deposit was better.  $\text{B}_4\text{C}$  layers, in fact, resulted to be highly stressed, and shortly after the deposition the surface was covered by wrinkles in the whole surface (Figure VII. 8).

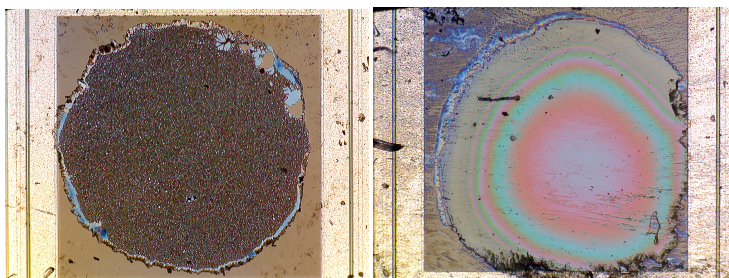


Figure VII. 7. Comparison between optical microscope images of  $\text{B}_4\text{C}$  1h and metallic B deposition.

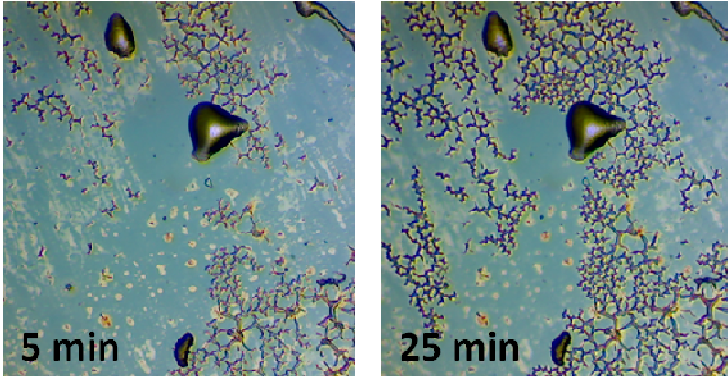


Figure VII. 8. Time evolution of the B<sub>4</sub>C deposit. The increased number of wrinkles is clear.

#### **7.2.4 Neutron Tests**

As already mentioned, 3D hybrid detectors were tested both with fast and thermal neutrons in different facilities. The read-out system was the same in all tests, and was composed by CREMAT CR-110 charge sensitive amplifier, Cremat CR-200 gaussian shaping amplifier (4  $\mu$ s peaking time) and AMPTEK MCA8000a multichannel analyzer.

##### **7.2.4.1 Fast neutrons**

A first test of the performances of the device was performed using fast neutrons at the Van de Graaff “CN” accelerator at INFN-LNL laboratories, exploiting the  ${}^7\text{Li}(p,n){}^7\text{Be}$  reaction of 4.0 MeV protons on a LiF target, producing 2.3 MeV neutrons, with a flux of about  $10^2$  neutrons  $\text{cm}^{-2} \text{s}^{-1}$  at a distance of 60 cm from the target, in forward direction, corresponding to the position of the sample during the irradiation. Each measurement was run for approximately one hour in order to acquire enough statistics.

Further tests with fast neutrons were performed at U-120M Isochronous Cyclotron in Rez (CZ), where fast neutrons with a wide energy range from 4 to 12 MeV were produced by the reaction of  ${}^2\text{H}$  ions on a thick Be target, with fluxes higher than  $10^6$  neutrons  $\text{cm}^{-2} \text{s}^{-1}$ . In this case, each sample was irradiated for 20 minutes.

##### **7.2.4.2 Thermal neutrons**

Tests with thermal neutrons on 3D sensors were firstly performed at the LVR-15 research nuclear reactor in Rez (CZ), using a collimated neutron beam, with a flux

about  $1.5 \cdot 10^7$  neutrons  $\text{cm}^{-2} \text{s}^{-1}$ . In this case, in order to compare different detectors, a scintillator counter was monitoring the effective dose.

Further measurements on 3D and planar sensors were performed at the TRIGA research nuclear reactor at Jožef Stefan Institute Ljubljana (SLO), having a thermal neutron flux of about  $10^6$  neutrons  $\text{cm}^{-2} \text{s}^{-1}$ . Measurements were run for one hour in case of planar sensors and only 20 minutes for 3D sensors, having a larger sensitive area.

### 7.3 Performances of 3D hybrid detectors

#### 7.3.1 Fast neutrons

First tests were performed at the “CN” accelerator at INFN-LNL laboratories, comparing the energy spectrum of 3D diodes, with and without polysiloxane converter, measured with neutrons and with a  $^{60}\text{Co}$  calibration source. Figure VII. 9 shows the comparison of the spectra measured by the same sensor with  $^{60}\text{Co}$  gamma rays and with fast neutrons. For low energies the spectra are very similar, while for energies above 0.25 MeV they start to diverge, showing higher counts number in case of fast neutrons. This effect is due to the interaction of fast neutrons with the polysiloxane converter, producing recoil protons that can be detected by the silicon sensor. The number of counts is quite small, due to the small detection volume and to the non-optimized geometry. This first test however showed the feasibility of the concept, even if large improvements were needed.

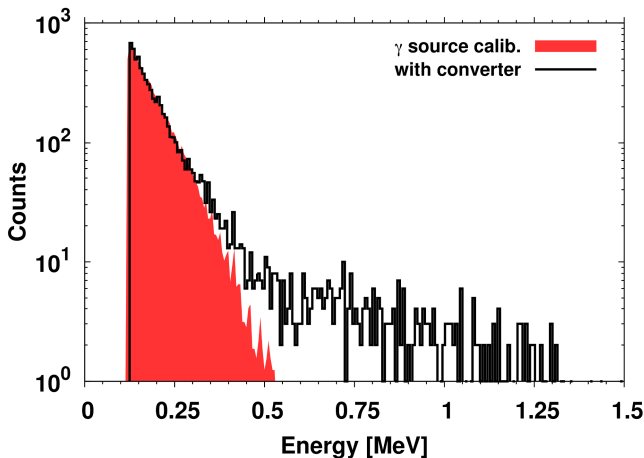


Figure VII. 9. Energy spectrum of fast neutrons compared with that of  $^{60}\text{Co}$  gamma rays, for a sample filled by 22PDPS.

A second test, employing higher energies, was performed at the U-120M Cyclotron in Rez (CZ). In this case, the neutron flux was much higher, so that, even if the measurements were run for a shorter time (20 min instead than 1 hour), the number of counts was much higher.

Figure VII. 10 shows the comparison of the spectra produced by fast neutrons on 3D sensors filled by PDMS (two different samples) and by PDMS with 10% o-carborane. Data acquired without polysiloxane converter are also shown for comparison. The improvement in the detection rate due to the presence of the converter is clear, with much higher counts in the case of polysiloxane filled cavities in comparison to the empty ones. It is interesting to notice that the presence of 10 % o-carborane concentration, aimed at improving thermal neutron detection capability, doesn't affect the performances of the detector, and a greater variability can instead be due to geometrical factors like converter thickness (compare sample 1 and sample 2, having same composition), that needs also to be optimized in dependence of neutron energies.

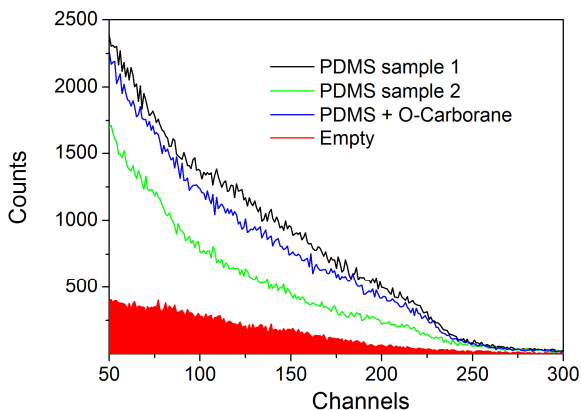


Figure VII. 10. Energy spectra produced by fast neutron on 3D silicon diodes filled with different types of converters.

### 7.3.2 Slow neutrons

As regarding thermal neutron detection, different 3D sensors employing different types of converter were tested at the LVR-15 research reactor in Rez (CZ). In this first test, sensors filled with  ${}^6\text{LiF}$  powder, with PDMS + 30% metallic  ${}^{10}\text{B}$  and with PDMS + 10% o-carborane were analyzed and compared to empty sensor. Energy spectra measured during these runs are shown in Figure VII. 11. In this figure, is clear that  ${}^6\text{LiF}$  powder represents the best solution, despite the lower neutron capture cross section of  ${}^6\text{Li}$  in comparison to  ${}^{10}\text{B}$ , due to the combined effects of the

longer ranges and of the higher energies deposited in silicon by  ${}^6\text{Li}$  reaction products, that allows to record more events at energies above the discrimination threshold [McGregor2013]. Very rough estimates of thermal neutron efficiency (Table VII. 3) indicated for  ${}^6\text{LiF}$  powder an efficiency almost 20 times higher than the best boron containing sample. It is interesting to notice that in the  ${}^6\text{LiF}$  spectrum, the signal produced by the two different reaction products can be clearly distinguished: at higher channels 2.72 MeV tritium peak and at about channel 60 the signal produced by 2.05 MeV  $\alpha$  particles.

Furthermore, the use of metallic boron converters seems to be more effective than the use of o-carborane, that doesn't allow the introduction of very high amount of boron.

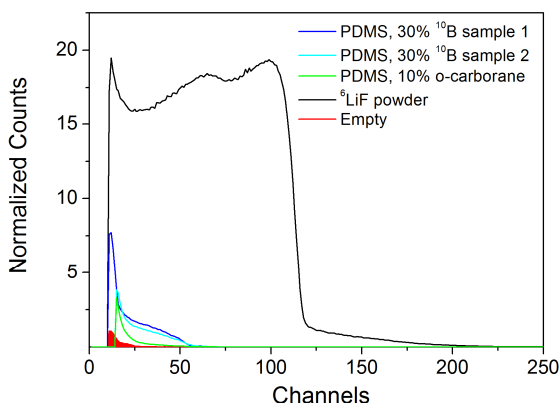


Figure VII. 11. Energy spectra of 3D sensors filled with different converters for thermal neutrons.

Table VII. 3. Roughly estimated neutron detection efficiency for the tested samples.

Sample	Estimated efficiency (%)
${}^6\text{LiF}$ powder	$0.4 \pm 0.2$
PDMS, 30% ${}^{10}\text{B}$ sample 1	$0.02 \pm 0.01$
PDMS, 30% ${}^{10}\text{B}$ sample 2	$0.01 \pm 0.005$
PDMS, 10% o-carborane	$0.004 \pm 0.002$

In case of  ${}^{10}\text{B}$  converters, the signal of the neutron capture reaction products were not so clear, but they could be anyway distinguished in the log scale plot (Figure VII. 12), thus confirming that the signal was produced by  ${}^{10}\text{B}$  capture reaction. In this

case, indeed, the two shoulders can be ascribed to  $\alpha$  particles produced in the two different possible neutron capture reactions (Chapter I), while  ${}^7\text{Li}$  has a too shorter range in the material, and only very few particles can reach the detector with high enough energy to be detected. A confirmation of that can be found in the rough estimation of the number of counts for the two shoulders, with the least energetic one having a number of counts approximately 20 times higher than the other, in good agreement with the probability ratio of the two  ${}^{10}\text{B}$  reaction (respectively 94% and 6%). The sensor without converter instead showed only the signal produced by the gamma background.

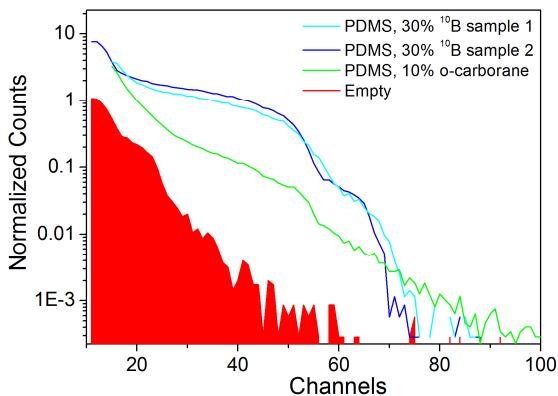


Figure VII. 12. Energy spectra in log scale, signals from different conversion products can be distinguished.

Similar tests were performed also at the TRIGA reactor in Ljubljana, and in this case, for comparison, the same tests were performed both on planar and on 3D sensors having the same converter layers. In all cases the peaks from boron alpha particles were clearly distinguished, once again with very good agreement with the expected ratio between high energy and low energy  $\alpha$  particles.

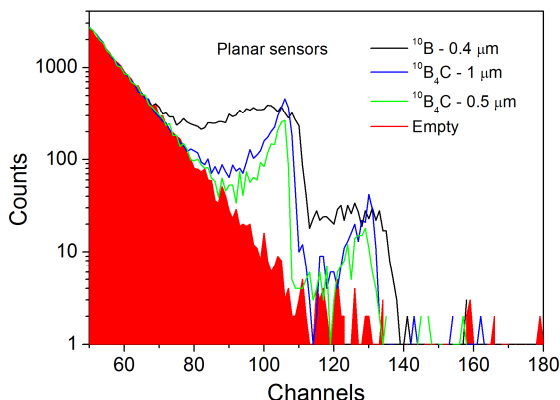


Figure VII. 13. Recorded energy spectra produced by thermal neutrons on planar detectors with different converters.

Also in 3D sensors employing the same converter layer, similar results were observed, with the clear appearance of the two  $\alpha$  particles peaks (Figure VII. 14). In this case, the sample filled by  ${}^6\text{LiF}$  powder was also tested, showing very similar spectrum to the one already measured in the previous tests (Figure VII. 11).

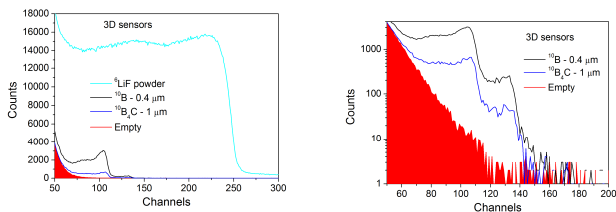


Figure VII. 14. Measured pulse height spectra produced by thermal neutrons on 3D sensors with different neutron converters. Both linear scale and log scale spectra are shown.

In Table VII. 4, an estimation of the neutron detection efficiency is reported. The estimation is very rough since the high gamma background prevents the less energetic  ${}^7\text{Li}$  particles to be distinguished, and the uncertainty in the neutron flux, due to the reactor power fluctuations during the measurements are close to 50%. From the data reported in Table VII. 4, there seems to be a higher efficiency for 3D diodes, even if this result is not as high as expected, probably due to the incomplete deposition of the converter on the vertical walls of the detector.

Table VII. 4. Rough estimation of thermal neutron detection efficiency for planar and 3D sensors with different converters.

Sensor	Converter	Estimated efficiency (%)
3D	$^6\text{LiF}$ powder	$1.1 \pm 0.6$
3D	$^{10}\text{B}$ , $0.4 \mu\text{m}$	$0.06 \pm 0.03$
3D	$^{10}\text{B}_4\text{C}$ , $1 \mu\text{m}$	$0.03 \pm 0.02$
Planar	$^{10}\text{B}$ , $0.4 \mu\text{m}$	$0.02 \pm 0.01$
Planar	$^{10}\text{B}_4\text{C}$ , $0.5 \mu\text{m}$	$0.004 \pm 0.002$
Planar	$^{10}\text{B}_4\text{C}$ , $1 \mu\text{m}$	$0.008 \pm 0.004$

## 7.4 Conclusions

In this chapter, some results on the detection of fast and slow neutrons with 3D hybrid detectors were presented. From the data, it is clear that the detection of both fast and slow neutrons is possible, but several issues were encountered. The detection of fast neutrons, showed a very low efficiency, mainly due to the low cross-section of the elastic scattering process. This is an intrinsic limit of the system, and the only way to overcome it would be the increase of the dimensions of the system, leading to completely different setups. Furthermore, the use of the same detector geometry for both fast and thermal neutrons has the consequence of a non-optimized system for both types of radiation. As an example, it is worth recalling that the range of 2 MeV protons in PDMS is about  $90 \mu\text{m}$ , while the range of the reaction products of  $^{10}\text{B}$  is respectively  $4 \mu\text{m}$  for Li and  $8 \mu\text{m}$  for  $\alpha$  particles. For this reason, a silicon cavity dimension of  $200 \mu\text{m}$  seems to be suitable for the detection of fast neutrons in that energy range, but is ineffective in the detection of thermal neutrons, since most of the useful energy is lost before reaching the silicon walls. Following these considerations, and given the larger field of application of thermal neutron detection, and especially thermal neutron imaging, new detector geometry was recently designed and its production is on-going.

## Conclusions and Future Perspectives

This work dealt with the development and the characterization of both liquid and plastic polysiloxane based scintillators.

With the aim of developing a new non-toxic liquid scintillator exploiting the interesting properties of polysiloxanes, several different solvents were tested, characterized by very good thermal and chemical stability, very low volatility and low toxicity. The optical characterization was connected with the phenyl group distribution and concentration, and special attention was paid at the formation of intramolecular excited state dimers (excimers). These results allowed to explain the outcome of the gamma ray scintillation measurements, showing better performances in the sample with the smaller excimer formation, 1,1,5,5-tetraphenyl-1,3,3,5-tetramethyltrisiloxane (TPTMTS). After this first selection, the work focused on the investigation of the time response of polysiloxane liquid scintillators based on TPTMTS. In particular, different mixtures with different concentrations of PPO were studied, analyzing their pulse shape under various excitations: UV light, neutrons and gamma rays. The results were finally correlated with the pulse shape discrimination (PSD) capabilities of the mixtures. Figure of Merit (FoM), calculated by means of the charge comparison algorithm, was employed to analyze the PSD performances and a clear dependence with PPO concentration was noticed. It has been observed that at low energies FoM depends on the scintillation light output, so that commercial EJ-309 resulted to be the best material, followed by TPTMTS with 2% PPO and 0.02% LV. At higher energies instead, the difference in the slow component intensity between neutrons and gamma rays is the most important feature. Since this difference increases with PPO concentration, for energies above 900 keVee, the best mixture resulted to be the one with the highest PPO concentration (4%), reaching even slightly better performances than the commercial reference (EJ-309). Despite the good results, the optimization of the PSD performances of this new class of materials is not completed yet. The comparison of the time response of TPTMTS samples with that of EJ-309, showed that the fast component for the latter was shorter than for polysiloxane samples. This decay time depends mostly on the secondary dye employed in the scintillating mixture. A shorter value for its fast decay is an advantage in term of PSD since it allows further reducing the contribution of the fast component to the delayed signal, with a consequent better separation of the PSD distribution peaks and a larger FoM value. In this view, the replacement of LV with a faster secondary dye would allow to improve the PSD performances of the materials, outreaching those of EJ-309 even at energies below 900 keVee.

The second part of this thesis dealt with the development and characterization of polysiloxane based plastic scintillators. These materials have some very interesting properties, like good chemical and thermal stability (up to 200 °C) and good radiation

hardness. They also exhibit higher chain mobility that could be exploited to achieve PSD in plastic materials also with reasonable primary dye concentrations. With this aim, the time responses of polysiloxane plastics doped with different PPO concentrations up to 8 wt% and 0.02 wt% LV were analyzed with the goal of evaluating their PSD performances. Previous fluorescence emission measurements, also on PPO solutions in toluene, allowed to observe the formation of excimers between PPO molecules, and consequently to connect this phenomenon with the pulse shape analysis performed by UV excitation, time resolved ion beam induced luminescence (TRIBIL) and neutron and gamma excitation. Also in this case, an increase in the delayed component intensity with PPO concentration was observed. TRIBIL measurements, showed no clear difference between  $H^+$ ,  $O^{3+}$  and  $C^{3+}$  pulse shapes, also due to the fact that high dye concentrations are not stable in high vacuum, because of PPO diffusion and sublimation.

This outcome was in contrast with neutron and gamma scintillation pulse shape analysis that showed instead a clear difference in the intensity of the delayed component between neutrons and gammas, and also a dependence of this component from the primary dye concentration. These last results were very important since they were never reported before, at these low concentrations, for plastic scintillators and could pave the way to the development of stable, polysiloxane plastic scintillators, capable of efficient PSD. The differences with TRIBIL measurements can be explained by the different setup and by the different type of interaction between heavy charged particles and neutrons and gammas. Nevertheless, a more detailed analysis is needed in order to investigate the long term stability of the materials and in order to analyze more in detail the PSD capability of the polysiloxane samples, evaluating the FoM of the system at different PPO concentrations and investigating the effect of samples dimensions on the PSD performances. Furthermore, similarly to what already mentioned for polysiloxane liquids, the pulse shape discrimination capability of the material could be further improved by the replacement of LV with a faster dye, allowing to better separate the fast component from the slow component, and thus to increase the FoM value.

Important results were also achieved with red emitting polysiloxane scintillators coupled to avalanche photodiode (APD). The addition of a third dye, Lumogen Red, having emission above 600 nm, allowed to increase the spectral matching with APD responsivity, achieving very good improvements in comparison to the light output measured by the same detector with blue emitting polysiloxane scintillators. To reach this result, the energy transfer between different dyes was studied by means of spectrofluorimetry and spectrophotometry, and by scintillation measurements performed with red enhanced PMT. This work, paves the way to the development of more compact systems, replacing awkward and fragile PMT with more compact and robust APD, reducing the sensitivity to magnetic fields of the system, and improving its radiation hardness thanks to the use of polysiloxane scintillators.

Finally, in the last chapter, some preliminary results on the development of hybrid detectors for neutrons are presented. These sensors combine 3D silicon diode with a proper neutron absorber, allowing to convert fast or slow neutrons in detectable particles. These results proves the feasibility of the concept, showing the detection of both fast and thermal neutrons using respectively a polysiloxane converter and different types of  $^{10}\text{B}$  or  $^6\text{Li}$  based materials. The reported efficiencies are however low, due to the non-optimized geometrical structure of sensor and converter deposition. A new design is in production, optimized for thermal neutron detection with boron converters that is expected to improve the efficiency by several orders of magnitude. If this result was achieved, the development of a high efficiency pixel sensor for thermal neutrons would become possible, finding wide applications in many fields.



## List of Abbreviations and Acronyms

100PMPS	Poly(methyl-phenylsiloxane) elastomer
22PDPS	Poly(22-25mol% diphenylsiloxane-co-dimethylsiloxane) elastomer
ADC	Analog to Digital Converter
APD	Avalanche Photodiode
DPDM20	Poly(18-22mol%-diphenyl-co-dimethylsiloxane) liquid
DIN	Di-isopropylnaphtalene
FoM	Figure of Merit
HMIS	Hazardous Material Identification System
keVee	keV electron equivalent
LAB	Linear alkylbenzene
LR	BASF Lumogen F Red 305
LV	BASF Lumogen F Violet 570
MSDS	Materials Safety Data Sheet
PDMS	Poly(dimethylsiloxane)
PM100	Poly(methyl-phenylsiloxane) liquid
PMDM50	Poly(48-52mol%-phenylmethylsiloxane-co-dimethylsiloxane) liquid
PMPS	Poly(methyl-phenylsiloxane)
PMT	Photomultiplier tube
PPO	2,5-diphenyloxazole
PPTMTS	1,1,3,5,5-pentaphenyl-1,3,5-trimethyltrisiloxane
PS	Polystyrene
PSD	Pulse Shape Discrimination
PVT	Polyvinyltoluene
PXE	Phenyl-o-xylylethane
RTV	Room Temperature Vulcanization
THF	Tetrahydrofuran
ToF	Time of Flight
TPTMTS	1,1,5,5-tetraphenyl-1,3,3,5-tetramethyltrisiloxane
TRIBIL	Time Resolved Ion Beam Induced Luminescence



## References

- [Abbasi2010] Abbasi et al, *Calibration and characterization of the IceCube photomultiplier tube*, Nucl. Instr. Meth. A, **2010**, 618 (1-3): p. 139-152.
- [Aberle2012] C. Aberle, C. Buck, F.X. Hartmann, M. Lindner, S. Schonert, S. Wagner, H. Watanabe, *Large Scale Production of the Liquid Scintillator for the Double Chooz Experiment*, Nucl. Phys. B (Proc. Suppl.), **2012**, 229-232:448.
- [Adadurov2011] A.F. Adadurov, D.A. Yelyseev, V.D. Titskaya, V.N. Lebedev, P.N. Zhmurin, *Plastic scintillators based on polymers with eliminated excimer forming*, Rad. Measur., **2011**, 46: p. 498-502.
- [Agosteo2016] S. Agosteo, A. Fazzi, M.V. Introini, M. Lorenzoli, A. Pola, *A telescope detection system for direct and high resolution spectrometry of intense neutron fields*, Radiat. Meas., **2016**, 85: p. 1-17.
- [Annand1987] J. R. M. Annand, *A fast module for pulse shape analysis*, Nucl. Instrum. Meth. A, **1987**, 262: p. 371-377.
- [Araki2005] T. Araki, et al., *Experimental investigation of geologically produced antineutrinos with KamLAND*, Nature, **2005**,
- [ASTMC1807] ASTM C1807-15, *Standard guide for Nondestructive Assay of Special Nuclear Material (SNM) Holdup Using Passive Neutron Measurement Methods*.
- [Athanasiasdes2005] A. Athanasiasdes, N. N. Shehad, L. Sun, T. D. Lyons, C. S. Martin, L. Bu, J. L. Lacy, *High sensitivity portable neutron detector for fissile materials detection*, Proc. IEEE Nucl. Sci. Symp. Conf., **2005**: p. 1009–1013.
- [Back2008] H.O. Back et al., *Study of phenylxylylethane (PXE) as scintillator for low energy neutrino experiments*, Nucl. Instrum. Methods A, **2008**, 85: p. 48–60.
- [Balaban2014] B. Balaban, S. Doshay, M. Osborn, Y. Rodriguez, S. A. Carter, *The role of FRET in solar concentrator efficiency and color tunability*, J. Lumin., **2014**, 146: p. 256-262.
- [Barashkov1996] N. N. Barashkov, O. A. Gunder, N. I. Voronkina, V. K. Milinchuk, *Factors determining radiation stability of plastic scintillators*, Appl. Radiat. Isotopes, **1996**, 47(11/12): p. 1557-1559.
- [Bariguete2014] W. Beriguete et al., *Production of a gadolinium-loaded liquid scintillator for the Daya Bay reactor neutrino experiment*, Nucl. Instrum. Meth. A., **2014**, 763: p. 82-88.
- [BASF\_LR] BASF. *BASF Lumogen F Red Technical Data Sheet*, **2004**.
- [BASF\_LV] BASF. *BASF Lumogen F Violet 570 Technical Data Sheet*, **2004**.
- [Bass2013] C.D. Bass, E.J. Beise, H. Breuer, C.R. Heimbach, T.J. Langford, J.S. Nico, *Characterization of a <sup>6</sup>Li-loaded liquid organic scintillator for fast neutron spectrometry and thermal neutron detection*, Appl. Radiat. Isotopes, **2013**, 77: p. 130-138.
- [Baumberg2001] I. Baumberg, O. Berezin, A. Drabkin, B. Gorelik, L. Kogan, M. Voskoboynik, M. Zaidman, *Effect of polymer matrix on photo-stability of photo-*

- luminescent dyes in multi-layer polymeric structures*, Polym. Degrad. Stab., **2001**, 73: p. 403-410.
- [BC-454ds] Saint Gobain Crystals, *BC-454 Natural Boron-loaded Premium Plastic Scintillator*, available at <http://www.crystals.saint-gobain.com>
- [BC-521ds] Saint Gobain Crystals, *BC-521 Gadolinium Loaded Liquid Scintillators*, available at <http://www.crystals.saint-gobain.com>.
- [Bell2002] Z. W. Bell, G. M. Brown, C. H. Ho, F. V. Sloop Jr., *Organic scintillators for neutron detection*,<sup>9</sup> in X-Ray and Gamma Ray Detectors and Applications IV (Proc. SPIE), R. B. James, L. A. Franks, A. Burger, E. M. Westbrook, R. D. Hurst editors. Norfolk, U.K.: Bertrams, **2002**, 4784: p. 150-163.
- [Bell2004] Z.W. Bell, M.A. Miller, L. Maya, G.M. Brown, F.V. Sloop Jr., *Boron-Loaded Silicone Rubber Scintillators*, IEEE Trans. Nucl. Sci., **2004**, 51: p. 1773-1776.
- [Bellinger2011] S.L. Bellinger, R.G. Fronk, W.J. McNeil, T.J. Sobering, D.S. McGregor, *Enhanced variant designs and characteristics of the microstructured solid-state neutron detector*, Nucl. Instr. Meth. A, **2011**, 652(1): p. 387-391.
- [Bellinger2012] S. L. Bellinger, R. G. Fronk, W. J. McNeil, T. J. Sobering, D. S. McGregor, *Improved High Efficiency Stacked Microstructured Neutron Detectors Backfilled With Nanoparticle <sup>6</sup>LIF*, IEEE Trans. Nucl. Sci., **2012**, 59(1): p. 167-173.
- [Bellini2013] Borexino Collaboration, *Measurement of geo-neutrinos from 1353 days of Borexino*, Phys. Lett. B, **2013**, 722:p. 295-300.
- [Bentoumi2013] G. Bentoumi, X. Dai, H. Fritzsche, G. Jonkmans, L. Li, G. Marleau, B. Sur, *Characterization of a liquid scintillator based on linear alkyl benzene for neutron detection*, Nucl. Instrum Methods A, **2013**, 701: p. 221-224.
- [Beriguete2014] W. Beriguete, J. Cao, Y. Ding, S. Hans, K. M. Heeger, L. Hu, A. Huang, K.-B. Luk, I. Nemchenok, M. Qi, R. Rosero, H. Sun, R. Wang, Y. Wang, L. Wen, Y. Yang, M. Yeh, Z. Zhang, L. Zhou, *Production of a gadolinium-loaded liquid scintillator for the Daya Bay reactor neutrino experiment*, Nucl. Instr. Meth. A, **2014**, 763: p. 82-88.
- [Berman1961a] I. Berman, *Luminescence in a scintillation solution excited by  $\alpha$  and  $\beta$  particles and related studies in quenching*, J. Chem. Phys., **1961**, 34(2): p. 598-603.
- [Berman1961a] I. Berman, *Luminescence in a Scintillation Solution Excited by  $\alpha$  and  $\beta$  Particles and Related Studies in Quenching*, J. Chem. Phys., **1961**, 34:p. 598-603.
- [Berman1961b] I. B. Berman, *Transient Dimer Formation by 2,5-Diphenyloxazole*, J. Chem. Phys., **1961**, 34: p. 1083-1084.
- [Berman1973] I. B. Berman, O. J. Steingraber, *Liquid Scintillation Solutions for Pulse-Shape Discrimination*, Nucl. Instrum. Methods, **1973**, 108: p. 587-591.
- [Bertrand2014] G. H. V. Bertrand, F. Sguerra, C. Dehé-Pittance, F. Carrel, R. Coulon, S. Normand, E. Barat, T. Dautremer, T. Montagu, M. Hamel, *Influence of bismuth loading in polystyrene-based plastic scintillators for low energy gamma spectroscopy*, J. Mater. Chem. C, **2014**, 2: p. 7304-7312.

- [Bertrand2015] G. H. V. Bertrand, M. Hamel, S. Normand, F. Sguerra, *Pulse shape discrimination between (fast or thermal) neutrons and gamma rays with plastic scintillators: State of the art*, Nucl. Instrum. Meth. A, **2015**, 776: p. 114-128.
- [Birks1964] J. B. Birks. *Theory and Practice of Scintillation Counting*, **1964**, Pergamon Press LTD.
- [Birks1966] J.B. Birks, J.M. de C. Conte, G. Walker, *The influence of excimer formation on solvent-solute energy transfer in organic liquid scintillators*, IEEE Trans. Nucl. Sci., **1966**, 13: p. 148–153.
- [Birks1967] J. B. Birks, *Excimers and Exciplexes*, Nature, **1967**, 214: p. 1187-1190.
- [Birks1968] J. B. Birks, *Energy transfer in organic systems VI. Fluorescence response functions and scintillation pulse shapes*, J. Phys. B At. Mol. Phys., **1968**, 1: p. 946-957.
- [Birks1970a] J. B. Birks, M. Salet, S. C.P. Leite, *Energy transfer in organic systems IX. Effect of diffusion on transfer efficiency*, J. Phys. B: Atom. Molec. Phys., **1970**, 3(4): p. 513-525.
- [Birks1970b] J.B. Birks, *Liquid scintillators solvents*, in *Organic Scintillators and Liquid Scintillation Counting*, D.L. Horrocks, C.-T. Peng Editors, **1970**, Academic Press, p. 3–23.
- [Blasse1994] G. Blasse, B. C. Grabmaier, *Luminescent Materials*, **1994**, Springer Berlin Heidelberg.
- [Bollinger1957] L. M. Bollinger, G. E. Thomas, *Boron-loaded liquid scintillation neutron detectors*, Rev. Sci. Instrum., **1957**, 28(7): p. 489-496.
- [Bowen1989a] M. Bowen, S. Majewski, D. Pettey, J. Walker, R. Wojcik, C. Zorn. *A new radiation-resistant plastic scintillator*. IEEE T. Nucl. Sci., **1989**, 36(7): p. 562-566.
- [Bowen1989b] M. Bowen, S. Majewski, D. Pettey, J. Walker, R. Wojcik, C. Zorn. *A new radiation-hard plastic scintillator*, Nucl. Instrum. Meth. A, **1989**, 276: p.391-393.
- [Breukers2013] R.D. Breukers, C.M. Bartle, A. Edgar, *Transparent lithium loaded plastic scintillators for thermal neutron detection*, Nucl. Instrum. Methods A, **2013**, 701: p. 58-61.
- [Britvich2001] G. I. Britvich, V. G. Vasil'chenko, V. A. Lishin, V. A. Polyakov, A. S. Solov'ev, *New Scintillation Materials for Particle Detectors*, Instrum. Exp. Tech., **2001**, 44:p.472-484.
- [Britvich2005] G.I. Britvich, V.G. Vasil'chenko, Y.V. Gilitsky, A.P. Chubenko, A.E. Kushnirenko, E.A. Mamidzhanyan, V.P. Pavluchenko, V.A. Pikalov, V.A. Romakhin, A.P. Soldatov, O.V. Sumaneev, S.K. Chernichenko, I.V. Shein, A.L. Shepetov, *A neutron detector on the basis of a boron-containing plastic scintillator*, Nucl. Instrum. Methods A, **2005**, 550: p. 343-358.
- [Brooks1959] F. D. Brooks, *A Scintillation Counter With Neutron And Gamma-Ray Discriminators*, Nucl. Instrum. Methods, **1959**, 4:p. 151-163.
- [Brooks1960] F. D. Brooks, R. W. Pringle, B. L. Funt, *Pulse Shape Discrimination in a Plastic Scintillator*, IRE Trans. Nucl. Sci., **1960**, 7 (2-3): p. 35-38.

- [Brooks1979] F. D. Brooks, *Development of organic scintillators*, Nucl. Instrum. Methods, **1979**, 162: p. 477-505.
- [Busjan1999] W. Busjan, K. Wick, T. Zoufal, *On the behaviour of plastic scintillators during an experiment in a high dose rate environment*, Nucl. Instrum. Methods B, **1999**, 151: p. 434-437.
- [Byrd1992] R. C. Byrd, G. F. Auchampaugh, C. E. Moss, W. C. Feldman, *Warhead Counting using neutron scintillators: Detector development testing, and demonstration*, IEEE Trans. Nucl. Sci., **1992**, 39 (4):p.1051–1055.
- [Carturan2011] S. Carturan, A. Quaranta, T. Marchi, F. Gramegna, M. Degerlier, M. Cinausero, V. L. Kravchuk, M. Poggi, *Novel polysiloxane-based scintillators for neutron detection*, Rad. Prot. Dosim., **2011**, 143: p. 471-476.
- [Caruso2010] A. N. Caruso, *The physics of solid-state neutron detector materials and geometries*, J. Phys.: Condens. Matter, **2010**, 22(44): 443201.
- [Cester2014] D. Cester, G. Nebbia, L. Stevanato, F. Pino, G. Viesti, *Experimental tests of the new plastic scintillator with pulse shape discrimination capabilities EJ-299-33*, **2014**, Nucl. Instr. Meth. A, 735: p. 202–206.
- [Cester2014] D. Cester, G. Nebbia, L. Stevanato, F. Pino, G. Viesti, *Experimental tests of the new plastic scintillator with pulse shape discrimination capabilities EJ-299-33*, Nucl. Instr. Meth. A, **2014**, 735: 202-206.
- [Chang2015] Z. Chang, N.C. Okoye, M.J. Urffer, A.D. Green, K.E. Childs, L.F. Miller, *On the scintillation efficiency of carborane-loaded liquid scintillators for thermal neutron detection*, Nucl. Instrum. Methods A, **2015**, 769: p. 112-122.
- [Chen1999] R. Chen, A. Fremout, S. Tavernier, P. Bruyndonckx, D. Clément, J.-F. Loude, C. Morel, *Readout of scintillator light with avalanche photodiodes for positron emission tomography*, Nucl. Instrum. Meth. A, **1999**, 433: p. 637–345.
- [Cho1975] Z. H. Cho, C. M. Tsai, L. A. Eriksson, *Tin and lead loaded plastic scintillators for low energy gamma-ray detection with particular application to high rate detection*, IEEE T. Nucl. Sci., **1975**, 22(1), p. 72-80.
- [Chu1990] D. Y. Chu, J. K. Thomas, *Photophysical Studies of Molecular Mobility in Polymer Films and Bulk Polymers. 3. Dynamic Excimer Formation of Pyrene in Bulk PDMS*, Macromolecules, **1990**, 23: p. 2217-2222.
- [Comrie2015] A. C. Comrie, A. Buefler, F. D. Smit, H. J. Wörtche, *Digital neutron/gamma discrimination with an organic scintillator at energies between 1 MeV and 100 MeV*, Nucl. Instrum. Meth. A, **2015**, 772: p. 43-49.
- [Tiwari2014] A. Tiwari, M. D. Soucek, *Concise Encyclopedia of High Performance Silicones*, **2014**, Hoboken, New Jersey: J. Wiley and Sons, p. 1990.
- [CRSreport2010] Congressional Research Service, CRS report for Congress, *The Helium-3 Shortage: Supply, Demand, and Options for Congress*, Sep. **2010**.
- [DallaBetta2012] G.-F. Dalla Betta, C. Da Via, M. Povoli, S. Parker, M. Boscardin, G. Darbo, S. Grinstein, P. Grenier, J. Hasi, C. Kenney, A. Kok, C.-H. Lai, G. Pellegrini, S. Watts, *Recent developments and future perspectives in 3D silicon radiation sensors*, JINST, **2012**, 7: c10006.
- [DallaPalma2014] M. Dalla Palma, A. Quaranta, T. Marchi, G. Collazuol, S. Carturan, M. Cinausero, M. Degerlier, F. Gramegna, *Red Emitting Phenyl-Polysiloxane*

- Based Scintillators for Neutron Detection*, IEEE Trans. Nucl. Sci., **2014**, 61: p. 2052-2058.
- [Deiters2000] K. Deiters, Y. Musienko, S. Nicol, B. Patel, D. Renker, S. Reucroft, R. Rusack, T. Sakhelashvili, J. Swain, P. Vikas, *Properties of the most recent avalanche photodiodes for the CMS electromagnetic calorimeter*, Nucl. Instrum. Meth., **2000**, 442: p. 193–197.
- [EJ-254ds] Eljen Technology, *EJ-254 data sheet*, available at <http://www.eljentechnology.com> .
- [EJ-299-33] <http://www.eljentechnology.com/index.php/products/plastic-scintillators/114-ej-299-33>.
- [EJ-309ds] Eljen Technology, *EJ-309 data sheet*, available at <http://www.eljentechnology.com> .
- [EJ-331ds] Eljen Technology, *EJ-331 data sheet*, available at <http://www.eljentechnology.com> .
- [ENDF] <https://www-nds.iaea.org/exfor/endl.htm>
- [Enqvist2013] A. Enqvist, C.C. Lawrence, B.M. Wieger, S.A. Pozzi, T.N. Massey, *Neutron light output response and resolution functions in EJ-309 liquid scintillation detectors*, Nucl. Instrum. Methods A, **2013**, 715: p. 79-86.
- [Evans1958] R. B. Evans, *Compton Effect, in Corpuscles and Radiation in Matter*, R. Kollath, R. D. Birhoff, L. Simons, E. Merzbacher, W. Whaling editors **1958**, Springer Berlin Heidelberg, 6/34: p. 218-298.
- [Feng2012] P. L. Feng, J. Villone, K. Hattar, S. Mrowka, B. M. Wong, M. D. Allendorf, F. P. Doty, *Spectral- and Pulse-Shape Discrimination in Triplet-Harvesting Plastic Scintillators*, IEEE Trans. Nucl. Sci., **2012**, 59(6): p. 3312-3319.
- [Feygelman1990a] V. M. Feygelman, J. K. Walker, J. P. Harmon, *Polysiloxane-based scintillators doped with oligophenylenes: Effect of color centers on radiation stability*, Nucl. Instrum. Meth. A, **1990**, 290: p. 131-135.
- [Feygelman1990b] V. M. Feygelman, J. K. Walker, J. P. Harmon, *Polysiloxane-based scintillators: 1,1,4,4-tetraphenylbutadiene as a secondary fluor*, Nucl. Instrum. Meth. A, **1990**, 295: p. 94-98.
- [Forster1959] Th. Förster, *Transfer mechanism of electronic excitation*, Discuss. Faraday Soc., **1959**, 27: p. 7-17.
- [Foster2008] M. Foster and D. Ramsden, *A compact neutron detector based on the use of a SiPM detector*, Proc. IEEE Nucl. Sci. Symp. Conf., **2008**: p. 1882–1886.
- [Fronk2015] R. G. Fronk, S. L. Bellinger, L. C. Henson, T. R. Ochs, C. T. Smith, J. K. Shultis, D. S. McGregor, *Dual-sided microstructured semiconductor neutron detectors (DSMSNDs)*, Nucl. Instrum. Meth. A, **2015**, 804: p.201-206.
- [Fuchs1970] C. Fuchs, F. Heisel, R. Voltz, A. Coche, *Scintillation decay and absolute efficiencies in organic liquid scintillators*, in *Organic Scintillators and Scintillation Counting*, D. Horrocks, C.-T. Peng, Editors **1971**, Academic Press: New York, p. 171-186.
- [Furst1956] M. Furst, H. Kallmann, F.H. Brown, *Fluorescence Efficiencies of Organic Compounds*, J. Appl. Phys., **1956**, 26: p. 1321.

- [Geiger1909] H. Geiger, E. Marsden, *On a Diffuse Reflection of the  $\alpha$  Particles*, Proc. R. Soc. Lond. A, **1909**, 82: p. 495-500.
- [GelestMSDS] Gelest, *Material Safety Data Sheet*, available at <http://www.gelest.com>.
- [Haas2008] J. T. M. de Haas, P. Dorenbos, *Advances in Yield Calibration of Scintillators*, IEEE Trans. Nucl. Sci., **2008**, 55(3): p.1086-1092.
- [Hallam1978] A. Hallam, J. B. Birks, *Energy transfer in organic systems XIII. Plastic scintillators*, J. Phys. B: Atom. Molec. Phys., **1978**, 11(18): p. 3273-3289.
- [Hall-Wilton2012] ] R. Hall-Wilton, C. Høglund, M. Imam, K. Kanaki, A. Khaplanov, O. Kirstein, T. Kittelmann, B. Nilsson, J. Scherzinger, *Detectors for the European Spallation Source*, IEEE Nucl. Sci. Symp. Med. Imag. Conf. (NSS/MIC), **2012**, p. 4283-4289.
- [HamamtsuPMT] Hamamatsu, Photomultiplier tubes, basics and applications, Third edition. Available at: [https://www.hamamatsu.com/resources/pdf/etd/PMT\\_handbook\\_v3aE.pdf](https://www.hamamatsu.com/resources/pdf/etd/PMT_handbook_v3aE.pdf).
- [Hamanishi1993] K. Hamanishi, H. Shizuka, *Relaxation processes in the excited state of phenylsiloxanes*, J. Chem. Soc. Faraday Trans., **1993**, 89: p. 3007–3013.
- [Hamel2008] M. Hamel, V. Simic, and S. Normande. *Fluorescent 1,8-naphthalimides-containing polymers as plastic scintillators. An attempt for neutron-gamma discrimination*, React. Funct. Polym., **2008**, 68: p. 1671-1681.
- [Hamel2011a] M. Hamel, G. Turk, A. Rousseau, S. Darbon, C. Reverdin, S. Normand, *Preparation and characterization of highly lead-loaded red plastic scintillators under low energy x-rays*, Nucl. Instr. Meth. A, **2011**, 660: p. 57-63.
- [Hamel2011b] M. Hamel, G. Turk, A. Rousseau, S. Darbon, C. Reverdin, S. Normand, *Preparation and characterization of highly lead-loaded red plastic scintillators under low energy x-rays*, Nucl. Instrum. Methods A, **2011**, 660: p. 57-63.
- [Hamel2014] M. Hamel, A.-M. Frelin-Labalme, S. Normand, *The influence of the solvent in fast neutron/gamma discrimination*, EPL, **2014**, 106: 52001.
- [Harmon1991] J. Harmon, J. Gaynor, V. Feygelman, J. Walker, *Linear polydiorganosiloxanes as plastic bases for radiation hard scintillators*, Nucl. Instrum. Methods B, **1991**, 53: 309-314.
- [Harvey1979] J. A. Harvey, N. W. Hill, *Scintillation detectors for neutron physics research*, Nucl. Instrum. Methods, **1979**, 162: p. 507-529.
- [Herwig2009] K.W. Herwig *Introduction to the Neutron in Neutron Imaging and Applications*, I. S. Anderson, R. L. McGreevy, H. Z. Bilheux editors, **2009**, Springer Science + Business Media, New York: 3-12.
- [Hirayama1965] F. Hirayama, *Intramolecular Excimer Formation. I. Diphenyl and Triphenyl Alkanes*, J. Chem Phys., **1965**, 42: p. 3163-3171.
- [Hirayama1968] F. Hirayama, F.J. Basile, C. Kikuchi, *Energy Transfer and Quenching in Plastic Scintillators*, Mol. Cryst., **1968**, 4: p. 83–108.
- [Hirayama1968] F. Hirayama, F.J. Basile, C. Kikuchi, *Energy Transfer and Quenching in Plastic Scintillators*, Mol. Cryst., **1968**, 4: p. 83-108.

- [Holl1995] I. Holl, E. Lorenz, S. Natkaniec, D. Renked, C. Schmelz, and B. Shwartz, *Some studies of avalanche photodiode readout of fast scintillators*, IEEE Trans. Nucl. Sci., **1995**, 42(4): p. 351-356.
- [Horrocks1974] D. L. Horrocks, *Applications of Liquid Scintillation Counting*, **1974**, New York, USA: Academic Press.
- [Horta1991] A. Horta, I.F. Pièrola, A. Rubio, J.J. Freire, *Conformational analysis of cyclic poly(methylphenylsiloxane): excimer-forming sites and side-group rotation*, Macromolecules **1991**, 24: p.3121-3126.
- [Hurd2014] A. J. Hurd, R. T. Kouzes, *Why new neutron detector materials must replace helium-3*, Eur. Phys. J. Plus, **2014**, 129: p. 236.
- [Itoh1996] T. Itoh, M. H. Yang, C. Chou, *Intramolecular excimer formation in diphenylsiloxane-based copolymers*, J.Chem. Soc. Faraday Trans., **1996**, 92(19), 3593-3597.
- [Itoh2001] T. Itoh, *Spectroscopy and photophysics of methylphenylsiloxane and diphenylsiloxane-based molecules and polymers*, Res. Chem. Intermed., **2001**, 27: p. 669–685.
- [Itoh2001] T. Itoh, *Spectroscopy and photophysics of methylphenylsiloxane and diphenylsiloxane-based molecules and polymers*, Res. Chem. Intermed., **2001**, 27: p. 669-685.
- [Itoh2002] T. Itoh, M.-H. Yang, *Intramolecular Excimer Formation of the Copolymers Based on Methylphenylsiloxane and Dimethylsiloxane Units in Solution*, J. Phys. Chem. B, **2002**, 106: p. 2196-2202.
- [Jakubek2006] J. Jakubek, T. Holy, E. Lehmann, S. Pospisil, J. Uher, J. Vacik, D. Vavrik, *Neutron imaging with Medipix-2 chip and a coated sensor*, Nucl. Instr. Meth. A, **2006**, 560: p. 143-147.
- [Jones2013] R.G. Jones, W. Ando, J. Chojnowski, *Silicon-Containing Polymers: The Science and Technology of Their Synthesis and Applications*, 2013, Springer Science and Business Media, Berlin, Germany: p. 192-194.
- [Joyce2012] M.J. Joyce, M.D. Aspinall, F.D. Cave, A.D. Lavietes, *Real-Time, Digital Pulse-Shape Discrimination in non-Hazardous Fast Liquid Scintillation Detectors: Prospects for Safety and Security*, IEEE Trans. Nucl. Sci., **2012**, 59: p. 1245-1251.
- [Kalivas2012] N. Kalivas, I. Costaridou, I. Kandarakis, D. Cavouras, C. D. Nomicos, G. Panayiotakis, *Optical gain signal-to-noise ratio transfer efficiency as an index for ranking of phosphor-photodetector combinations used in X-ray medical imaging*, Appl. Phys. A: Mater. Sci. Process., **2012**, 78: p. 915-919.
- [Karar1999] A. Karar, Y. Musienko, and J. Ch Vanel, *Characterization of avalanche photodiodes for calorimetry application*, Nucl. Instrum. Meth. A, **1999**, 428: p. 413-431.
- [Kaschke1988] M. Kaschke, K. Vogler, *Time-resolved Studies of Intermolecular Electronic Energy Transfer Processes between Molecules in Solution*, Laser Chem., **1988**, 8: p. 19-38.
- [Kaschuck2000] Y. A. Kaschuck, B. Esposito, L. A. Trykov, V. P. Semenov, *Fast neutron spectrometry with organic scintillators applied to magnetic fusion experiments*, Nucl. Instrum. Methods A, **2002**, 476(1-2): p. 511-515.

- [Katagiri2004] M. Katagiri, M. Matsubayashi, K. Sakasai, T. Nakamura, M. Ebine, A. Birumachi, N. Rhodes, *A compact neutron detector using scintillators with wavelength shifting fibres by backside readout method*, Nucl. Instrum. Meth. A, **2004**, 529: p. 313–316.
- [Keivanidis2008] P. E. Keivanidis, N. C. Greenham, H. Sirringhaus, R. H. Friend, J. C. Blakesley, R. Dpeller, M. Campoy-Quiles, T. Agostinelli, D. D. C. Bradley, J. Nelson. *X-ray stability and response of polymeric photodiodes for imaging applications*, Appl. Phys. Lett., **2008**, 92: 023304.
- [King1966] T. A. King, R. Voltz, *Time dependence of scintillation intensity in aromatic materials*, P. Roy. Soc. Lond. A Mat., **1966**, 289(1418): p. 424-439.
- [Kirov2005] A.S. Kirov, J.Z. Piao, N.K. Mathur, T.R. Miller, S. Devic, S. Trichter, M. Zaider, C.G. Soares, T. LoSasso, *The three-dimensional scintillation dosimetry method: test for a 106Ru eye plaque applicator*, Phys. Med. Biol., **2005**, 50: p. 3063-3081.
- [Klein1929] O. Klein, Y. Nishina, *Über die Streuung von Strahlung durch freie Elektronen nach der neuen relativistischen Quantendynamik von Dirac*, Z. Physik, **1929**, 52: p. 853-868.
- [Knoll2000] G. F. Knoll, *Radiation Detection and Measurements*, **2000**, John Wiley & Sons Inc., New York.
- [Koike1960] M. Koike, A. Danno, *Radiation effects on dimethyl-diphenyl siloxane copolymer. I. protective effect of phenyl radical on the cross-linking*, J. Phys. Soc. Jpn., **1960**, 15(11): p. 1501-1508.
- [Koshimizu2015] M. Koshimizu, G. H. V. Bertrand, M. Hamel, S. Kishimoto, R. Haruki, F. Nishikido, T. Yanagida, Y. Fujimoto, K. Asai, *X-ray detection capability of bismuth-loaded plastic scintillators*, Jpn. J. Appl. Phys., **2015**, 54: 102202.
- [Kouzes2010] R. T. Kouzes, J. H. Ely, L. E. Erikson, W. J. Kernan, A. T. Lintereur, E. R. Siciliano, D. L. Stephens, D. C. Stromswold, R. M. Van Ginhoven, M. L. Woodring, *Neutron detection alternatives to <sup>3</sup>He for national security applications*, Nucl. Instrum. Meth. A, **2010**, 623: p. 1035-1045.
- [Kouzes2011] R. T. Kouzes, J. H. Ely, A. T. Lintereur, E. K. Mace, D. L. Stephens, M. L. Woodring, *Neutron detection gamma ray sensitivity criteria*, Nucl. Instrum. Meth. A, **2011**, 654: p. 412-416.
- [Kraus2006] C. Kraus, *SNO with liquid scintillator: SNO+*, Prog. Part. Nucl. Phys., **2006**, 57:150-152.
- [Lakowicz2006] J. R. Lakowicz, *Principles of Fluorescence Spectroscopy*, **2006**, New York, NY, USA: Springer Science+Business Media.
- [Laustriat1968] G. Laustriat, *The luminescence decay of organic scintillators*, Molec. Cryst., **1968**, 4: p. 127-145.
- [Leo1987] W. R. Leo, *Techniques for Nuclear and Particle Physics Experiments*, **1987**, Springer Berlin Heidelberg.
- [Levin2003] C. S. Levin, *Detector design issues for compact nuclear emission cameras dedicated to breast imaging*, Nucl. Instrum. Meth A, **2003**, 497: p. 60-74.
- [Li2012] S. Li, X. Xu, H. Cao, S. Tang, B. Ding, and Z. Yin, *A novel compact real time radiation detector*, Appl. Radiat. Isot., **2012**, 70: p.1667-1670.

- [Lipsky1956] S. Lipsky, *Non-Radiative Electronic Energy Transfer in Organic Liquids at High Donor Concentration*, Air Force Cambridge Research Laboratories Final Report, **1956**.
- [Lombardi2013] P. Lombardi, F. Ortica, G. Ranucci, A. Romani, *Decay time and pulse shape discrimination of liquid scintillators based on novel solvents*, Nucl. Instrum. Methods A, **2013**, 701: p. 133–144.
- [Lumogen] BASF, *BASF Lumogen F Collector dyes Technical Information*, **1997**. Available at: <http://www2.basf.us/additives/pdfs/p3201e.pdf>
- [Luo2014] X. L. Luo, V. Modamio, J. Nyberg, J. J. Valiente-Dobón, Q. Nishada, G. deAngelis, et al., *Test of digital neutron–gamma discrimination with four different photomultiplier tubes for the Neutron Detector Array (NEDA)*, Nucl. Instrum. Meth. A, **2014**, 767: p. 83–91.
- [Malimath1997] G.H. Malimath, G.C. Chikkur, H. Pal, T. Mukherjee, *Role of internal mechanisms in energy transfer processes in organic liquid scintillators*, Appl. Radiat. Isot., **1997**, 48: p.359-364.
- [Mark2005] J. E. Mark, H. R. Allcock, R. West. *Inorganic Polymers*, **2005**, Oxford, UK: Oxford University Press.
- [Marrodan2009] T. Marrodán Undagoitia, F. von Feilitzsch, L. Oberauer, W. Potzel, A. Ulrich, J. Winter, M. Wurm, *Fluorescence decay-time constants in organic liquid scintillators*, Rev. Sci. Instrum., **2009**, 80: p. 043301.
- [Mathad1986] R.D. Mathad, G.C. Chikkur, N. Umakantha, *Electronic excitation energy transfer in organic liquid scintillators*, J. Chem. Phys., **1986**, 84: p. 2187–2195.
- [Mathad1986] R.D. Mathad, G.C. Chikkur, N. Umakantha, *Electronic excitation energy transfer in organic liquid scintillators*, J. Chem. Phys., **1986**, 84: p. 2187-2195.
- [McGregor2003] D. S. McGregor, M. D. Hammig, Y.-H. Yang, H. K. Gersch, R.T. Klann, *Design considerations for thin film coated semiconductor thermal neutron detectors—I: basics regarding alpha particle emitting neutron reactive films*, Nucl. Instr. Meth. A, **2003**, 500: p. 272-308.
- [McGregor2009] D. S. McGregor, W. J. McNeil, S. L. Bellinger, T. C. Unruh, J. K. Shultis, *Microstructured semiconductor neutron detectors*, Nucl. Instrum. Methods A, **2009**, 608: p.125-131.
- [McGregor2013] D.S. McGregor, S. L. Bellinger, J. K. Shultis, *Present status of microstructured semiconductor neutron detectors*, J. Cryst. Growth, **2013**, 379: p. 99-110.
- [Mendicino2014] R. Mendicino, M. Boscardin, S. Carturan, M. Cinausero, G. Collazuol, G.-F. Dalla Betta, M. Dalla Palma, F. Gramegna, T. Marchi, E. Perillo, M. Povoli, A. Quaranta, S. Ronchin, N. Zorzi, *Novel 3D silicon sensors for neutron detection*, J. Inst., **2014**, 9(5): C05001.
- [Moszynski1979] M. Moszynski, B. Bengtson, *Status of Timing with Plastic Scintillation Detectors*, Nucl. Instrum. Methods, **1979**, 158: p. 1-31.

- [Moszynski2002] M. Moszynski, M. Szawlowski, M. Kapusta, M. Balcerzyk, *Large area avalanche photodiodes in scintillation and X-rays detection*, Nucl. Instrum. Meth. A, **2002**, 485: p. 504-521.
- [NIST2010] M. J. Berger, J. H. Hubbell, S. M. Seltzer, J. Chang, J. S. Coursey, R. Sukumar, D. S. Zucker, K. Olsen, *XCOM: Photon Cross Section Database (version 1.5)*. [Online] Available: <http://physics.nist.gov/xcom>, **2010**, National Institute of Standards and Technology, Gaithersburg, MD.
- [Normand2002] S. Normand, B. Mouanda, S. Haan, M. Louvel, *Study of a New Boron Loaded Plastic Scintillator (Revised)*, IEEE T. Nucl. Sci., **2002**, 49(4): p. 1603-1608.
- [O’Keeffe2011] H. M. O’Keeffe, E. O’Sullivan, M. C. Chen, *Scintillation decay time and pulse shape discrimination in oxygenated and deoxygenated solutions of linear alkylbenzene for the SNO+ experiment*, Nucl. Instr. Meth. A, **2011**, 640(1): p. 119-122.
- [Oberauer2013] L. Oberauer, *Liquid Scintillator Detectors*, Nuclear Physics B (Proc. Suppl.), **2013**, 235–236: 198-204.
- [Ott1956] D.G. Ott, F.N. Hayes, V.N. Kerr, R.W. Benz, *Inherent Inconsistencies in Fluorescence and Scintillation Spectra*, Science, **1956**, 123: p 1071.
- [Ovechkina2009] L. Ovechkina, K. Riley, S. Miller, Z. Bell, V. Nagarkar, *Gadolinium loaded plastic scintillators for high efficiency neutron detection*, Physics Procedia, **2009**, 2: p. 161-170.
- [Pawelczak 2014] I.A. Pawelczak, A.M. Glenn, H.P. Martinez, M.L. Carman, N.P. Zaitseva, S.A. Payne, *Boron-loaded plastic scintillator with neutron- $\gamma$  pulse shape discrimination capability*, Nucl. Inst. Meth. A, **2014**, 751: p. 62-69.
- [Pawelczak2013] I.A. Pawelczak, S.A.Ouedraogo, A. M.Glenn, R.E.Wurtz, L. F. Nakae, *Studies of neutron- $\gamma$  pulse shape discrimination in EJ-309 liquid scintillator using charge integration method*, Nucl. Instrum. Meth. A, **2013**, 711: p. 21–26.
- [Piemonte2005] C. Piemonte, M. Boscardin, G.-F. Dalla Betta, S. Ronchina, N. Zorzi, *Development of 3D detectors featuring columnar electrodes of the same doping type*, Nucl. Instrum. Meth. A, **2005**, 541(1-2): p. 441-448.
- [Pilcher1998] B. Pilcher, G. Böning, E. Lorenz, R. Mirzoyan, W. Pimpl, M.Schwaiger, S. I. Ziegler, *Studies with a prototype high resolution PET scanner based on LSO-APD modules*, IEEE Trans. Nucl. Sci., **1998**, 45: p. 1298–1302.
- [Polymer\_Ency] H. F. Mark, *Encyclopedia Of Polymer Science & Technology*, **2007**, Hoboken, New Jersey: J. Wiley and Sons.
- [Pozzi2013] S. A. Pozzi, M. M. Bourne, S. D. Clarke, *Pulse shape discrimination in the plastic scintillator EJ-299-33*, Nucl. Instrum. Meth. A, **2013**, 723: p. 19–23.
- [Pozzi2013] S. A. Pozzi, M. M. Bourne, S. D. Clarke, *Pulse shape discrimination in the plastic scintillator EJ-299-33*, Nucl. Instr. Meth. A, **2013**, 723: p. 19-23.
- [Quaranta2010a] A. Quaranta, S. M. Carturan, T. Marchi, V. L. Kravchuk, F. Gramegna, G. Maggioni, M. Degerlier, *Optical and scintillation properties of polydimethyl-diphenylsiloxane based organic scintillators*, IEEE T. Nucl. Sci., **2010**, 57(10): p. 891-900.

- [Quaranta2010b] A. Quaranta, S. Carturan, T. Marchi, M. Cinausero, C. Scian, V.L. Kravchuk, M. Degerlier, F. Gramegna, M. Poggi, G. Maggioni, *Doping of polysiloxane rubbers for the production of organic scintillators*, Opt. Mater., **2010**, 32: p. 1317-1320.
- [Quaranta2010c] A. Quaranta, S. Carturan, T. Marchi, A. Antonaci, C. Scian, V. L. Kravchuk, M. Degerlier, F. Gramegna, G. Maggioni, *Radiation hardness of polysiloxane scintillators analyzed by ion beam induced luminescence*, Nucl. Instrum. Methods Phys. Res. B, **2010**, 268(6):p. 3155-3159.
- [Quaranta2011] A. Quaranta, S. Carturan, T. Marchi, M. Buffa, M. Degerelier, M. Cinausero, G. Guastalla, F. Gramegna, G. Valotto, G. Maggioni, V. L. Kravchuk, *Doped polysiloxane scintillators for thermal neutrons detection*, J. Non-Cryst. Solids, **2011**, 357: p. 1921-1925.
- [Quaranta2013] A. Quaranta, S. Carturan, M. Cinausero, T. Marchi, F. Gramegna, M. Degerlier, A. Cemmi, S. Baccaro, *Characterization of polysiloxane organic scintillators produced with different phenyl containing blends*, Mater. Chem. Phys., **2013**, 137: p. 951-958.
- [Ranucci1998] G. Ranucci, A. Goretti, P. Lombardi, *Pulse-shape discrimination of liquid scintillators*, Nucl. Instrum. Meth. A, **1998**, 412: p. 374-386.
- [Robb1968] W. L. Robb, *Thin silicone membranes - their permeation properties and some applications*, Ann N Y Acad Sci., **1968**, 146(1): p. 119-37.
- [Salom1989] C. Salom, I. Hernandez Fuentes, I.F. Piérola, A. Horta, *Temperature Dependence of Poly(phenylsiloxane) Fluorescence. 2. Comparison of Poly(methylphenylsiloxane) with Copolymer of Methylphenylsiloxane and Dimethylsiloxane*, Macromolecules, **1989**, 22: p. 1874-1878.
- [Salom1991] C. Salom, J.A. Semlyen, S. Clarson, I. Hernandez Fuentes, A.L. Macanita, A. Horta, I.F. Piérola, *Viscosity dependence of the excimer to monomer fluorescence ratio. Cyclic and linear polysiloxanes*, Macromolecules, **1991**, 24: p. 6827-6831.
- [Schmelz1985] C. Schmelz, S. M. Bradbury, I. Holl, E. Lorenz, D. Renker, S. Ziegler, *Feasibility study of an avalanche photodiode readout for a high resolution PET with nsec time resolution*, IEEE Trans. Nucl. Sci., **1995**, 42(4): 1080-1084.
- [Seiden2012] A. Seiden, *Characteristics of the ATLAS and CMS detectors*, Phil. Trans. R. Soc. A, **2012**, 370: p. 892-906.
- [Seliger1956] H. H. Seliger, C. A. Ziegler, I. Jaffe, *Role of Oxygen in the Quenching of Liquid Scintillators*, Phys. Rev., **1956**, 101(3): p. 998-999.
- [Shao2013] Q. Shao, L. F. Voss, A. M. Conway, R. J. Nikolic, M. A. Dar, C. L. Cheung, *High aspect ratio composite structures with 48.5% thermal neutron detection efficiency*, App. Phys. Lett., **2013**, 102: 063505.
- [Smith2013] M. B. Smith, T. Achtzehn, H. R. Andrews, E. T. H. Clifford, H. Ing, V. D. Kovaltchouk, *Fast Neutron Spectroscopy Using Cs<sub>2</sub>LiYCl<sub>6</sub>:Ce (CLYC) Scintillator*, IEEE T. Nucl. Sci., **2013**, 60: p. 855-859.
- [Söderström2008] P.-A. Söderström, J. Nyberg, R. Wolters, *Digital pulse-shape discrimination of fast neutrons and  $\gamma$ -rays*, **2008**, Nucl. Instrum. Meth. A, 594: p. 79-89.

- [SRIM] [www.srim.org](http://www.srim.org).
- [Stevanato2012] L. Stevanato, D. Cester, G. Nebbia, G. Viesti, *Neutron detection in a high gamma-ray background with EJ-301 and EJ-309 liquid scintillators*, **2012**, Nucl. Instrum Methods A, 690: p. 96-101.
- [Strobl2009] M. Strobl, I. Manke, N. Kardjilov, A. Hilger, M. Dawson, J. Banhart, *Advances in neutron radiography and tomography*, J. Phys. D: Appl. Phys., **2009**, 42: 243001.
- [Swiderski2008] L. Swiderski, M. Moszynski, D. Wolski, T. Batsch, A. Nassalski, A. Syntfeld-Kazuch, T. Szczesniak, F. Kniest, M. R. Kusner, G. Pausch, J. Stein, W. Klamra, *Boron-10 Loaded BC523A Liquid Scintillator for Neutron Detection in the Border Monitoring*, IEEE T. Nucl. Sci., **2008**, 55(6): p.3710-3716.
- [Tarasenko2013] O. Tarasenko, N. Galunov, N. Karavaeva, I. Lazarev, V. Panikarskaya, *Stilbene composite scintillators as detectors of fast neutrons emitted by a  $^{252}\text{Cf}$  source*, Radiat. Meas., **2013**, 58: p. 61-65.
- [Tomanin2014] A.Tomanin, J.Paepen, P.Schillebeeckx, R.Wynants, R.Nolte, A.Lavietes, *Characterization of a cubic EJ-309 liquid scintillator detector*, **2014**, Nucl. Instrum. Methods A, 756: p. 45-54.
- [Uher2008] J. Uher, J. Jakubek, U. Koster, C. Lebel, C. Leroy, S. Pospisil, R. Skoda, Z. Vykydal, *Detection of fast neutrons with the Medipix-2 pixel detector*, Nucl. Instr. Meth. A, **2008**, 591: p. 71-74.
- [Valeur2001] B. Valeur, *Molecular Fluorescence: Principles and Applications*, **2001**, Weinheim, Germany: Wiley-VCH.
- [Van\_Eijk2012] C. W. E. van Eijk, *Inorganic scintillators for thermal neutron detection*, IEEE Trans. Nucl. Sci., **2012**, 59(5): p. 2242-2247.
- [VanLoef2014] E. V. van Loef, G. Markosyan, U. Shirwadkar, K. S. Shah, *Plastic Scintillators With Neutron/Gamma Pulse Shape Discrimination*, IEEE Trans. Nucl.Sci., **2014**, 61(1): p. 467-471.
- [Varga2009] Z. Varga, G. Suranyi, *Detection of previous neutron irradiation and reprocessing of uranium materials for nuclear forensic purposes*, Appl. Radiat. Isotopes, **2009**, 67(4): p. 516-522.
- [Vartsky2003] D. Vartsky, M.B. Goldberg, A. Breskin, R. Chechik, B. Guerard, J.F. Clergeau, *Large-area imaging detector for neutron scattering based on boron-rich liquid scintillator*, Nucl. Instrum. Methods A, **2003**, 504:p. 369-373.
- [Voltz1963] R. Voltz, G. Laustriat, A. Coche, *Mécanisme du transfert d'énergie dans les scintillateurs liquides*, C. R. Acad. Sci., **1963**, 257: p. 1473.
- [Voltz1966] R. Voltz, J. Lopes da Silva, G. Laustriat, A. Coche, *Influence of the Nature of Ionizing Particles on the Specific Luminescence of Organic Scintillators*, J. Chem. Phys., **1966**, 45: p. 3306-3311.
- [Walker1989] J. K. Walker, A. R. Katritzky, Z. Degaszfaran, *Radiation resistance of polysiloxane based scintillators doped with oxadiazole fluors*, Chem. Scripta, **1989**, 29(3): p. 245-248.
- [Weber2002] M. J. Weber, *Inorganic scintillators: today and tomorrow*, J. Lumin., **2002**, 100: p. 35-45.

- [Weinreb1962] A. Weinreb, *Fluorescence Energy Transfer and Oxygen Quenching in Solutions of Diphenyloxazole in Cyclohexane*, J. Chem. Phys., **1962**, 36: p. 890-894, 1962.
- [Wright1953] G. T. Wright, *Scintillation Response of Organic Phosphors*, Phys. Rev., **1953**, 91(5): p. 1282-1283.
- [Wurm2012] M. Wurm et al., *The next-generation liquid-scintillator neutrino observatory LENA*, Astropart. Phys., **2012**, 35: p. 685-732.
- [Yguerabide1962] J. Yguerabide, M. Burton, *Luminescence Decay Times: Concentration Effects*, J. Chem. Phys., **1962**, 37: p. 1757-1774.
- [Zaitseva2012] N. Zaitseva, B. L. Rupert, I. Pawelczak, A. Glenn, H. P. Martinez, L. Carman, M. Faust, N. Cherepy, S. Payne, *Plastic scintillators with efficient neutron/gamma pulse shape discrimination*, Nucl. Instrum. Meth. A, **2012**, 668: p. 88–93.
- [Zaitseva2013] N. Zaitseva, A. Glenn, H. P. Martinez, L. Carman, I. Pawelczak, M. Faust, S. Payne, *Pulse shape discrimination with lithium-containing organic scintillators*, Nucl. Instrum. Meth. A., **2013**, 729: p. 747-754.
- [Zhan2013] L. Zhan, *Daya Bay II and Future Reactor Experiments*, Nucl. Phys. B, **2013**, 237-238: p. 114-116.
- [Zhang1995] G. Zhang, J. K. Thomas, *Transport of Singlet Excitation in Solid Aromatic Polymers*, J. Phys. Chem., **1995**, 99(28): p. 11203-11215.
- [Zhang2001] L. Y. Zhang, K. J. Zhu, R.-Y. Zhu, D. T. Liu, *Monitoring Light Source for CMS Lead Tungstate Crystal Calorimeter at LHC*, IEEE T. Nucl. Sci, **2001**, 48: p. 372-378.
- [Zhu2004] R. Y. Zhu, *Precision Lead Tungstate Crystal Calorimeter for CMS at LHC*, IEEE T. Nucl. Sci, **2004**, 51: p. 1560-1567.
- [Zorn1990] C. Zorn, S. Majewski, R. Wojcik, C. Hurlbut, W. Moser, *Preliminary study of radiation damage in liquid scintillators*, IEEE T. Nucl. Sci, **1990**, 37(2): p. 487-491.



# Scientific production

## ***Published papers***

### **HYDE and scintillators**

R. Mendicino, M. Boscardin, S. Carturan, M. Cinausero, G. Collazuol, G.-F. Dalla Betta, M. Dalla Palma, F. Gramegna, T. Marchi, E. Perillo, M. Povoli, A. Quaranta, S. Ronchin, N. Zorzi, *Novel 3D silicon sensors for neutron detection*, J. Inst., **2014**, 9: C05001.

M. Dalla Palma, A. Quaranta, T. Marchi, G. Collazuol, S. Carturan, M. Cinausero, M. Degerlier, F. Gramegna, *Red Emitting Phenyl-Polysiloxane Based Scintillators for Neutron Detection*, IEEE Trans. Nucl. Sci., **2014**, 61: p. 2052-2058.

M. Dalla Palma, S.M. Carturan, M. Degerlier, T. Marchi, M. Cinausero, F. Gramegna, A. Quaranta, *Non-toxic liquid scintillators with high light output based on phenyl-substituted siloxanes*, Optical Materials, **2015**, 42, p. 111-117.

R. Mendicino, M. Boscardin, S. Carturan, G.-F. Dalla Betta, M. Dalla Palma, G. Maggioni, A. Quaranta, S. Ronchin, *Characterization of 3D and planar Si diodes with different neutron converter materials*, Nucl. Instrum. Meth. A, **2015**, 796: p. 23-28.

M. Dalla Palma, T. Marchi, S. Carturan, C. Checchia, G. Collazuol, F. Gramegna, N. Daldosso, V. Paterlini, A. Quaranta, M. Cinausero, M. Degerlier, *Pulse shape discrimination in polysiloxane based liquid scintillator*, IEEE Trans. Nucl. Sci., **accepted for publication**.

### **Other activities**

D. De Salvador, G. Maggioni, S. Carturan, M. Bazzan, N. Argiolas, A. Carnera, M. Dalla Palma, et al., *Highly bent (110) Ge crystals for efficient steering of ultrarelativistic beams*, J. Appl. Phys., **2013**, 114:154902.

A. Quaranta, S. Carturan, A. Campagnaro, M. Dalla Palma, M. Giarola, N. Daldosso, G. Maggioni, G. Mariotto, *Highly fluorescent xerogels with entrapped carbon dots for organic scintillators*, Thin Solid Films, **2014**, 553: p. 188-192.

## Proceedings

M. Dalla Palma, A. Quaranta, S. Carturan, F. Gramegna, T. Marchi, G. Collazuol, M. Cinausero, *Red emitting silicones for particles detection: coupling with APD*, in PoS(Bormio2013), Italy: Proceedings of science, **2013**. Atti di: 51st International Winter Meeting on Nuclear Physics, Bormio (SO), Italy, 21-25 January 2013.

M. Dalla Palma, A. Quaranta, T. Marchi, G. Collazuol, S. Carturan, M. Cinausero, F. Gramegna, *Red emitting phenyl-polysiloxane based scintillators for neutron detection* in 2013 3rd International Conference on Advancements in Nuclear Instrumentation, Measurement Methods and Their Applications, ANIMMA 2013, Marseille; France: IEEE, **2013**.

M. Dalla Palma, G.Franco Dalla Betta, G. Collazuol, T. Marchi, M. Povoli, R. Mendicino, M. Boscardin, S. Ronchin, N. Zorzi, G. Giacomini, A. Quaranta, S. Carturan, M. Cinausero, F. Gramegna, *Hybrid detectors for neutrons combining phenyl-polysiloxanes with 3D silicon detectors* in **2013** 3rd International Conference on Advancements in Nuclear Instrumentation, Measurement Methods and their Applications (ANIMMA).

G.F. Dalla Betta, M. Boscardin, S. Carturan, M. Cinausero, G. Collazuol, M. Dalla Palma, G. Giacomini, F. Gramegna, C. Granja, T. Marchi, R. Mendicino, E. Perillo, M. Povoli, A. Quaranta, S. Ronchin, T. Slavíček, M. Štefánek, J. Vacík, N. Zorzi, *Hybrid Detectors of Neutrons Based on 3D Silicon Sensors with Polysiloxane Converter* in Conference Record of Workshop on Room Temperature Semiconductor Detectors , **2013**.

S. M. Carturan, T. Marchi, G. Maggioni, F. Gramegna, M. Degerlier, M. Cinausero, M. Dalla Palma, A. Quaranta, *Thermal neutron detection by entrapping  $^6\text{LiF}$  nanocrystals in siloxane scintillators*, **2015**, Journal of Physics: Conference Series, 620 (1), art. no. 012010.

M. Degerlier, S.M. Carturan, F. Gramegna, T. Marchi, M. Dalla Palma, M. Cinausero, G. Maggioni, A. Quaranta, G. Collazuol, J. Bermudez, *Novel scintillating materials based on phenyl-polysiloxane for neutron detection and monitoring*, **2014**, Springer Proceedings in Physics, 154, pp. 151-157.

## LNL annual reports

M. Dalla Palma, T. Marchi, S. Carturan, A. Quaranta, F. Gramegna, G. Collazuol, M. Cinausero, N. Daldosso, V. Peterlini, *Fluorescence Lifetimes in Polysiloxane Based Scintillators: Effects of Primary Dye Concentration*. LNL-INFN Annual Report **2013**

S. Carturan, M. Dalla Palma, T. Marchi, G. Collazuol, M. Degerlier, J. Bermudez, A. Quaranta, M. Cinausero, F. Gramegna., *Non-toxic Liquid Silicones: Preliminary Tests as Scintillators*, LNL-INFN Annual Report **2013**.

S.M. Carturan, T. Marchi, G. Maggioni, F. Gramegna, M. Degerlier, M. Cinausero, M. Dalla Palma, A. Quaranta, *Thermal Neutron Detection by Entrapping 6LiF Nanocrystals in Siloxane Scintillators*, LNL-INFN Annual Report **2014**.

## **Conferences**

Poster presented at 51. International Winter Meeting on Nuclear Physics, Bormio (SO). From 21st to 25th of January **2013**. *Red emitting silicones for particles detection: coupling with APD*. Awarded with best poster prize. Proceedings published on PoS (Proceedings of Science).

Poster presented at the 3rd ANIMMA (Advancements in Nuclear Instrumentation Measurement Methods and their Applications) conference in Marseille (France). From the 22nd to the 27th of June **2013**. *Hybrid Detectors for Neutrons Combining Phenyl-Polysiloxanes with 3D Silicon Detectors*. Proceedings available on IEEEXplore.

Oral presentation at the 3rd ANIMMA (Advancements in Nuclear Instrumentation Measurement Methods and their Applications) conference in Marseille (France). From the 22nd to the 27th of June **2013**. *Red Emitting Phenyl-Polysiloxane Based Scintillators for Neutron Detection*. Proceedings available on IEEEXplore. Paper published on IEEE Trans. Nucl. Sci.

Poster presentation at E-MRS conference in Strasbourg (France). From the 27th to the 31st of May **2013**. *Highly fluorescent xerogels with entrapped carbon dots for organic scintillators*. Paper published on Thin Solid Films.

Oral presentation at the 2nd Topical Workshop on Modern Aspects in Nuclear Structure: *Pulse Shape Discrimination in Polysiloxane Based Scintillators*, Bormio (SO, Italy) 19th-22th February **2014**

Poster presentation at the NDRA2014 Summer School: *Polysiloxane based scintillators for neutron detection* Riva Del Garda (TN), 30th June- 4th July **2014**.

Oral presentation at the 4th ANIMMA (Advancements in Nuclear Instrumentation Measurement Methods and their Applications) conference in Lisbon (Portugal) *Development of new polysiloxane based liquid scintillators*, Lisbon, 20th-24th April 2015.

Part of this work was supported by the Fifth Commission of Istituto Nazionale di Fisica Nucleare (INFN), HYDE experiment and by the Italian Ministry of Education (Prin 2010-2011-2010TPSCSP\_005).

# Acknowledgment

*This work comes at the end of a long path, begun 9 years ago. Along the way, I had the opportunity to meet many fantastic people, who gave me the chance to grow personally and professionally. I am grateful to all of them, even if it is impossible to mention every single person.*

*Some people however gave a special contribution to this work, and without them this thesis would not have been possible. First of all I am thankful to Prof. Alberto Quaranta, who gave me this opportunity and who followed me constantly during these years, never refusing his help, his advices and his opinions.*

*I'm deeply grateful to Dott.sa Sara Carturan, who introduced me to the chemical preparation of polysiloxane materials, and has always been helpful and available for suggestions and to Dott. Tommaso Marchi and Dott.sa Fabiana Gramegna, for the fundamental help in the testing of the samples with radiation sources and in pulse shape analysis, their contribution to this thesis has been priceless.*

*I'm also thankful to Dott. Marco Cinausero, Dott. Gianmaria Collazuol, Dott. Gianluigi Maggioni, for their help in data acquisition, sample production, paper writing and discussions, to Dott. Nicola Daldosso and to Veronica Paterlini for fluorescence lifetime measurements and to Dott.sa Caroline Czelusniak for TRIBIL measurements.*

*I need to thank my colleague and friend Roberto Mendicino, for being my comrade-in-arms in Lubljana and Prague and for his work on the HYDE experiment: he has been the one who put the biggest efforts on it, and the results presented herein on that topic are mainly due to his efforts. I'm thankful to Prof. Gian-Franco Dalla Betta for having provided financial support for the last period, and for his help in the HYDE experiment.*

*I have also to mention my friends and colleagues Walter Raniero and Matteo Campostrini, with whom I spent a nice time inside and outside the laboratories in Legnaro and Prof. Gianantonio Della Mea, who introduced me to Legnaro laboratories thus allowing this experience to begin...*

*... ma più di tutti devo ringraziare i miei genitori Paola e Claudio, per non avermi mai fatto mancare nulla e per avermi trasmesso quei valori, di cui sono orgoglioso, che sono il faro che guida le mie scelte passate, presenti e future. E Marta per il suo incondizionato sostegno e incoraggiamento. La sua presenza costante al mio fianco mi ha dato la serenità e la sicurezza necessarie a raggiungere quest'obiettivo e la certezza che con lei accanto anche il percorso più tortuoso sarà niente più che una bella avventura.*

*Ringrazio infine tutta la "Gentaglia" di Feltre, compagnia di mille serate (e non solo). Essi sono uno dei principali motivi per cui, dovunque sia il mio futuro, dentro di me io sarò sempre innanzitutto feltrino.*

